Supporting Information

Controlling the Triplet Dynamics for Efficient Room Temperature Phosphorescence by Molecular Engineering

Ramar Arumugam,[a] Akkarakkaran Thayyil Muhammed Munthasir,[b] Pagidi Sudhakar,[c] Niharika Pradhan,[d] Gobbilla Sai Kumar,[a] Sambit Pradhan,[b] Venugopal Rao Soma,[d] Pakkirisamy Thilagar*[b] and Vadapalli Chandrasekhar*[a]

[a] Tata Institute of Fundamental Research, Hyderabad 500046, India.

[b] Department of Inorganic and Physical Chemistry, Indian Institute of Science, Bangalore 560012, India.

[c] Department of Chemistry, Indian Institute of Technology Tirupati, Tirupati 517619, India

[d] School of Physics and DIA-CoE (formerly ACRHEM), University of Hyderabad, Hyderabad 500046, India.

Table of Contents

1. General experimental procedures

1.1. Materials

All reactions were performed under an inert argon atmosphere using standard Schlenk techniques.[1] Starting materials such as *n*-butyl lithium (2.5 M in hexane), 1,4-dibromonaphthalene,1-bromo-4-methoxynaphthalene, BBr_3 (2.5 M in n-hexane), Sodium azide, Copper(I) iodide, L-proline, and dimesitylboron fluoride, were obtained and used as received. Tetrahydrofuran, *n*-hexane, *n*-pentane, diethyl ether, and DCM were dried and distilled by standard procedures.[2]

1.2. Methods

Multi-nuclear NMR (^1H, ^{11}B, and ^{13}C) spectra were recorded in $CDCl_3$ and DMSO-d_6 at 25 °C on a Bruker Avance 400 MHz/300 MHz NMR spectrometer operating at a frequency of 300 MHz for ^1H, ^{11}B for 128 MHz, and ^{13}C for 75 MHz. ^1H NMR spectra were referenced to TMS (0.00 ppm) as an internal standard. Chemical shift multiplicities are reported as singlet (s), doublet (d), triplet (t), and multiplet (m). ^{13}C resonances were referenced to the $CDCl_3$ signal at ~77.67 ppm. ^{11}B NMR chemical shift values were referenced to the external standard boron signal of $BF_3 \cdot Et_2O$. The ESI (HR-MS) mass spectra were recorded on a Bruker maXis mass spectrometer. Electronic absorption spectra, fluorescence emission spectra, and time-resolved fluorescence (TRF) decay measurements were recorded on a SHIMADAZU UV-2600 spectrophotometer and FLS-980 EDINBURGH spectrometer, respectively. Time-gated emission spectra were recorded using the same FLS 980 fluorimeter by excitation source of a pulsed microsecond flash lamp (μF1) with a pulse width of 1.1 μs. Temperature-dependent emission studies were also performed using the same instrument with the help of an OXFORD cryostat. All compound solutions for spectral measurements were prepared using anhydrous spectrophotometric grade solvents and standard volumetric glassware. Quartz cuvettes with sealing screw caps were used for the solution state spectral measurements. The intensity data of crystals **NB-Br, NB-OMe, NB-OH, NH_2**, and **NB-COOH** were collected on an XtaLAB AFC12 (RINC) [λ(Mo Kα) = 0.71073 Å] (Rigaku Oxford Diffraction, 2017) diffractometer. The data were integrated using CrysAlisPro 1.171.39.29d software. [3a,c] The structures were solved by direct methods using SHELXS-97 and refined using the SHELXL-2018/3 program (within the WinGX program package) [3b], and non-H atoms were refined anisotropically. The CCDC numbers **NB-Br, NB-OMe, NB-OH, NH_2**, and **NB-COOH** are 2291486 and 2487699-2487702, respectively. Density functional theory (DFT) calculations

were done using B3LYP functional with 6-31G(d) basis set as incorporated in the Gaussian 09 package for all the atoms. [4] The optimized structures and the frontier molecular orbitals (FMOs) were viewed using Gaussview 5.0. SOC calculations were done by ORCA 5.0 software, using B3LYP functional with a 6-31G (d, p) basis set. RP-HPLC analysis was performed on a Shimadzu HPLC system using a C18 column. The mobile phase consisted of water (A) and acetonitrile (B). The gradient method was as follows: solvent B was increased from 50% to 100% over 0.01–5.0 minutes, followed by 100% B from 5.0 to 20.0 minutes. The flow rate was maintained at 1.0 mL/min, the injection volume was 20 µL and detection was carried out at 254 nm. The compounds were dissolved in methanol prior to injection.

Synthesis of NB-Br

The precursor (4-bromonaphthalen-1-yl)dimesitylborane (**NB-Br**) was synthesised using a modified literature protocol [5]. Yield: 90%. ^{1}H NMR (300 MHz, $CDCl_3$): δ (ppm) 8.21 (d, *J* = 8.4 Hz, 1H), 7.78 (d, *J* = 8.4 Hz, 1H), 7.64 (d, *J* = 7.5 Hz, 1H), 7.44 (t, *J* = 7.6 Hz, 1H), 7.23-7.16 (m, 2H), 6.70 (s, 4H), 2.21 (s, 6H), 1.85 (s, 12H);^{13}C NMR (75 MHz, $CDCl_3$): δ (ppm) 140.60, 139.31, 137.01, 134.12, 131.61, 129.88, 128.51, 128.42, 128.15, 127.57, 127.37, 127.18, 127.02, 23.18, 21.31; ^{11}B NMR (128 MHz, $CDCl_3$): δ (ppm) 75.60; ESI (HR-MS). Calculated for $C_{28}H_{28}BBr$ [M + H]: m/z 455.1546, found: m/z 455.35.

Synthesis of NB-OMe

To a solution of 1-bromo-4-methoxynaphthalene (500 mg, 2.11 mmol) in dry Et_2O (15 mL) at –78 °C under N_2, ^{n}BuLi (2.5 M in hexane, 1.06 mL, 2.65 mmol) was added dropwise and stirred for 30 minutes. Dimesitylboron fluoride (565 mg, 2.11 mmol) in Et_2O (5 mL) was then added, and the mixture was allowed to warm to room temperature and stirred overnight. The reaction was quenched with saturated NH_4Cl, extracted with DCM, dried over Na_2SO_4, filtered, and concentrated. Purification by silica gel column chromatography (hexane/EtOAc, 98:2) yielded the product **NB-OMe** as a colourless solid. Yield: 90%. ^{1}H NMR (300 MHz, $CDCl_3$): δ (ppm) 8.33 (d, J = 8.4 Hz, 1H), 7.87 (d, J = 8.4 Hz, 1H), 7.54 (d, *J* = 7.5 Hz, 1H), 7.45 (t, *J* = 7.5 Hz, 1H), 7.31-7.28 (m, 1H), 6.82 (s, 4H), 4.07 (s, 3H), 2.34 (s, 6H), 2.00 (s, 12H); ^{13}C NMR (75 MHz, $CDCl_3$): δ (ppm) 158.71, 158.71, 158.71,143.71, 140.53, 138.47, 137.59, 138.47, 137.59, 138.47,137.59,136.98, 128.26, 127.52, 126.77, 126.77, 126.77, 126.77,125.40, 125.18, 125.18,

122.07, 122.07, 122.07,103.44, 55.48, 23.07, 21.27; ^{11}B NMR (128 MHz, $CDCl_3$): δ (ppm) 71.30; ESI (HR-MS). Calculated for $C_{28}H_{31}BO$ [M + H]: m/z 407.2546, found: m/z 407.2504

Synthesis of NB-OH

To a solution of **NB-OMe** (500 mg, 1.20 mmol) in dry DCM (10 mL) at 0 °C under N_2, BBr_3 (2.5 M in n-hexane, 1.2 mL, 3.0 mmol) was added dropwise. The mixture was stirred at rt for 12 h, then quenched with ice water. The organic layer was separated, dried (Na_2SO_4), and concentrated. Purification by column chromatography (hexane/EtOAc, 95:5) afforded **NB-OH** as a colourless solid. Yield: 50%. ^{1}H NMR (300 MHz, $CDCl_3$): δ (ppm) 8.21 (d, *J* = 8.4 Hz 1H), 7.84 (d, *J* = 9.0 Hz, 1H),7.42 (t, *J* = 8.8Hz, 2H), 7.25 (t, 2H and $CDCl_3$), 6.77 (s, 4H), 6.73 (d, *J*= 7.5 Hz, 1H),5.47 (s, 1H), 2.29 (s, 6H), 1.95 (s, 12H); ^{13}C NMR (75 MHz, $CDCl_3$): δ (ppm) 154.89, 143.65, 140.56, 138.56, 137.97, 136.66, 128.28, 127.70, 126.92, 125.26, 124.11, 121.72, 108.36, 23.08, 21.26; ^{11}B NMR (128 MHz, $CDCl_3$): δ (ppm) 71.34; ESI (HR-MS). Calcd for $C_{28}H_{29}BO$ [M + H]$^+$: *m*/*z* 393.2390 Found: *m*/*z* 393.2348.

Synthesis of NB-NH_2

A mixture of (4-bromonaphthalen-1-yl)dimesitylborane (**NB-Br**) (184 mg, 4.04 mmol), CuI (77 mg, 4.04 mmol), NaN_3 (58 mg, 8.92 mmol), and L-proline (61 mg, 5.30 mmol) was stirred in dry DMSO (5 mL) at 100 °C under nitrogen for 12 h. After completion (monitored by TLC), the reaction mixture was cooled to room temperature, diluted with water, and extracted with DCM (3 × 15 mL). The combined organic layers were dried over Na_2SO_4, filtered, and concentrated under reduced pressure. Purification by column chromatography (hexane/EtOAc) afforded the desired amine product NH_2 as a brown-colored solid. Yield: 20%. ^{1}H NMR (300 MHz, $CDCl_3$): δ (ppm) 7.91-7.77 (m, 2H),7.42-7.21(m, 3H), 6.76 (s, 6H), 6.68 (d, *J* = 7.2 Hz, 1H), 4.48 (s, 2H), 2.29 (s, 6H), 1.95 (s, 12H); ^{13}C NMR (75 MHz, $CDCl_3$): δ (ppm) 146.26, 140.57, 138.14, 138.04, 137.96, 128.61, 128.16, 126.33, 124.81, 122.87, 120.55, 23.08, 21.23; ^{11}B NMR (128 MHz, $CDCl_3$): δ (ppm) 70.58; ESI (HR-MS). Calcd for $C_{28}H_{30}BN$ [M + H]$^+$: *m*/*z* 392.2550 Found: *m*/*z* 392.2586.

Synthesis of NB-COOH

To a solution of (4-bromonaphthalen-1-yl)dimesitylborane (**NB-Br**) (500 mg, 1.01 mmol) in dry THF (10 mL) at –78 °C under N_2, ^{n}butyllithium (2.5 M in hexane, 0.5 mL, 1.31 mmol) was added dropwise. The reaction mixture was stirred at –78 °C for 30 min, then bubbled with dry CO_2 gas for 15 min. The reaction was allowed to warm to room temperature and quenched with dilute HCl

(10 mL). The aqueous phase was extracted with EtOAc (3 × 15 mL), and the combined organic layers were dried (Na_2SO_4), filtered, and concentrated. Purification by column chromatography (hexane/EtOAc) afforded the **NB-COOH** product as a colourless solid. Yield: 70%. ^{1}H NMR (300 MHz, DMSO-d_6): δ (ppm) 8.79 (d, *J*= 8.7 Hz, 1H), 8.03 (d, *J*= 7.5Hz, 1H), 7.81 (d, *J*= 8.1 Hz, 1H), 7.57(t, *J*= 7.8 Hz, 1H), 7.40- 7.32 (m, 2H), 6.80 (s, 4H), 2.24 (s, 6H), 1.86 (s, 12H); ^{13}C NMR (75 MHz, DMSO-d_6): δ (ppm) 169.30,152.70, 143.31,140.31, 139.58, 135.78, 131.94, 131.56, 128.93, 128.09, 127.71, 126.87,126.56, 23.10, 21.31; ^{11}B NMR (128 MHz, $CDCl_3$): δ (ppm) 75.41; ESI (HR-MS). Calcd for $C_{29}H_{29}BO_2$ $[M + H]^+$: *m*/*z* 421.2339 Found: *m*/*z* 421.2375.

3. Structural characterization

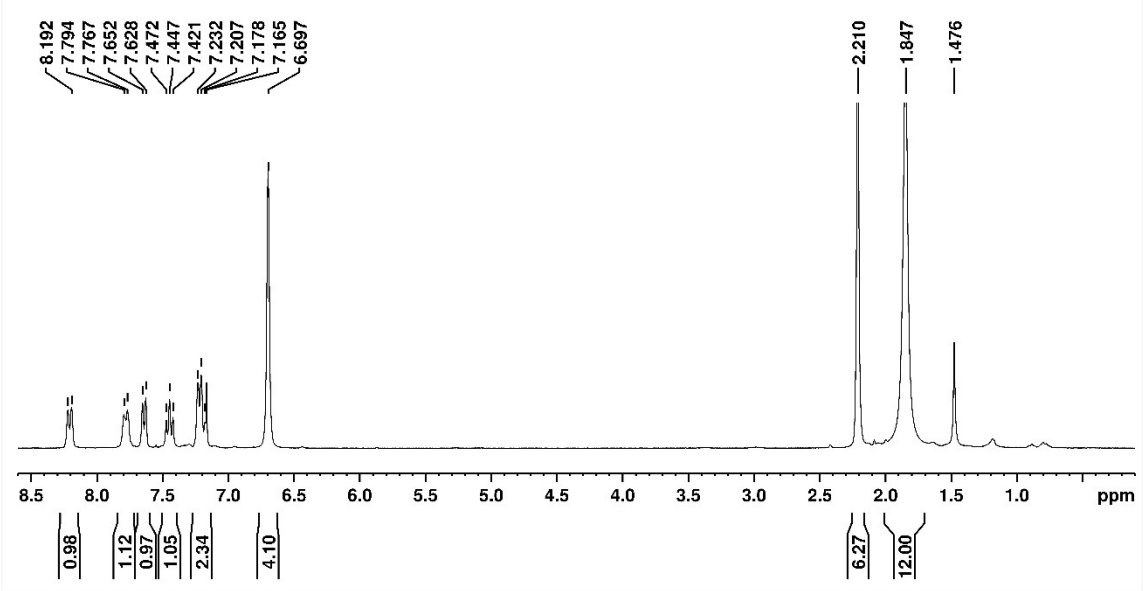

Figure S1. ^{1}H NMR spectrum of **NB-Br** in $CDCl_3$.

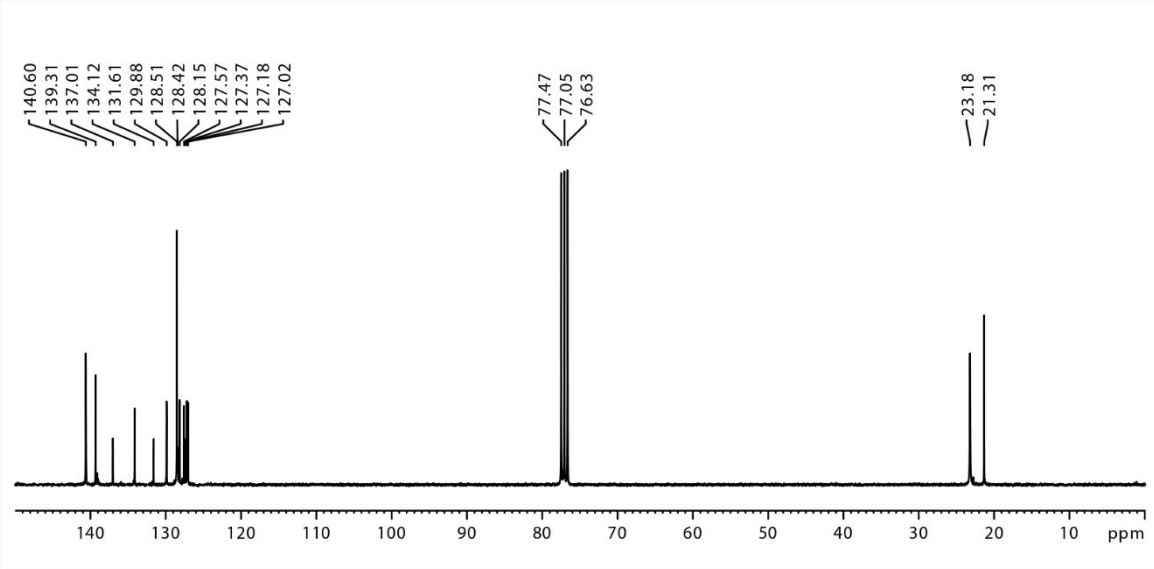

Figure S2. ^{13}C NMR spectrum of **NB-Br** in $CDCl_3$.

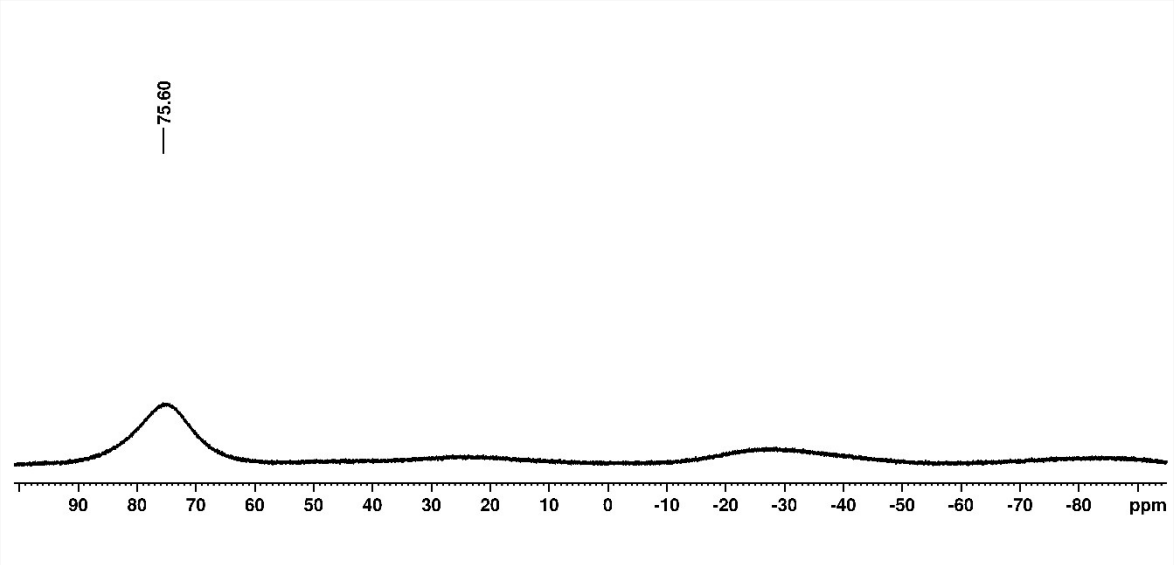

Figure S3. ^{11}B NMR spectrum of **NB-Br** in $CDCl_3$.

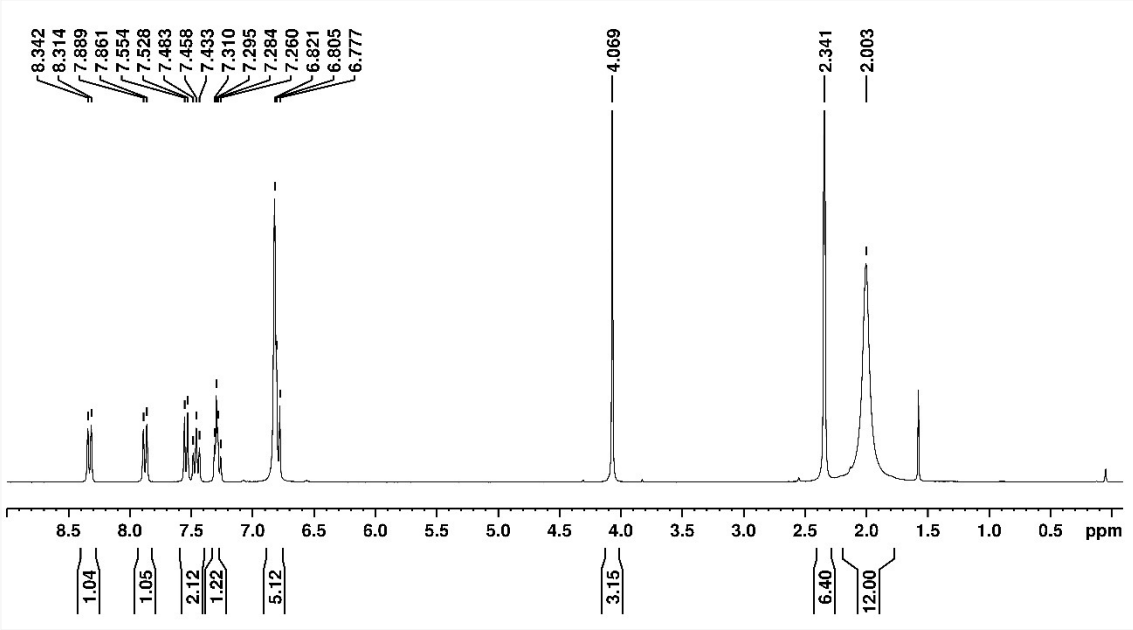

Figure S4. ^{1}H NMR spectrum of **NB-OMe** in $CDCl_3$.

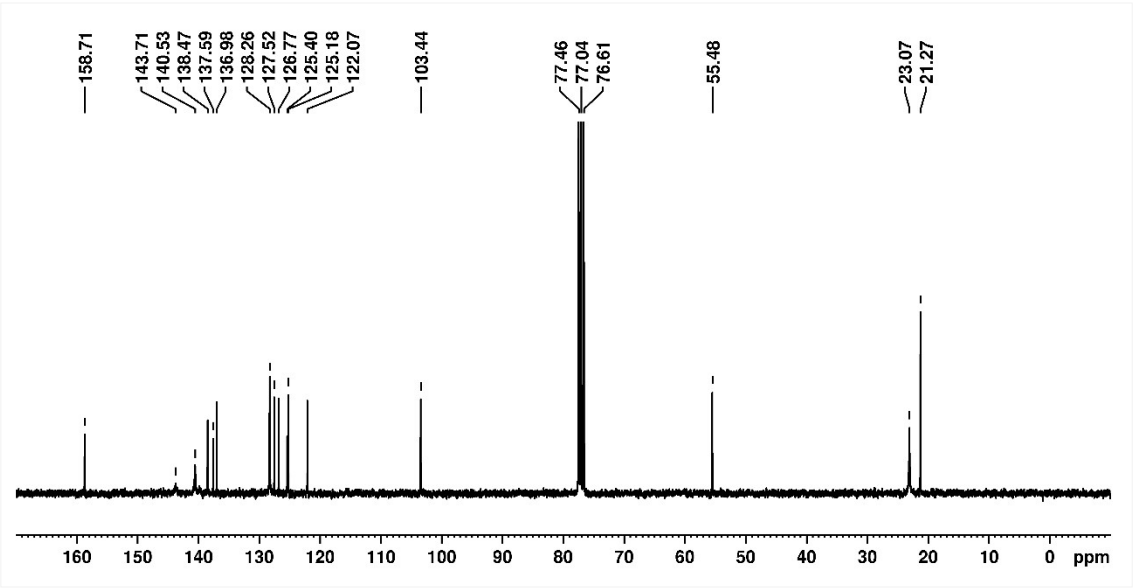

Figure S5. ^{13}C NMR spectrum of **NB-OMe** in $CDCl_3$.

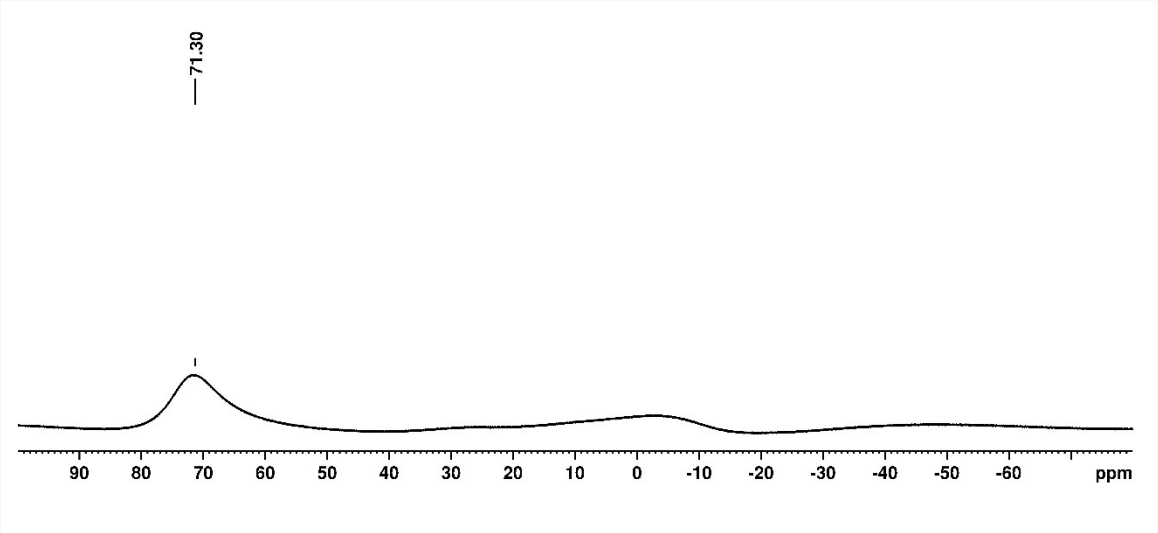

Figure S6. ^{11}B NMR spectrum of **NB-OMe** in $CDCl_3$.

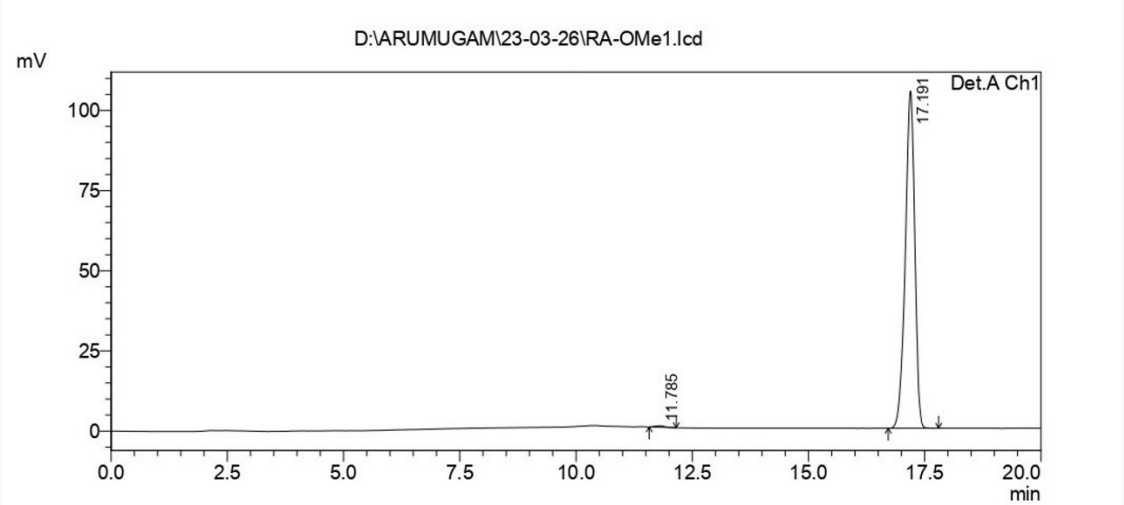

Detector A Ch1 254nm

Peak#	Ret. Time	Area	Height	Area %	Height %
1	11.785	6856	472	0.458	0.447
2	17.191	1491498	105152	99.542	99.553
Total		1498354	105624	100.000	100.000

Figure S7. HPLC trace report of NB-OMe

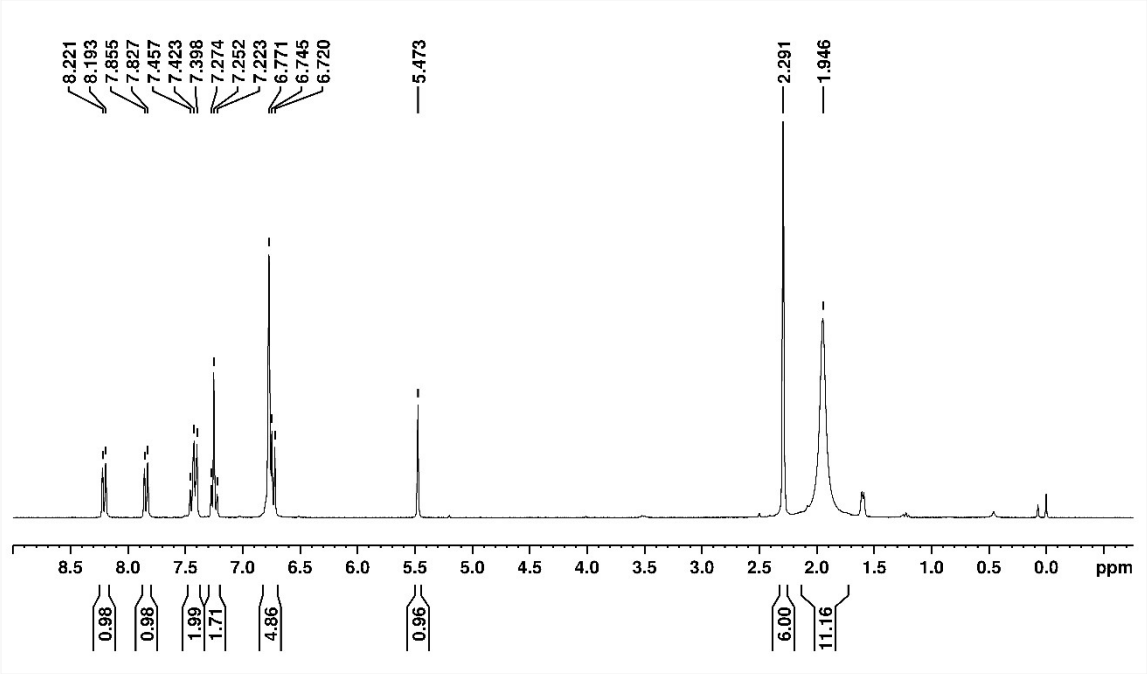

Figure S8. ^{1}H NMR spectrum of **NB-OH** in $CDCl_3$.

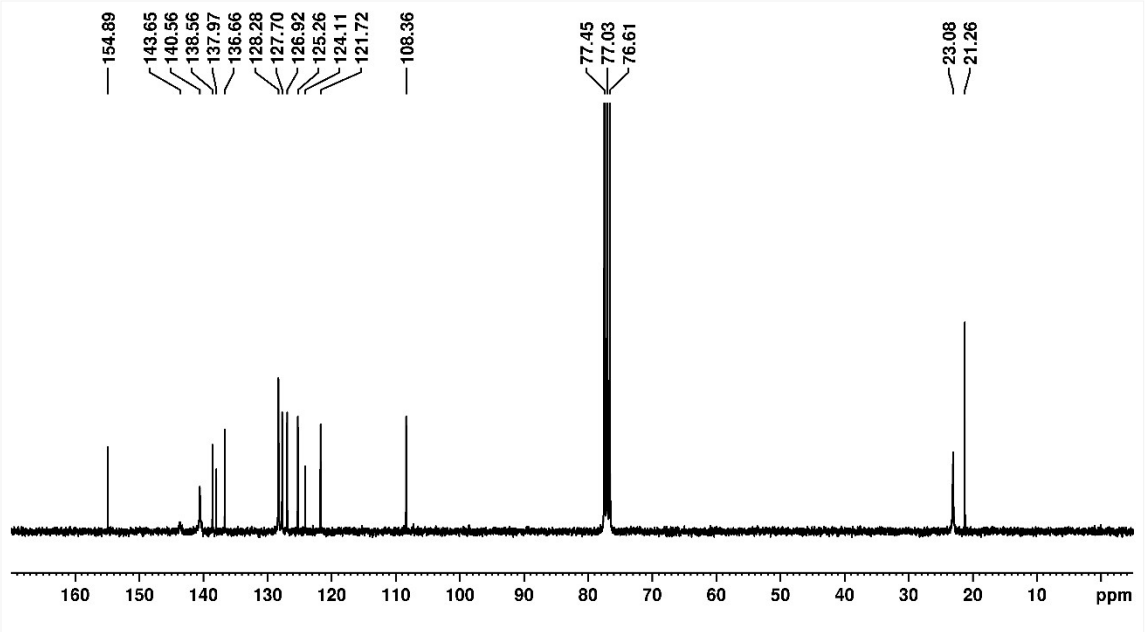

Figure S9. ^{13}C NMR spectrum of **NB-OH** in $CDCl_3$.

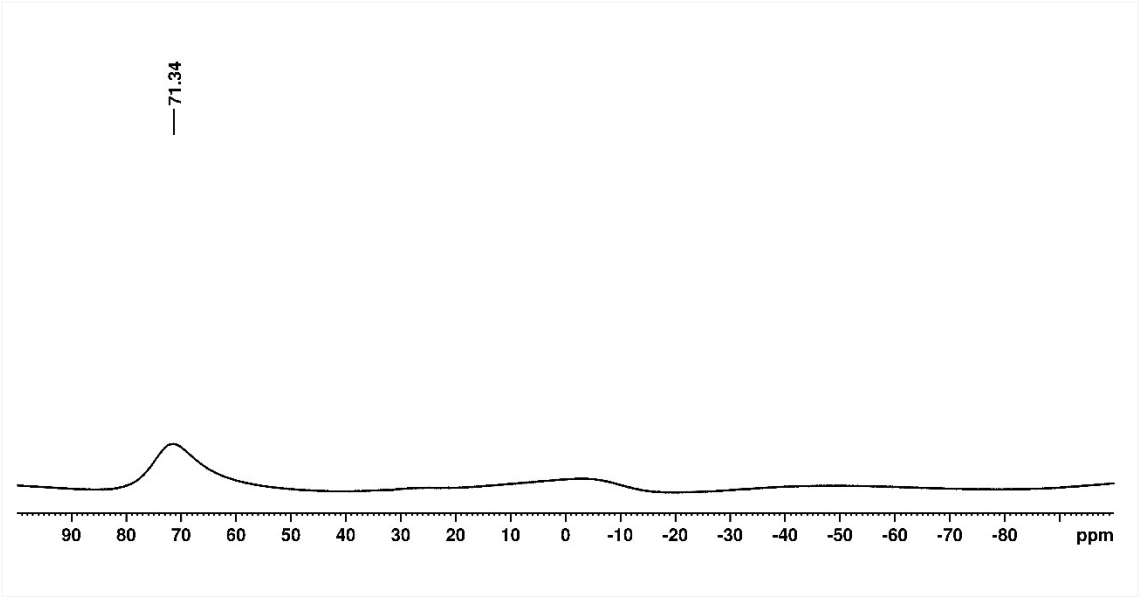

Figure S10. ^{11}B NMR spectrum of **NB-OH** in $CDCl_3$.

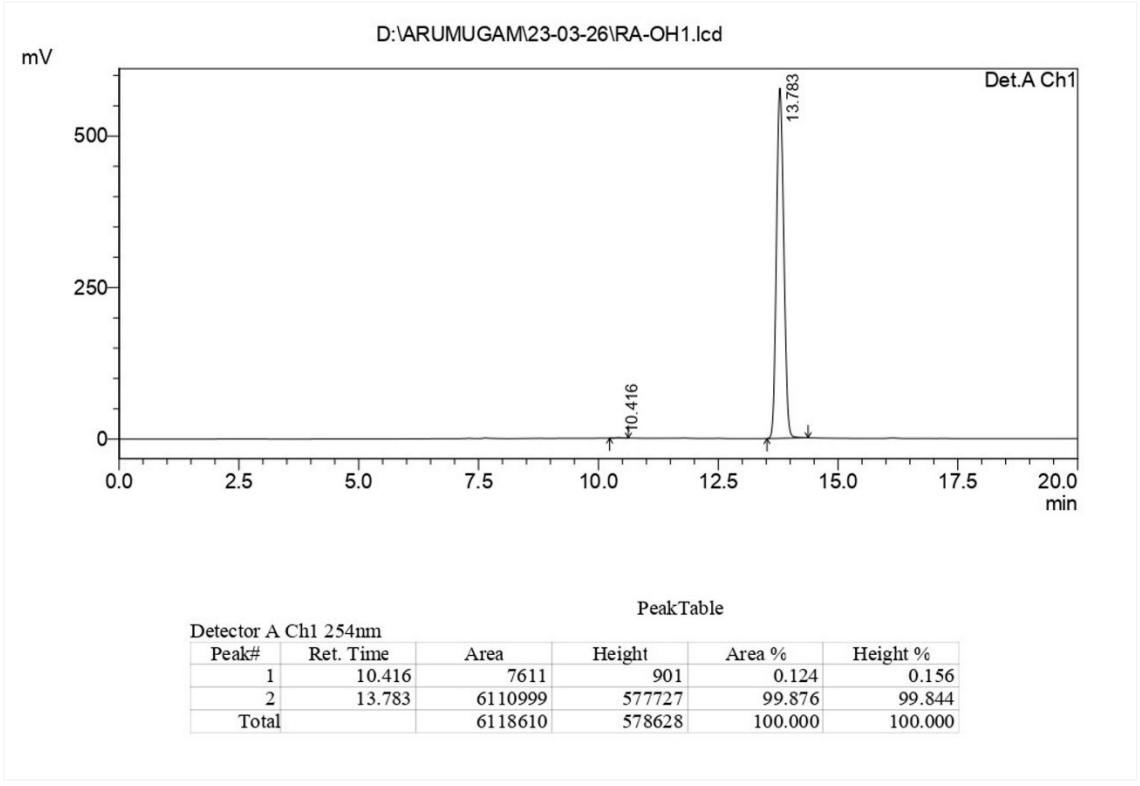

PeakTable

Detector A Ch1 254nm

Peak#	Ret. Time	Area	Height	Area %	Height %
1	10.416	7611	901	0.124	0.156
2	13.783	6110999	577727	99.876	99.844
Total		6118610	578628	100.000	100.000

Figure S11. HPLC trace report of **NB-OH**

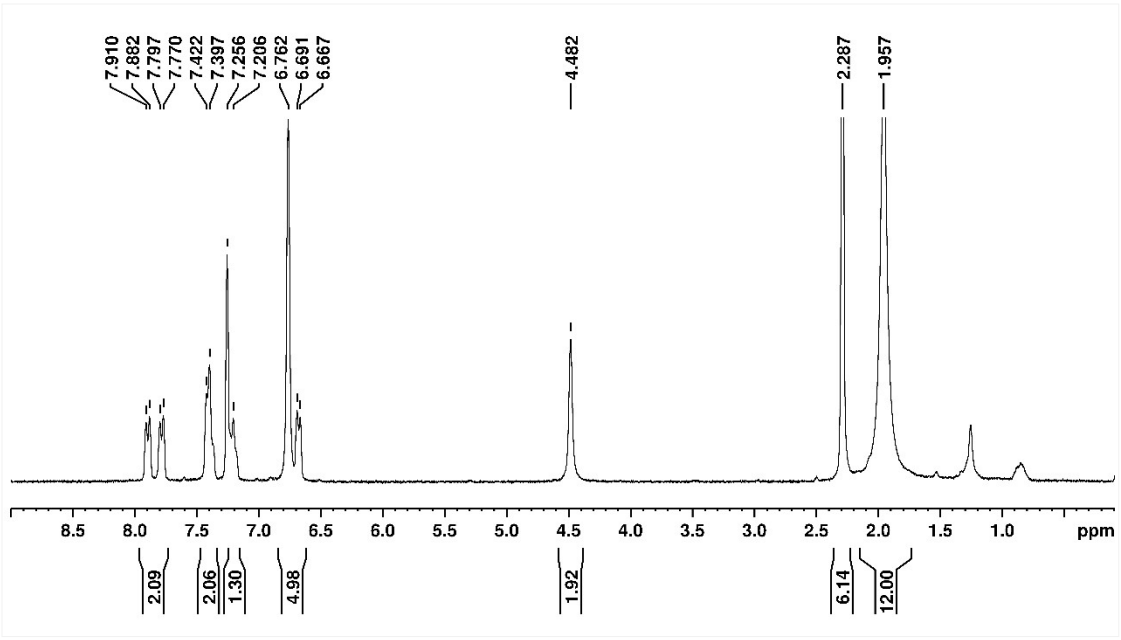

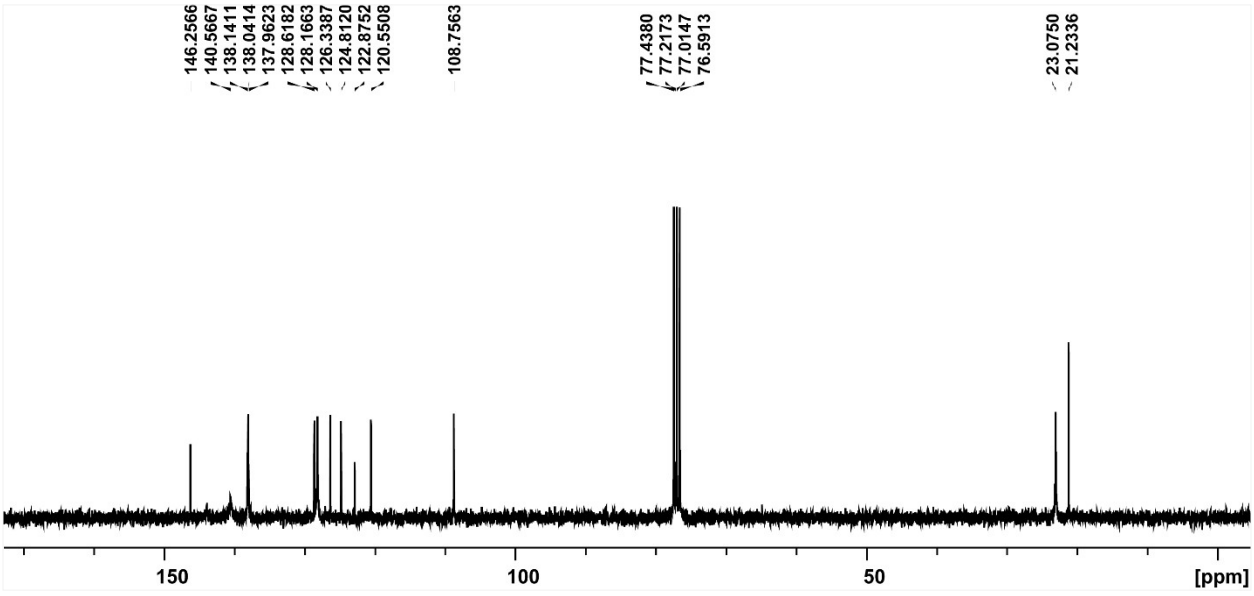

Figure S12. ^{1}H NMR spectrum of **NB-NH$_2$** in $CDCl_3$.

Figure S13. ^{13}C NMR spectrum of **NB-NH$_2$** in $CDCl_3$.

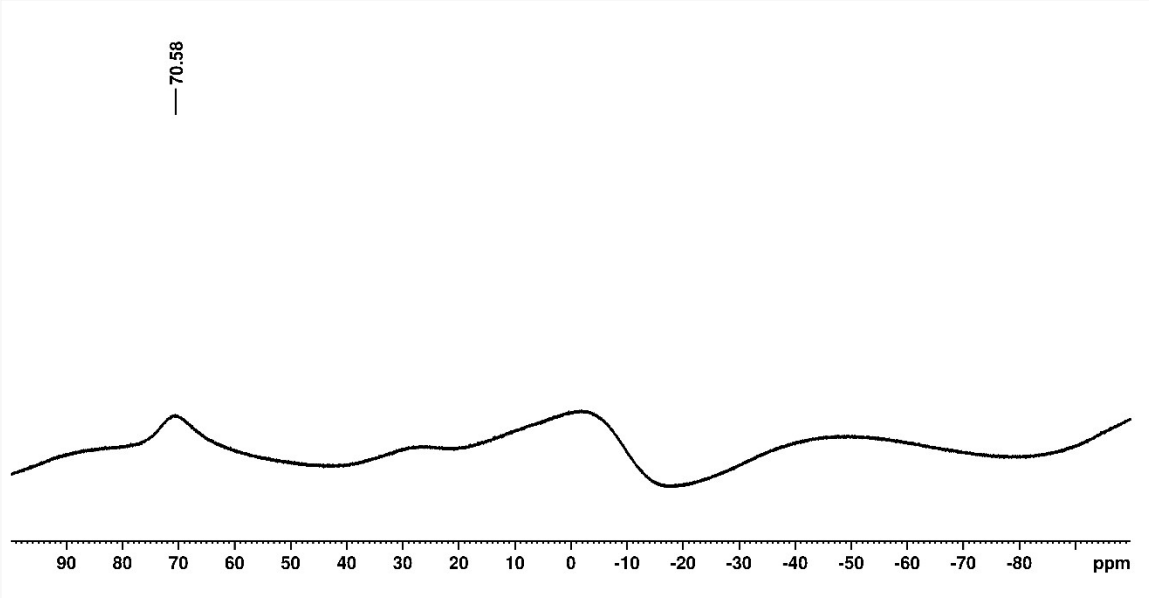

Figure S14. ^{11}B NMR spectrum of **NB-NH$_2$** in $CDCl_3$. The additional peaks and irregular baseline are due to the nmr tube used, even though it is a quartz tube.[8]

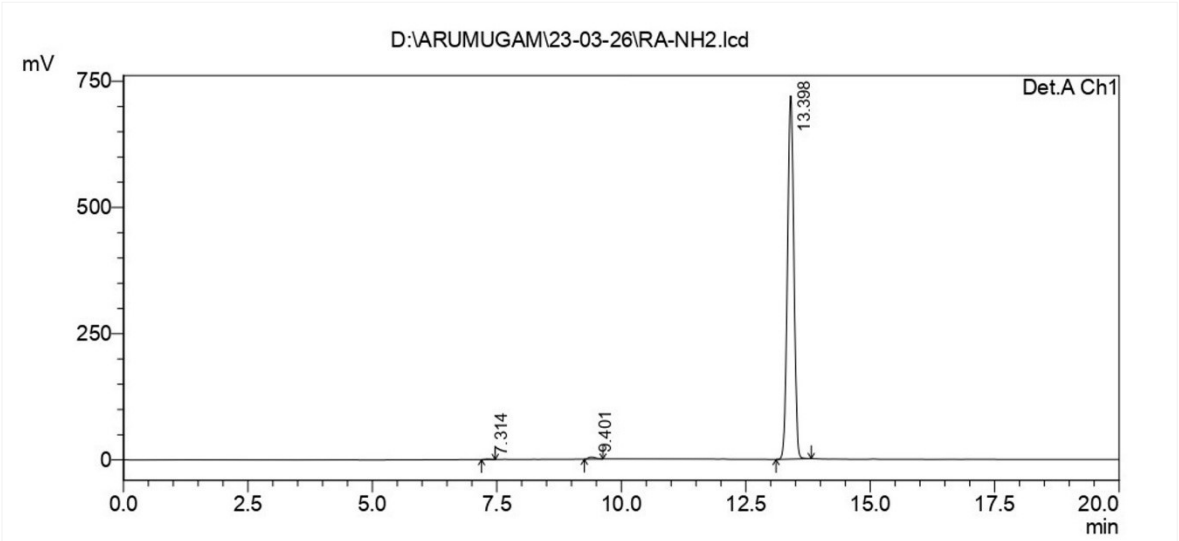

Detector A Ch1 254nm

Peak#	Ret. Time	Area	Height	Area %	Height %
1	7.314	6357	820	0.098	0.113
2	9.401	41241	3827	0.637	0.529
3	13.398	6425892	719341	99.265	99.358
Total		6473491	723988	100.000	100.000

Figure S15. HPLC trace report of **NB-NH$_2$**

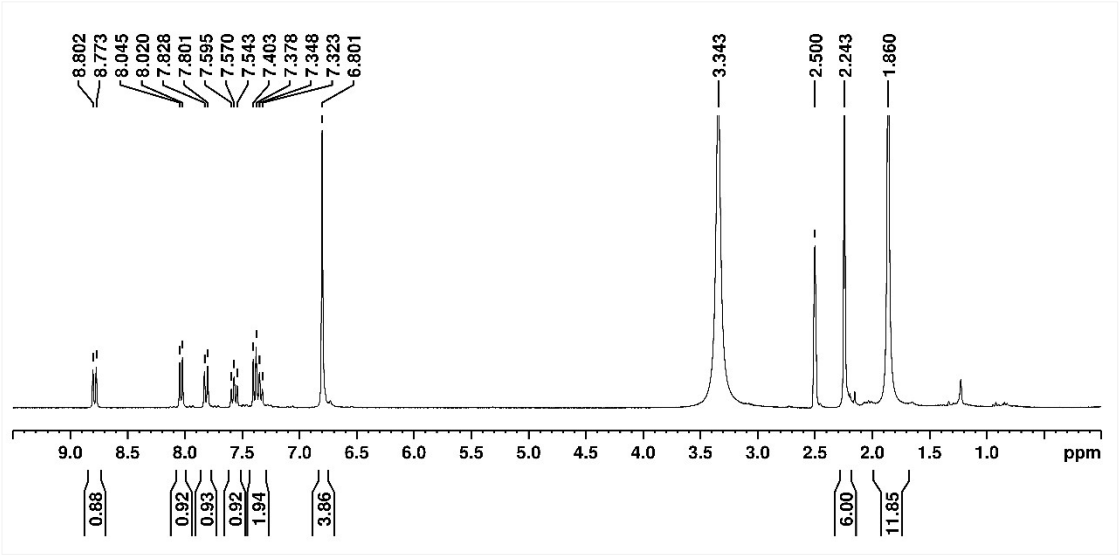

Figure S16. ^{1}H NMR spectrum of **NB-COOH** in DMSO- d_6.

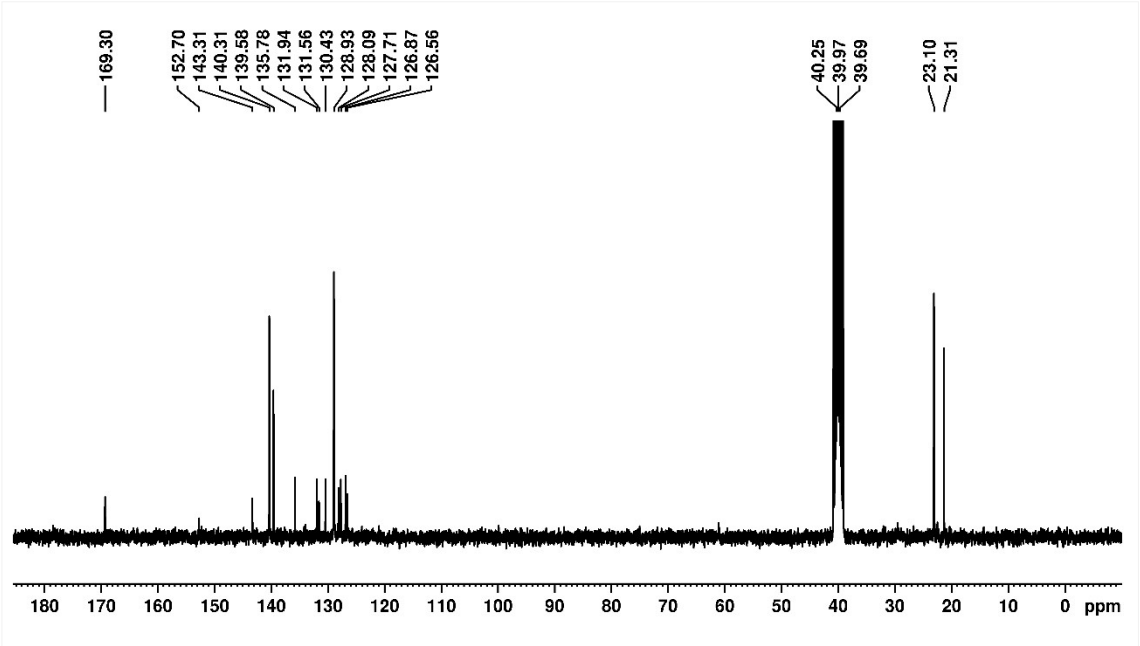

Figure S17. ^{13}C NMR spectrum of **NB-COOH** in DMSO- d_6.

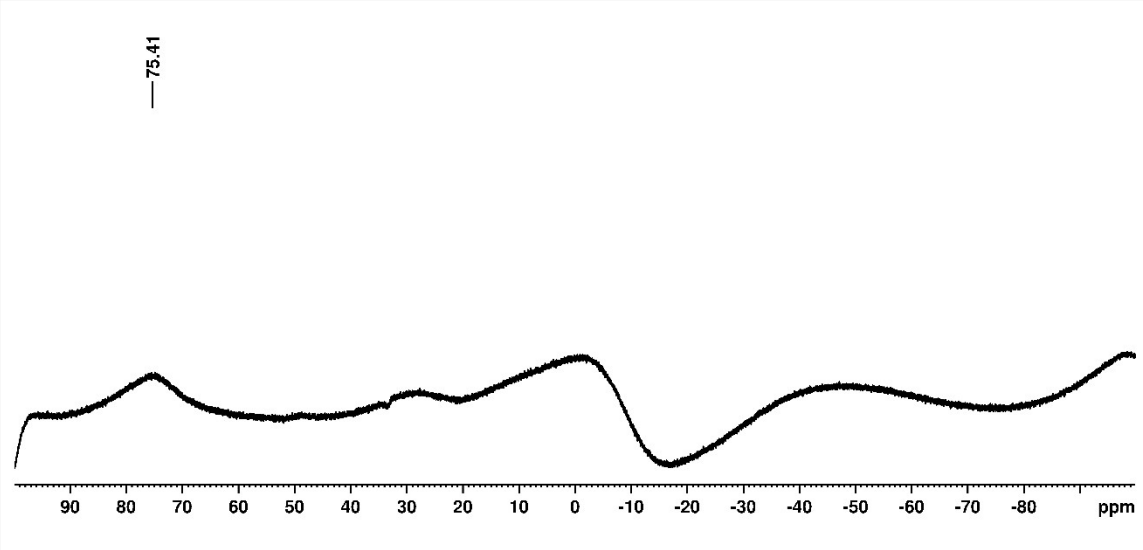

Figure S18. ^{11}B NMR spectrum of **NB-COOH** in $CDCl_3$.The additional peaks and irregular baseline are due to the nmr tube used, even though it is a quartz tube.[8]

4. Single-crystal X-ray diffraction Studies

Table S1: Crystallographic data and refinement parameters for compounds.

Compounds	NB-Br	NB-OMe	NB-OH	NB-NH_2	NB-COOH
Empirical formula	C28 H28 B Br	C29 H31 B O	C28 H29 B O [+ solvent]	C28 H30 B N	C29 H29 B O2
FW	455.21	406.35	392.32	391.34	420.33
T (K)	293 K	296 K	296 K	293 K	293 K
Crystal system	triclinic	orthorhombic	triclinic	monoclinic	triclinic
Space group	*P -1*	*P b c a*	*P -1*	*P 21/n*	*P -1*
a/Å	8.9277(7)	30.875(2)	8.7044(4)	8.3646(17)	8.3517(5)
b/Å	11.4441(7)	11.7008(7)	12.2005(5)	8.5059(17)	12.7415(5)
c/Å	12.0410(8)	12.4722(11)	13.3275(5)	32.466(3)	13.5443(6)
α/deg	78.049(5)	90	79.280(4)	90	87.233(4)
β/deg	85.965(6)	90	80.734(3)	90.079(12)	73.686(4)
γ/deg	67.940(6)	90	86.814(4)	90	83.611(4)
V/Å^3	1115.41(14)	4505.7(6)	1372.03(10)	2309.9(7)	1374.45(12)
Z	2	8	2	4	2
ρ_{calcd} (gcm^{-3})	1.355	1.198	0.950	1.125	1.016
μ (Mo Kα) (mm^{-1})	1.855	0.070	0.055	0.064	0.062
λ/Å	0.71073	0.71073	0.71073	0.71073	0.71073
F (000)	472.0	1744.0	420.0	840.0	448.0
Collected reflections	6097	2440	7483	2824	7517
Unique reflections	4565	2102	5799	1820	5415
Goodness of Fit (GOF) [F2]	0.730	1.037	1.069	0.914	4.342
R1 [I>2σ(I)][a]	0.0539	0.0427	0.0544	0.0867	0.4507
wR2 [I>2σ(I)][b]	0.1500	0.1172	0.1717	0.2725	0.8231
CCDC Number	2487699	2487700	2487701	2291486	2487702

[a] $R1 = \Sigma \| |Fo| - |Fc| | / \Sigma |Fo|$. [b] wR2 = [Σ {w (Fo 2 – Fc 2) 2}/Σ {w (Fo 2)

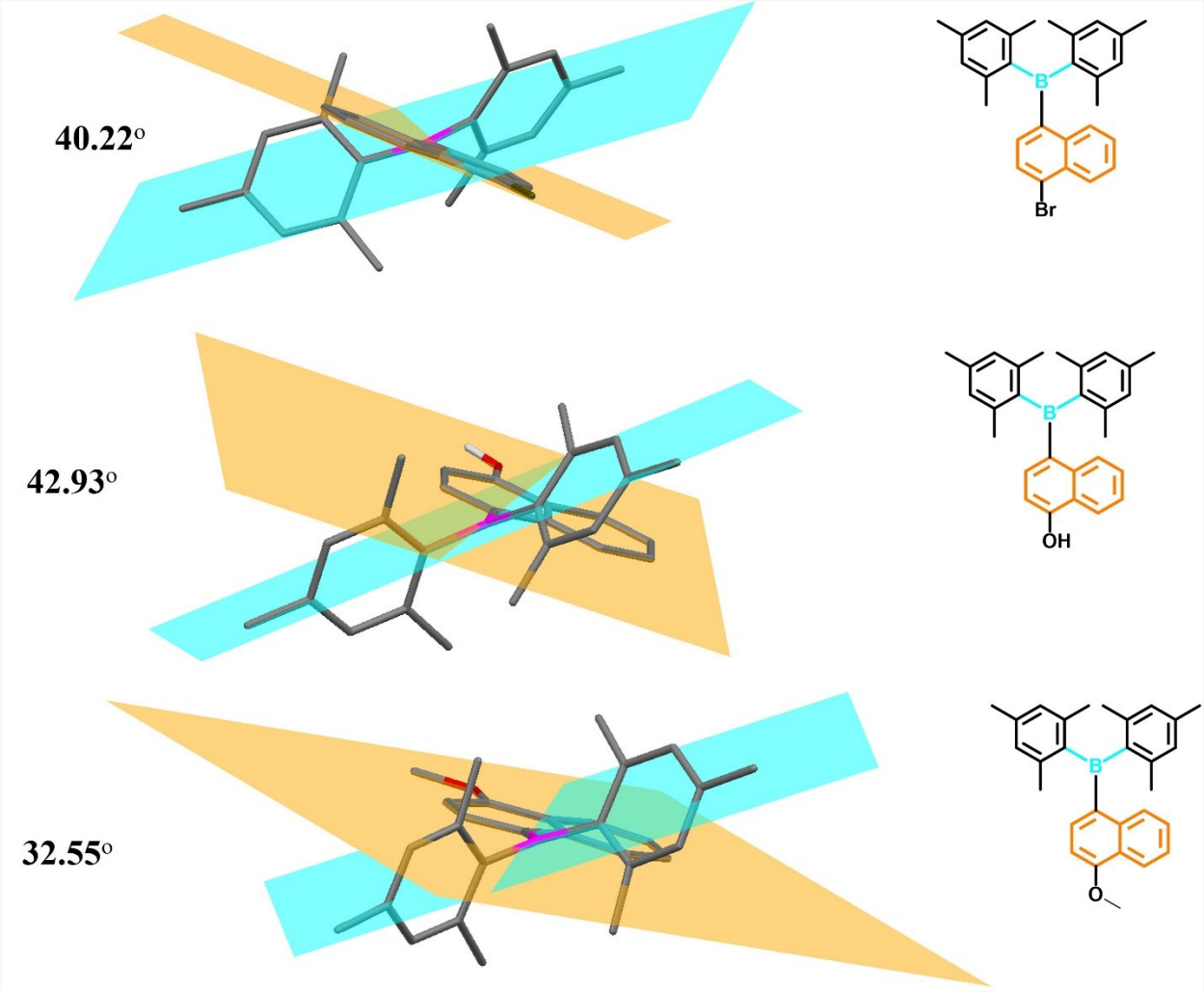

Figure S19. Dihedral angle (°) between the plane containing boron with carbons attached to B (cyan) and the mean plane containing all naphthalene carbon atoms (orange) [$\theta_{B\text{-}Nap}$] on **NB-Br**, **NB-OH** and **NB-OMe**. [Carbon: black, nitrogen: blue, boron: magenta, and hydrogen are omitted for clarity]. The angles mentioned in parentheses are obtained by subtracting the exact angle measured (from the crystal structure) from 180°.

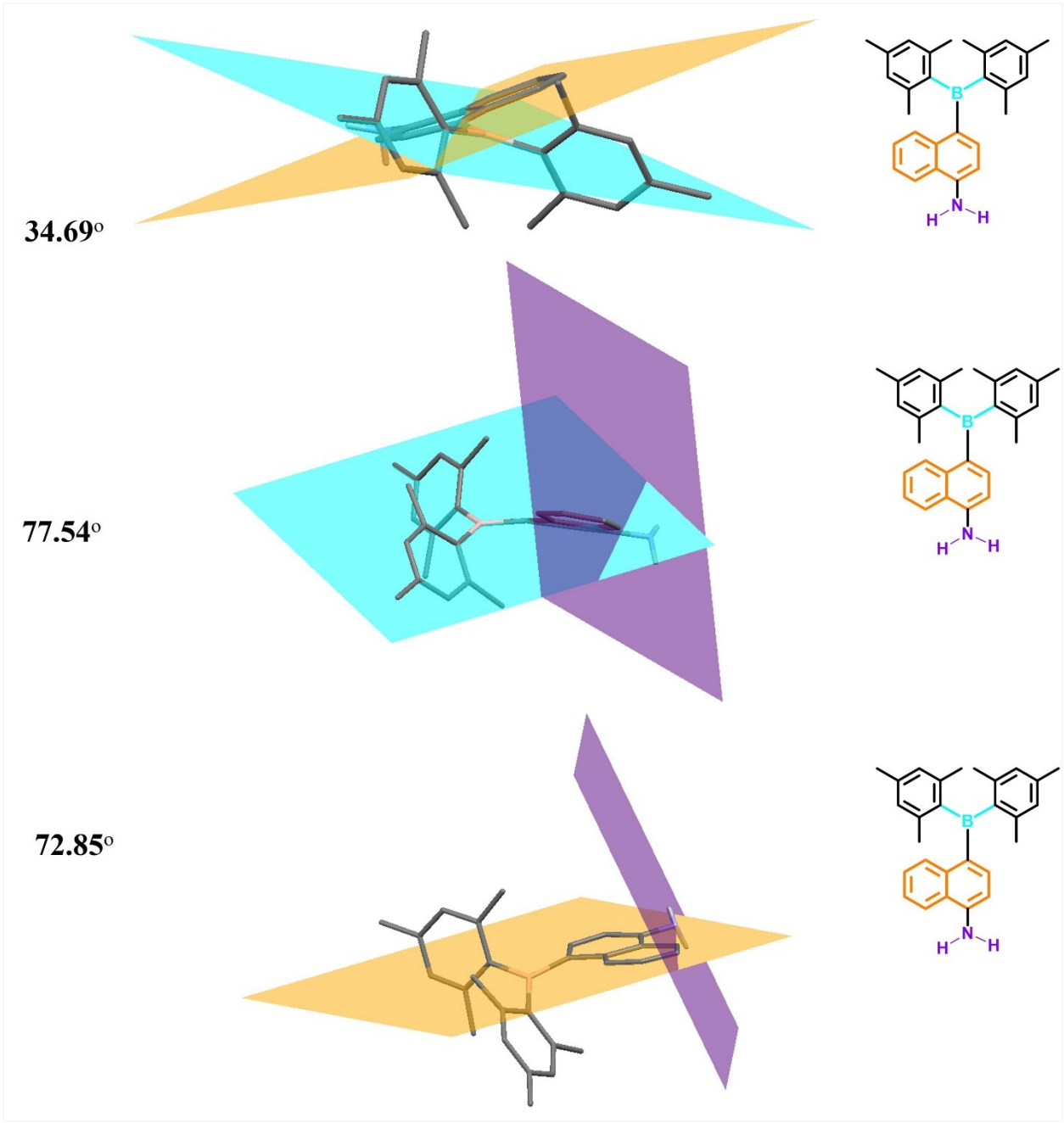

Figure S20. Dihedral angle (°) between the plane containing boron with carbons attached to B (cyan) and nitrogen with methyl carbon attached to N (magenta) [$\theta_{B\text{-}N}$], [$\theta_{B\text{-}Nap}$], and [$\theta_{N\text{-}Nap}$] on **NB-NH$_2$**. [Carbon: black, nitrogen: blue, boron: magenta, and hydrogen are omitted for clarity]. The angles mentioned in parentheses are obtained by subtracting the exact angle measured (from the crystal structure) from 180°.

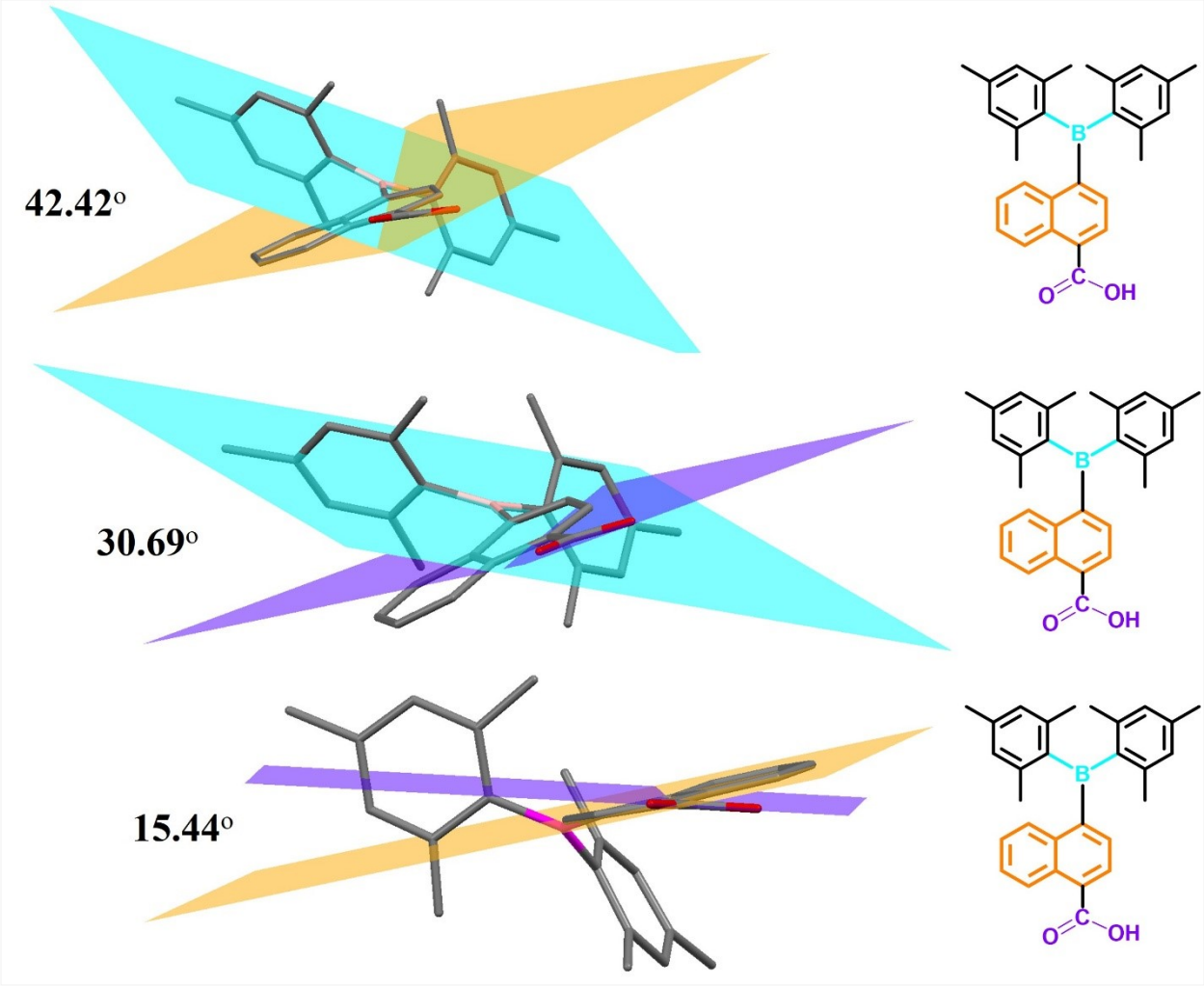

Figure S21. Dihedral angle (°) between the plane containing boron with carbons attached to B (cyan) and nitrogen with methyl carbon attached to N (magenta) [$\theta_{B\text{-}N}$], [$\theta_{B\text{-}Nap}$], and [$\theta_{N\text{-}Nap}$] on **NB-COOH**. [Carbon: black, nitrogen: blue, boron: magenta, and hydrogen are omitted for clarity]. The angles mentioned in parentheses are obtained by subtracting the exact angle measured (from the crystal structure) from 180°.

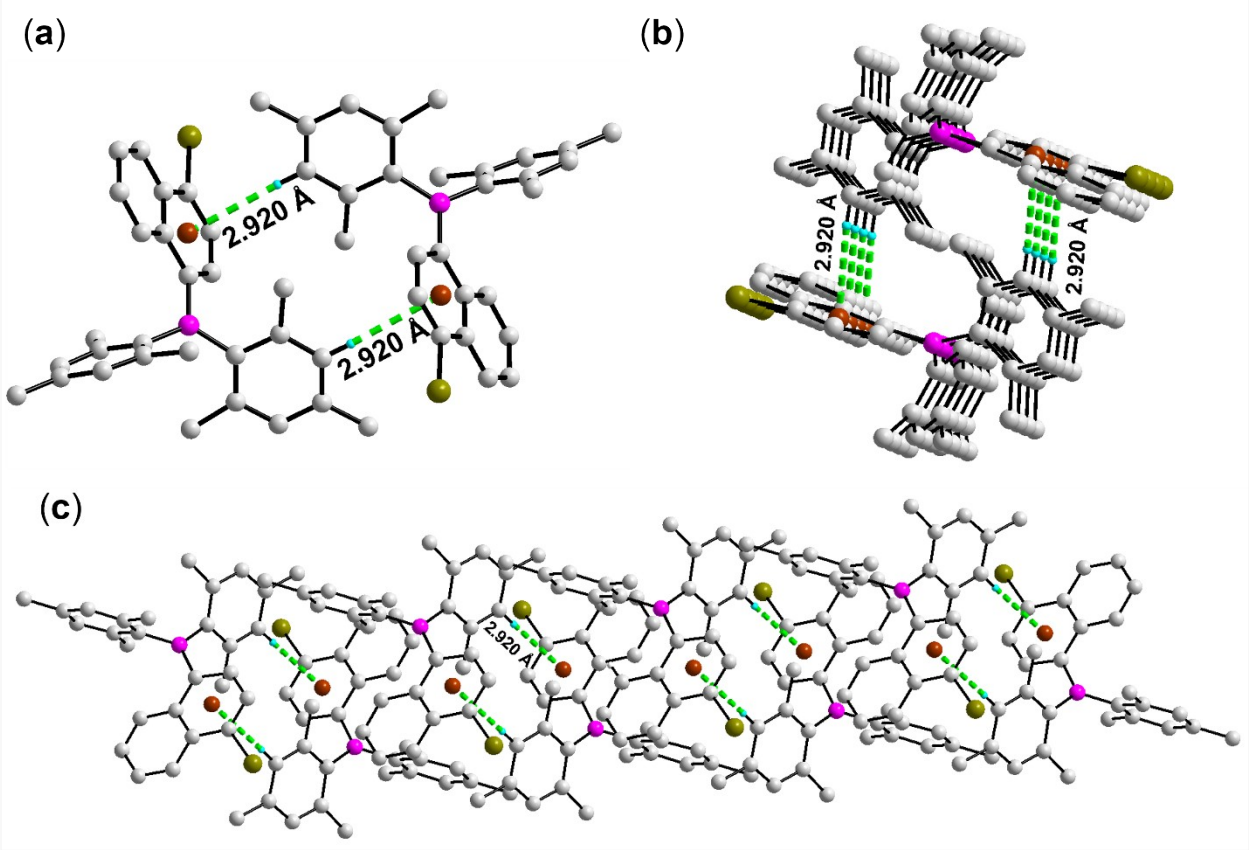

Figure S22. (a) Intermolecular interactions in **NB-Br** hold the molecule to form the crystal lattice. (b) The intramolecular interaction that forms the 3D chain. [Intermolecular C-H---πNap interaction between the mesityl hydrogen on one molecule with the π cloud of the naphthalene ring on the adjacent molecule (2.920 Å). (c) 1D chain. [Intermolecular C-H---πNap interaction between the mesityl hydrogen on one molecule with the π cloud of the naphthalene ring on the adjacent molecule (2.920 Å) Hydrogen atoms are omitted for clarity. Colour code: carbon (gray 50), and boron (pink).

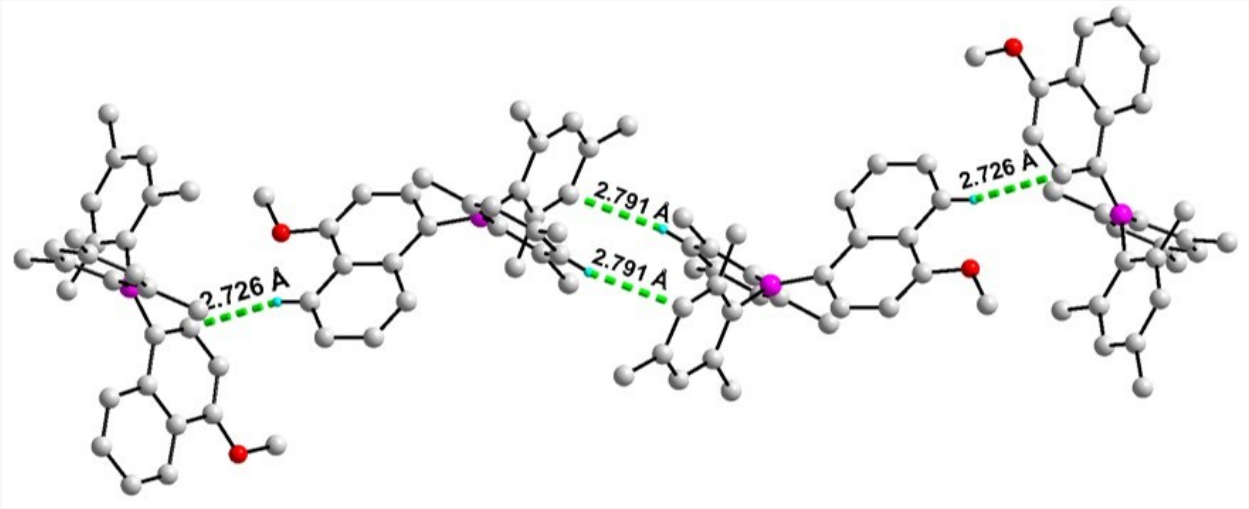

Figure S23. Crystal packing of **NB-OMe** highlighting intermolecular C–H···H–C interactions, including contacts between mesityl hydrogen atoms (2.791 Å) and between a naphthalene hydrogen and an adjacent carbon atom (2.726 Å).

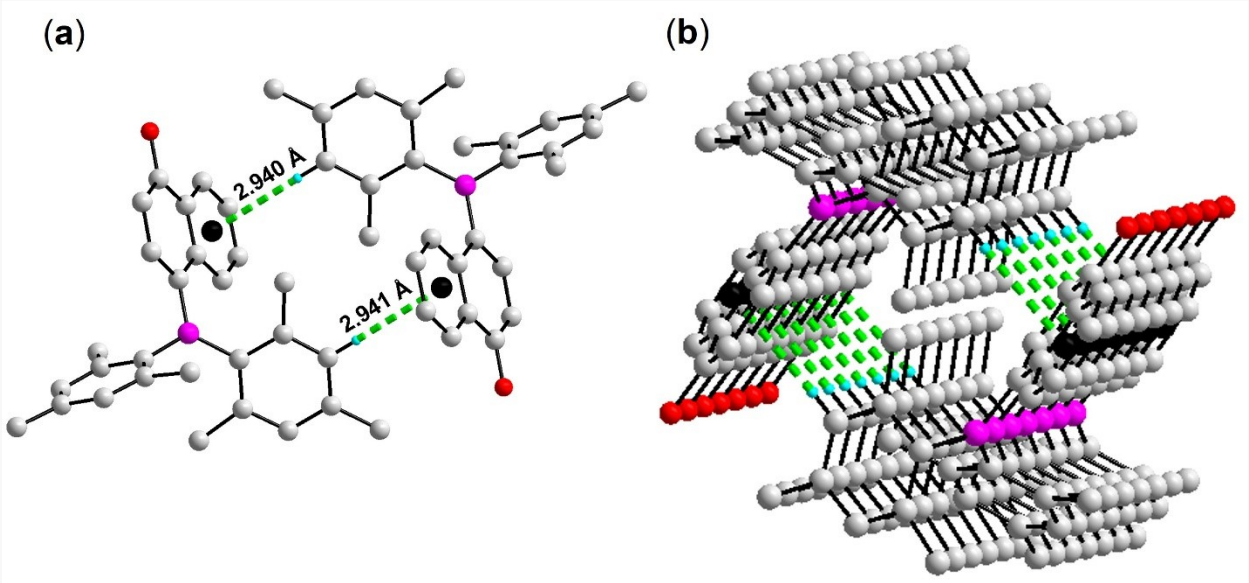

Figure S24. (a) Intermolecular interactions in **NB-OH** hold the molecule to form the crystal lattice. (b) The intramolecular interaction that forms the 3D chain. [Intermolecular C-H---π_{Nap} interaction between the mesityl hydrogen on one molecule with the π cloud of the naphthalene ring on the adjacent molecule (2.940 Å and 2.941Å). Hydrogen atoms are omitted for clarity. Colour code: carbon (gray 50), oxygen (red), and boron (pink).

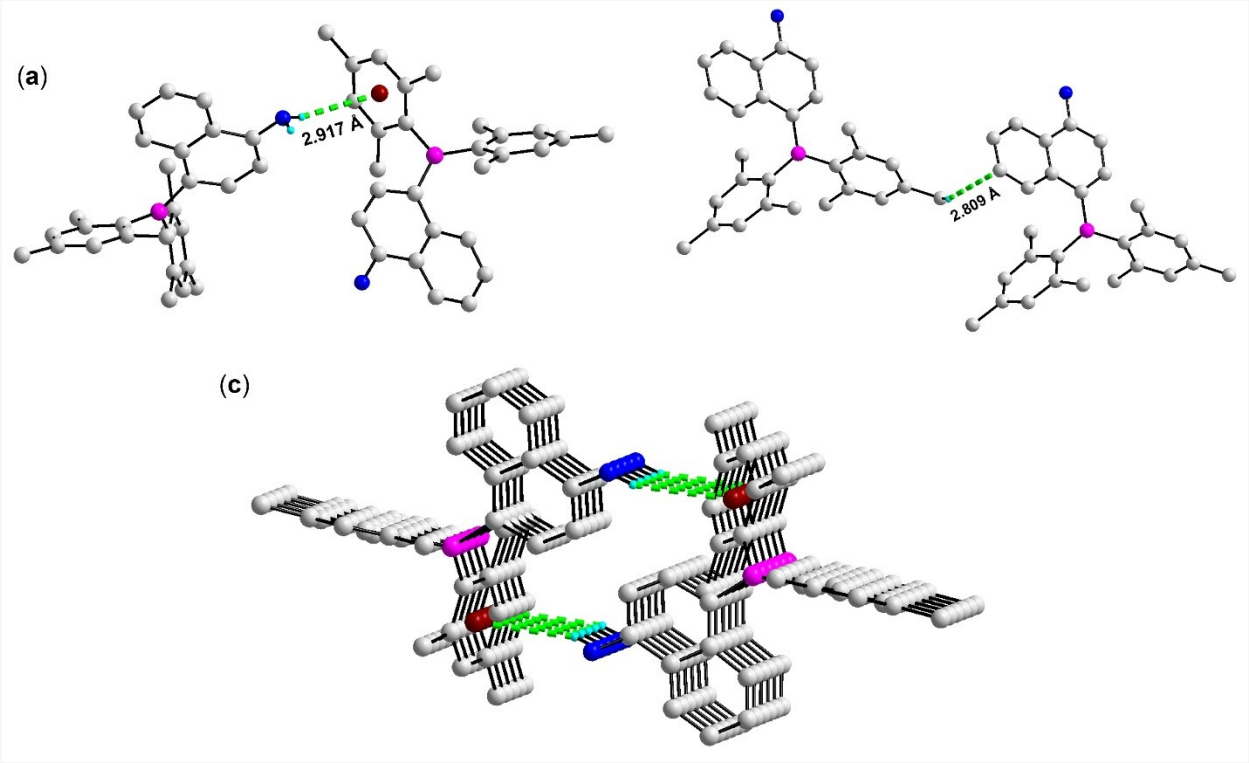

Figure S25. (a) Intermolecular interactions in NB-NH_2 hold the molecule to form the crystal lattice. (b) C–H···H–C interactions are observed, including contacts between mesityl hydrogen atoms (2.809 Å) and between a naphthalene carbon atom (c)The intramolecular interaction that forms the 3D chain. [Intermolecular N-H---π mesityl interaction between the NH_2 hydrogen on one molecule with the π cloud of the mesityl ring on the adjacent molecule (2.917 Å). Hydrogen atoms are omitted for clarity. Colour code: carbon (gray 50), boron (pink), and nitrogen (blue).

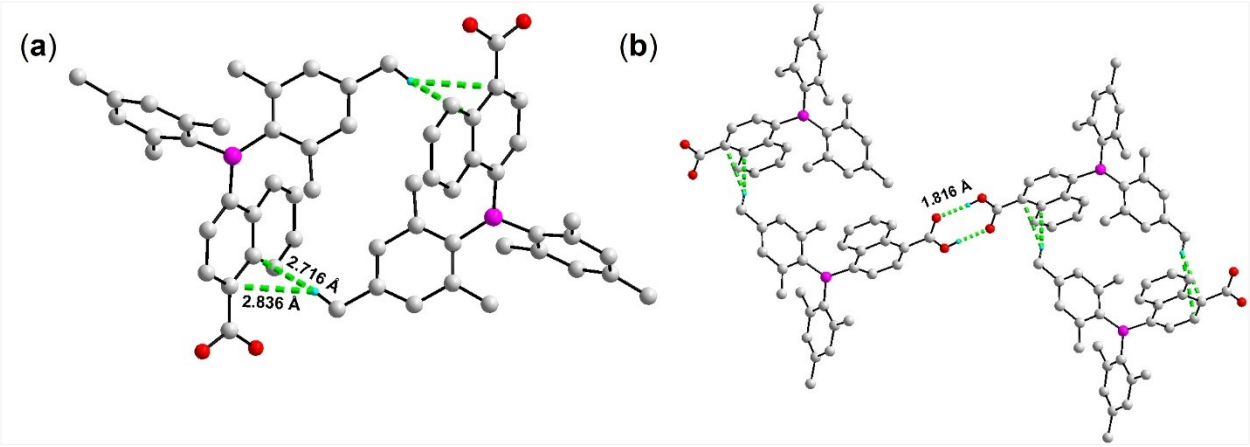

Figure S26. (a)Intramolecular interaction between the mesityl hydrogen and two carbon atoms of the naphthalene unit (C–H···H–C, 2.716 and 2.836 Å) observed in NB-COOH. (b) The intramolecular hydrogen bonding interaction O-H---O (1.816 Å) in NB-COOH. Hydrogen atoms are omitted for clarity. Colour code: carbon (gray 50), oxygen (red)and boron (pink).

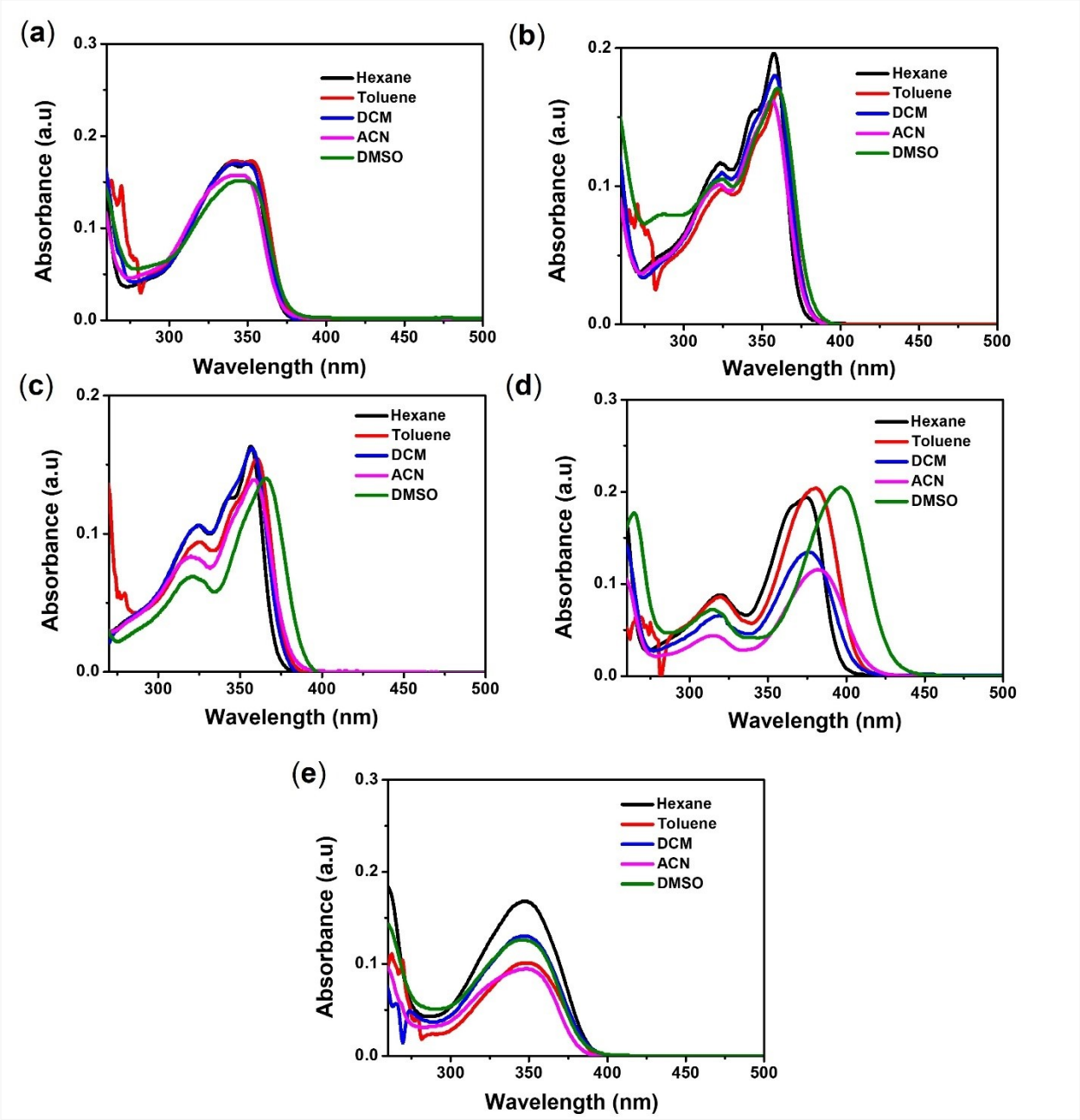

Figure S27. Solvent-dependent absorption spectra for (a) **NB-Br** (b) **NB-OMe**, (c) **NB-OH** (d) **NB-NH_2**, and (e) **NB-COOH** (conc 10^{-5} M)

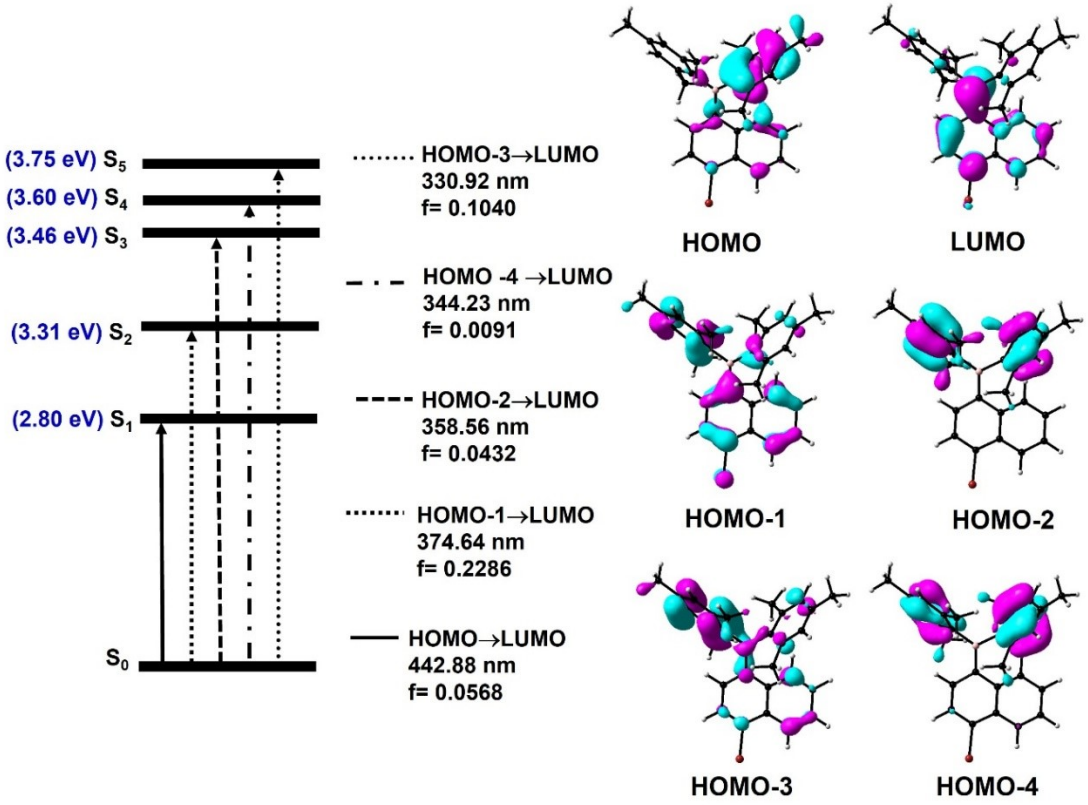

Figure S28. (a) Singlet energy level diagram, vertical transition involving the first five singlet states, and (b) molecular orbitals involved in the transitions calculated through TD-DFT calculation using PBE0/6-31G (d,p) level of theory for **NB-Br**.

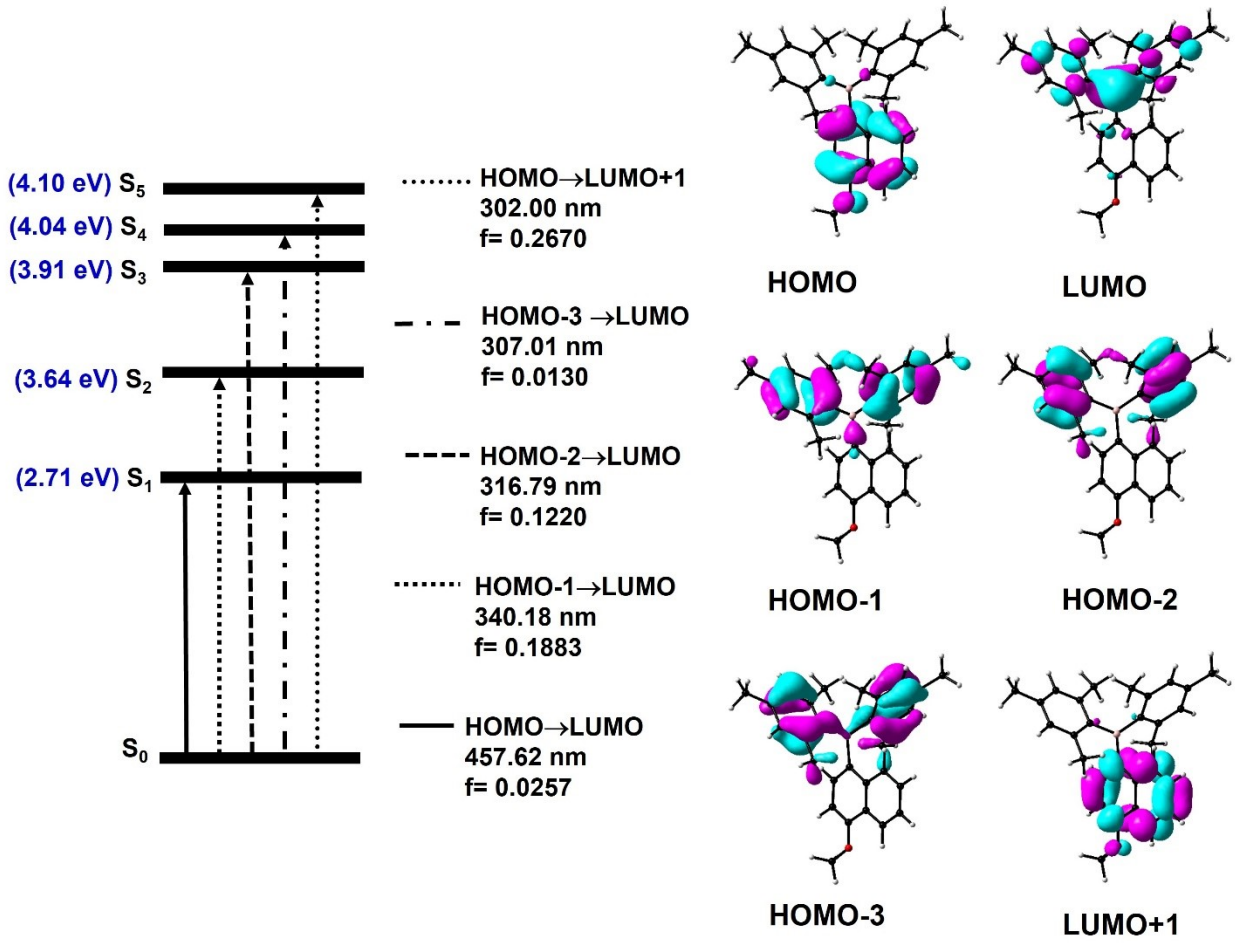

Figure S29. (a) Singlet energy level diagram, vertical transition involving first five singlet states, and (b) molecular orbitals involved in the transitions calculated through TD-DFT calculation using PBE0/6-31G (d,p)level of theory for **NB-OMe**.

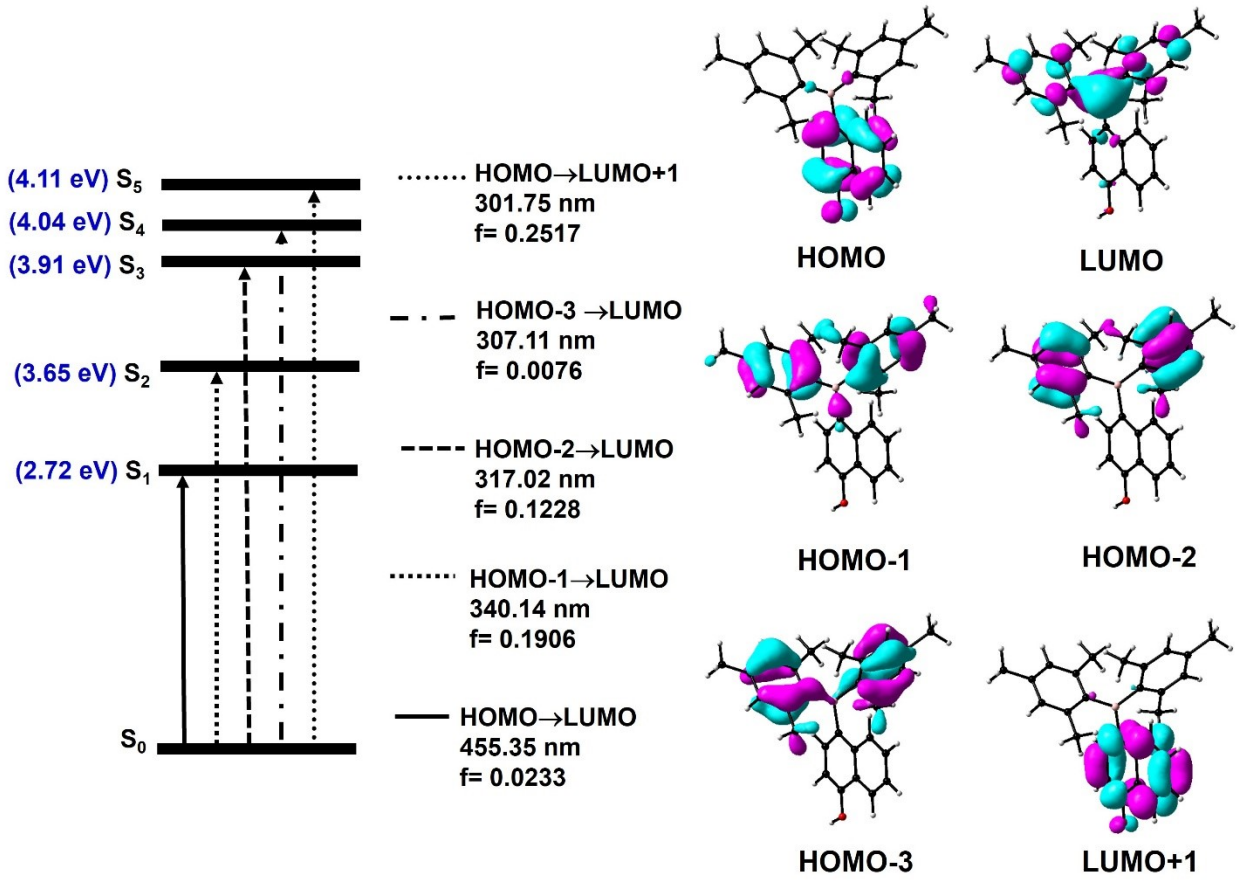

Figure S30. (a) Singlet energy level diagram, vertical transition involving first five singlet states, and (b) molecular orbitals involved in the transitions calculated through TD-DFT calculation using PBE0/6-31G (d,p) level of theory for **NB-OH**.

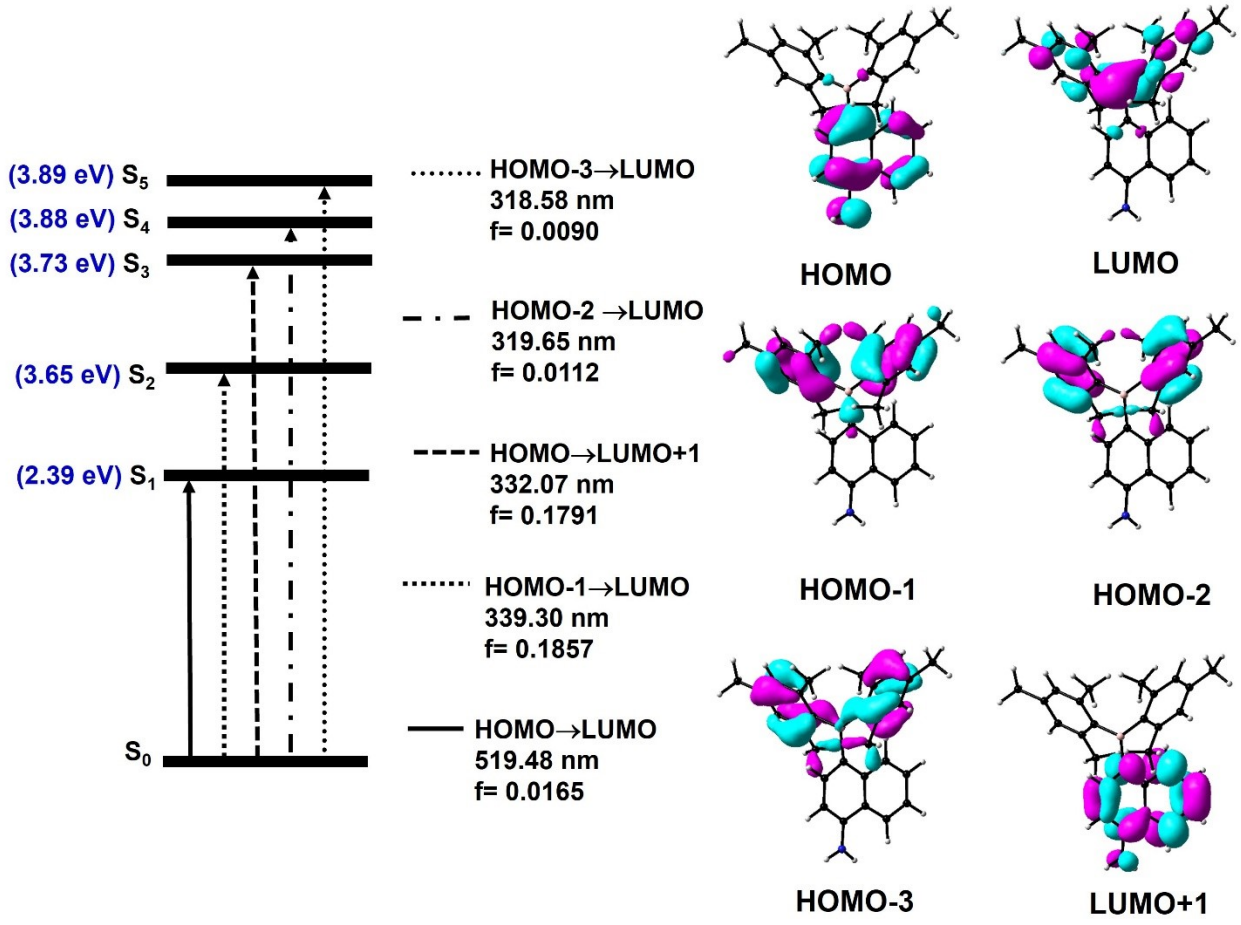

Figure S31. (a) Singlet energy level diagram, vertical transition involving first five singlet states, and (b) molecular orbitals involved in the transitions calculated through TD-DFT calculation using PBE0/6-31G (d,p) level of theory for **NB-NH$_2$**.

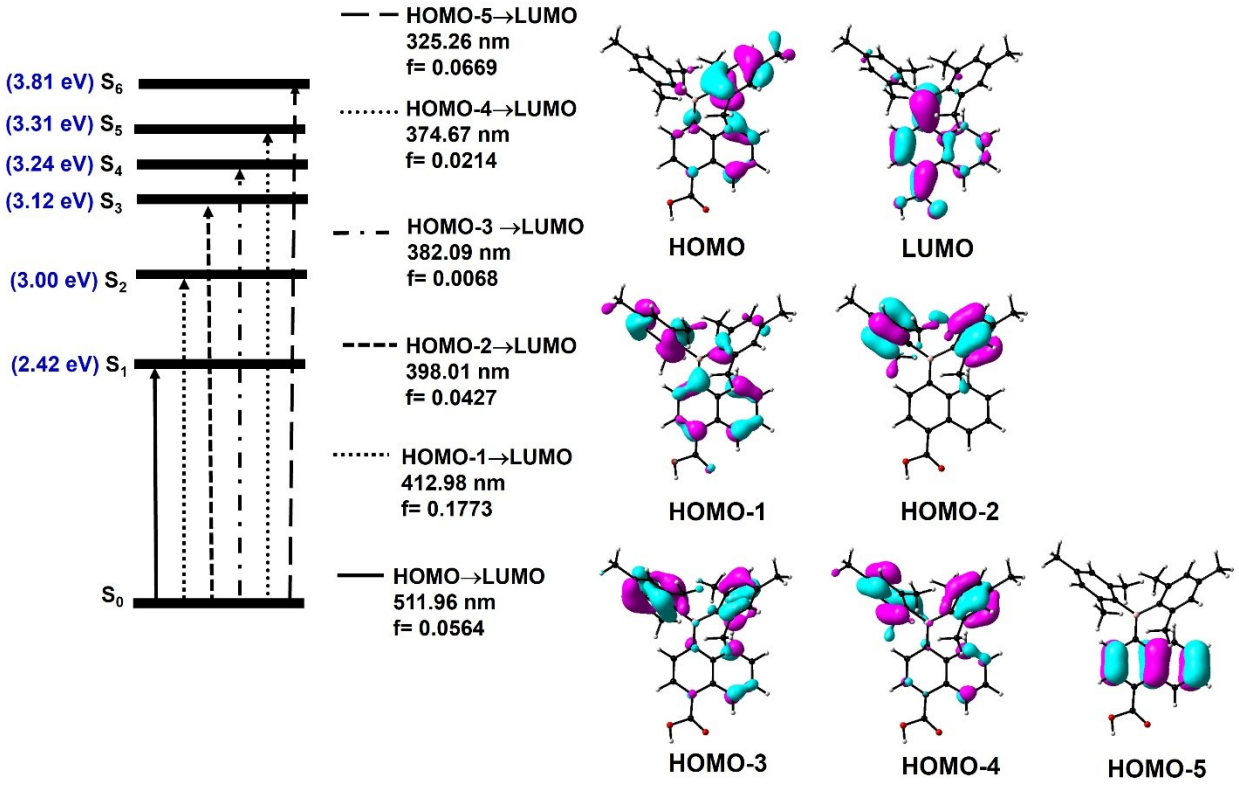

Figure S32. (a) Singlet energy level diagram, vertical transition involving first six singlet states, and (b) molecular orbitals involved in the transitions calculated through TD-DFT calculation using PBE0/6-31G (d,p) level of theory for **NB-COOH**

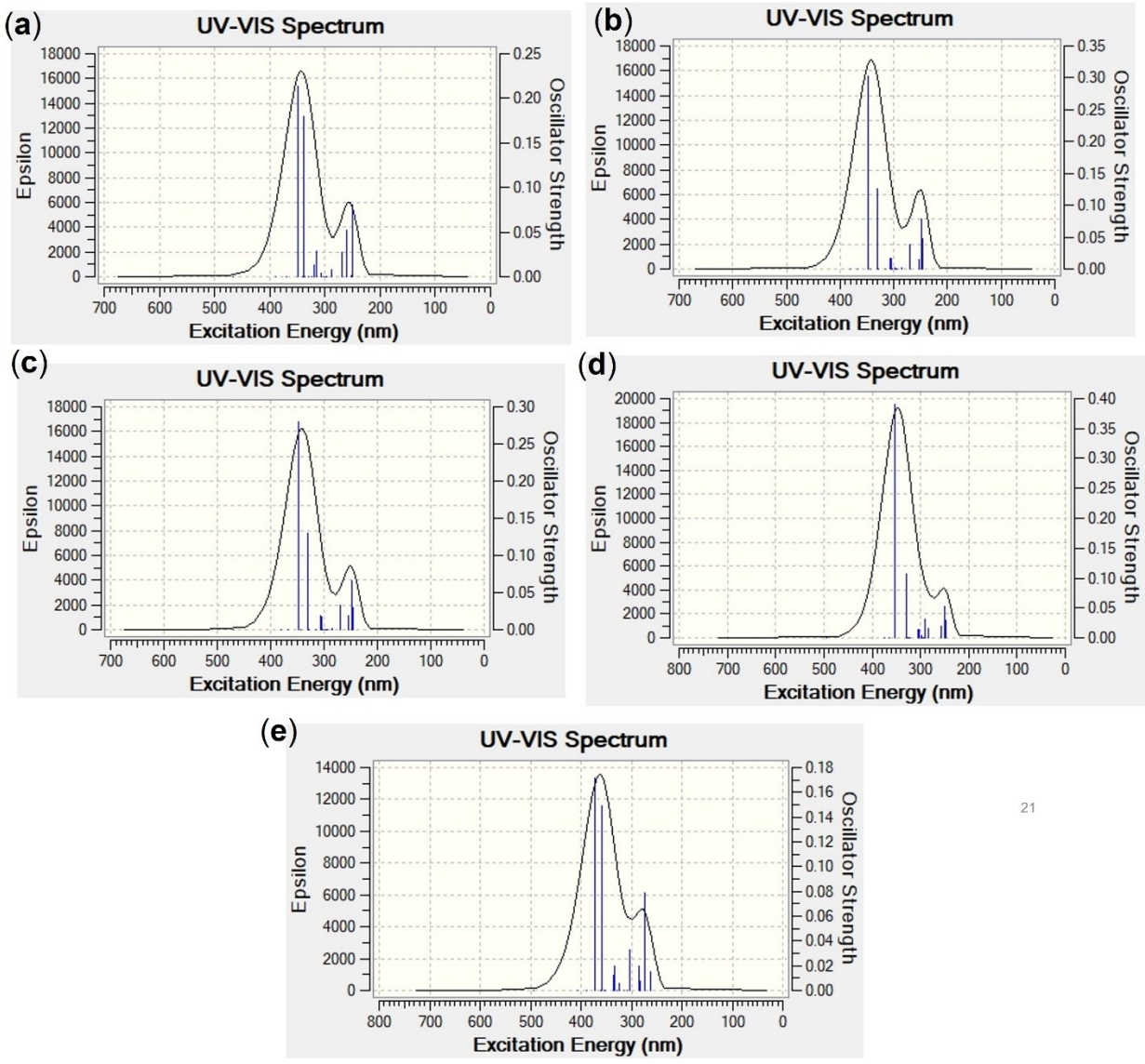

Figure S33. Theoretical UV-visible absorption spectra for (a) **NB-Br**, (b) **NB-OMe,** (c) **NB-OH,** (d) **NB-NH_2** and (e) **NB-COOH** through TD-DFT calculation using 6-31G (d, p)/B3LYP level of theory.

Table S2: Summary of computed singlet vertical transitions involved in **NB-Br** through TD-DFT calculation using PBE0/6-31G (d,p) level of theory.

Transitions	**E (eV)**	**λ (nm)**	***f***	**Dominant transitions (%)**
$S_0 \rightarrow S_1$	2.7995	442.88	0.0568	HOMO →LUMO (45.9)
$S_0 \rightarrow S_2$	3.3095	374.64	0.2286	HOMO-1 →LUMO (35.7)
$S_0 \rightarrow S_3$	3.4578	358.56	0.0432	HOMO-2 →LUMO (45.4)
$S_0 \rightarrow S_4$	3.6018	344.23	0.0091	HOMO-4 →LUMO (32.9)
$S_0 \rightarrow S_5$	3.7466	330.92	0.1040	HOMO-3 →LUMO (25.2)

Table S3: Summary of computed singlet vertical transitions involved in **NB-OCH_3** through TD-DFT calculation using PBE0/6-31G (d,p) level of theory.

Transitions	**E (eV)**	**λ (nm)**	***f***	**Dominant transitions (%)**
$S_0 \rightarrow S_1$	2.7093	457.62	0.0257	HOMO →LUMO (48.9)
$S_0 \rightarrow S_2$	3.6446	340.18	0.1883	HOMO-1 →LUMO(46.9)
$S_0 \rightarrow S_3$	3.9137	326.79	0.1220	HOMO-2 →LUMO (46.5)
$S_0 \rightarrow S_4$	4.0384	307.01	0.0130	HOMO-3 →LUMO (38.5)
$S_0 \rightarrow S_5$	4.1054	302.00	0.2670	HOMO →LUMO+1 (31.6)

Table S4: Summary of computed singlet vertical transitions involved in **NB-OH** through TD-DFT calculation using PBE0/6-31G (d,p) level of theory.

Transitions	**E (eV)**	**λ (nm)**	***f***	**Dominant transitions (%)**
$S_0 \rightarrow S_1$	2.7228	455.35	0.0233	HOMO →LUMO (48.9)
$S_0 \rightarrow S_2$	3.6451	340.14	0.1906	HOMO-1 →LUMO (46.8)
$S_0 \rightarrow S_3$	3.9109	317.02	0.1228	HOMO-2 →LUMO (46.5)
$S_0 \rightarrow S_4$	4.0371	307.11	0.0076	HOMO-3 →LUMO (39.4)
$S_0 \rightarrow S_5$	4.1089	301.75	0.2517	HOMO →LUMO+1 (32.6)

Table S5: Summary of computed singlet vertical transitions involved in **NB-NH$_2$** through TD-DFT calculation using PBE0/6-31G (d,p)level of theory.

Transitions	**E (eV)**	**λ (nm)**	***f***	**Dominant transitions (%)**
$S_0 \rightarrow S_1$	2.3867	519.48	0.0165	HOMO →LUMO (49.2)
$S_0 \rightarrow S_2$	3.6542	339.30	0.1857	HOMO-1 →LUMO (46.8)
$S_0 \rightarrow S_3$	3.7337	332.07	0.1791	HOMO→LUMO+1 (44.0)
$S_0 \rightarrow S_4$	3.8787	319.65	0.0112	HOMO-2→LUMO (46.5)
$S_0 \rightarrow S_5$	3.8918	318.58	0.0090	HOMO-3 →LUMO (39.2)

Table S6: Summary of computed singlet vertical transitions involved in **NB-COOH** through TD-DFT calculation using PBE0/6-31G (d,p)level of theory.

Transitions	**E (eV)**	**λ (nm)**	***f***	**Dominant transitions (%)**
$S_0 \rightarrow S_1$	2.4217	511.96	0.0564	HOMO →LUMO (47.3)
$S_0 \rightarrow S_2$	3.0022	412.98	0.1773	HOMO-1 →LUMO (39.5)
$S_0 \rightarrow S_3$	3.1151	398.01	0.0427	HOMO-2 →LUMO (44.8)
$S_0 \rightarrow S_4$	3.2449	382.09	0.0068	HOMO-4 →LUMO (19.9) HOMO-3 →LUMO (29.2)
$S_0 \rightarrow S_5$	3.3092	374.67	0.0214	HOMO-4 →LUMO (26.8) HOMO-3 →LUMO (17.1)
$S_0 \rightarrow S_6$	3.8118	325.26	0.0669	HOMO-5 →LUMO (41.7)

Table S7: Lifetime decay kinetics for **NB-Br, NB-OMe, NB-OH, NB-NH$_2$, and NB-COOH** in toluene (Con 10^{-5}M).

compound	λ_{ex} (nm)	λ_{em} (nm)	τ_1 [ns] (A1 [%])	τ_2 [ns] (A2 [%])	τ_{av} [ns]	PLQY	K_r ($x10^7$ S^{-1})	K_{nr} ($x10^8$ S^{-1})
NB-Br	330	400	2.98 (57.82)	7.02 (42.18)	4.67	2.75	0.58	2.08
NB-OMe	330	400	1.86 (87.89)	8.32 (12.11)	2.63	23.08	8.77	2.92
NB-OH	330	398	1.67 (96.07)	11.26 (3.93)	2.07	26.02	12.5	3.57
NB-NH$_2$	375	445	4.81 (100)	-	4.81	32.64	6.8	1.40
NB-COOH	347	445	4.13 (97.63)	22.39 (2.37)	4.49	36.23	8.1	1.42

λ_{ex}, λ_{em} = excitation and emission wavelength, τ = fluorescence lifetime, A= amplitude of intensity, τ_{av} =average fluorescence lifetime, Φ_{PL} = total absolute photoluminescence quantum yield, , k_r = radiative rate constant of fluorescence = Φ_{PL} / τ_{FL}, k_{nr} = non-radiative rate constant from singlet state (1 - Φ_{PL}) / τ_{av}.

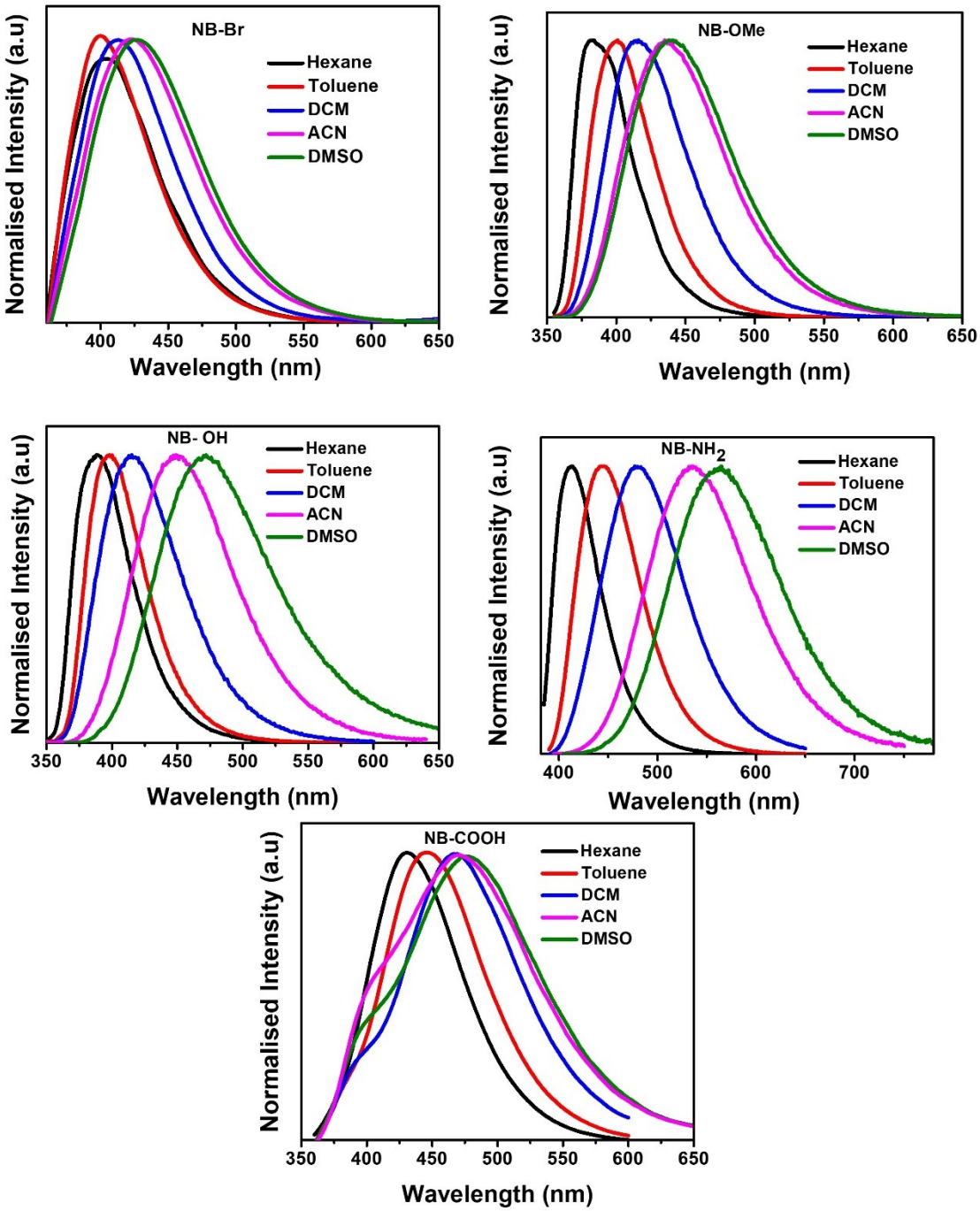

Figure S34. Solvent-dependent emission spectra for **NB-Br**, **NB-OMe**, **NB-OH**, **NB-NH_2**, and **NB-COOH** (conc 10^{-5} M)

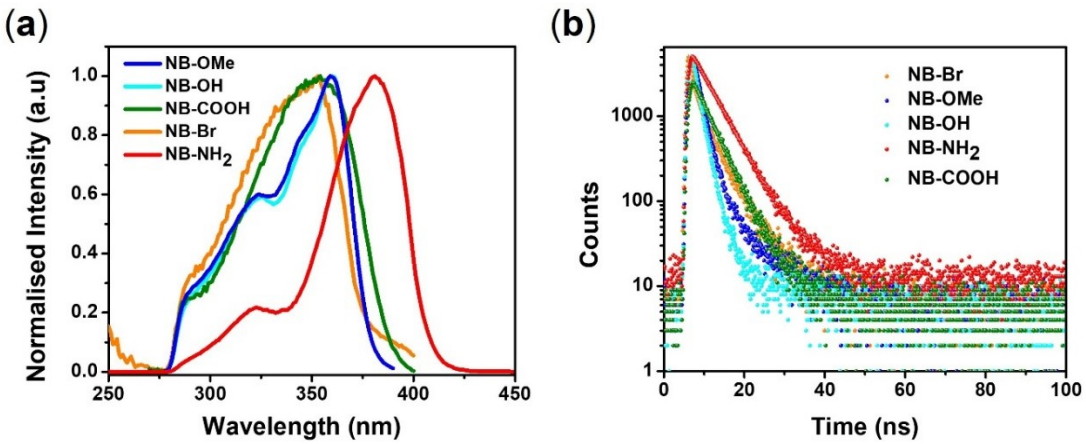

Figure S35. (a)Excitation spectra in toluene NB-Br, NB-OMe, NB-OH, NB-NH_2, NB-COOH (conc 10^{-5} M) (b) fluorescence decay curve for **NB-Br** [λ_{ex} = 330 nm, λ_{em} = 400 nm], **NB-Ome** [λ_{ex} = 330 nm, λ_{em} = 400 nm]**, NB-OH** [λ_{ex} = 330 nm, λ_{em} = 398 nm]**, NB-NH_2** [λ_{ex} = 375 nm, λ_{em} = 445 nm]**,** and **NB-COOH** [λ_{ex} = 330 nm, λ_{em} = 445 nm] in toluene (Conc = 10^{-5}M)

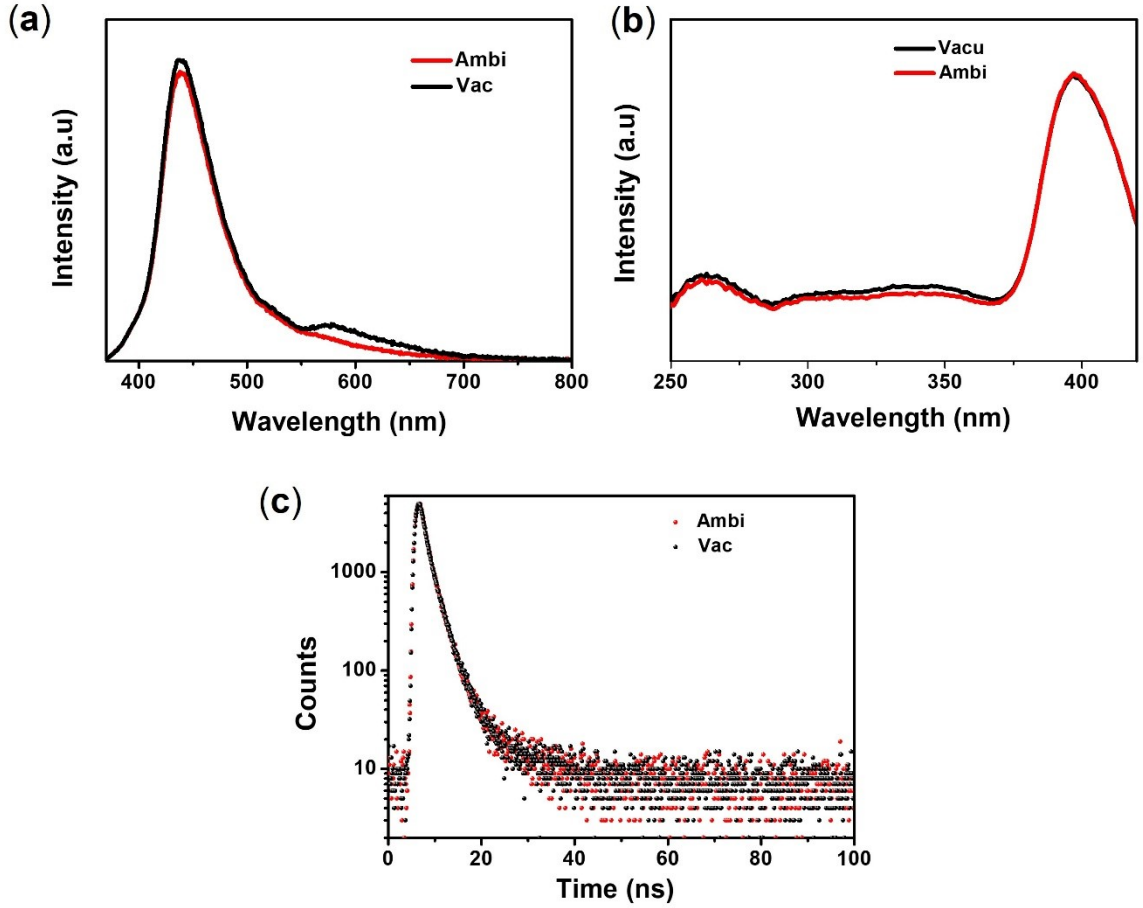

Figure S36. (a) Steady state FL spectra at λ_{ex} = 350 nm (b), Excitation spectra at λ_{em} = 430 nm and (c) Fluorescence lifetime decay [λ_{ex} = 350 nm, λ_{em} = 430 nm] for **NB-Br** under vacuum and ambient conditions at 298 K.

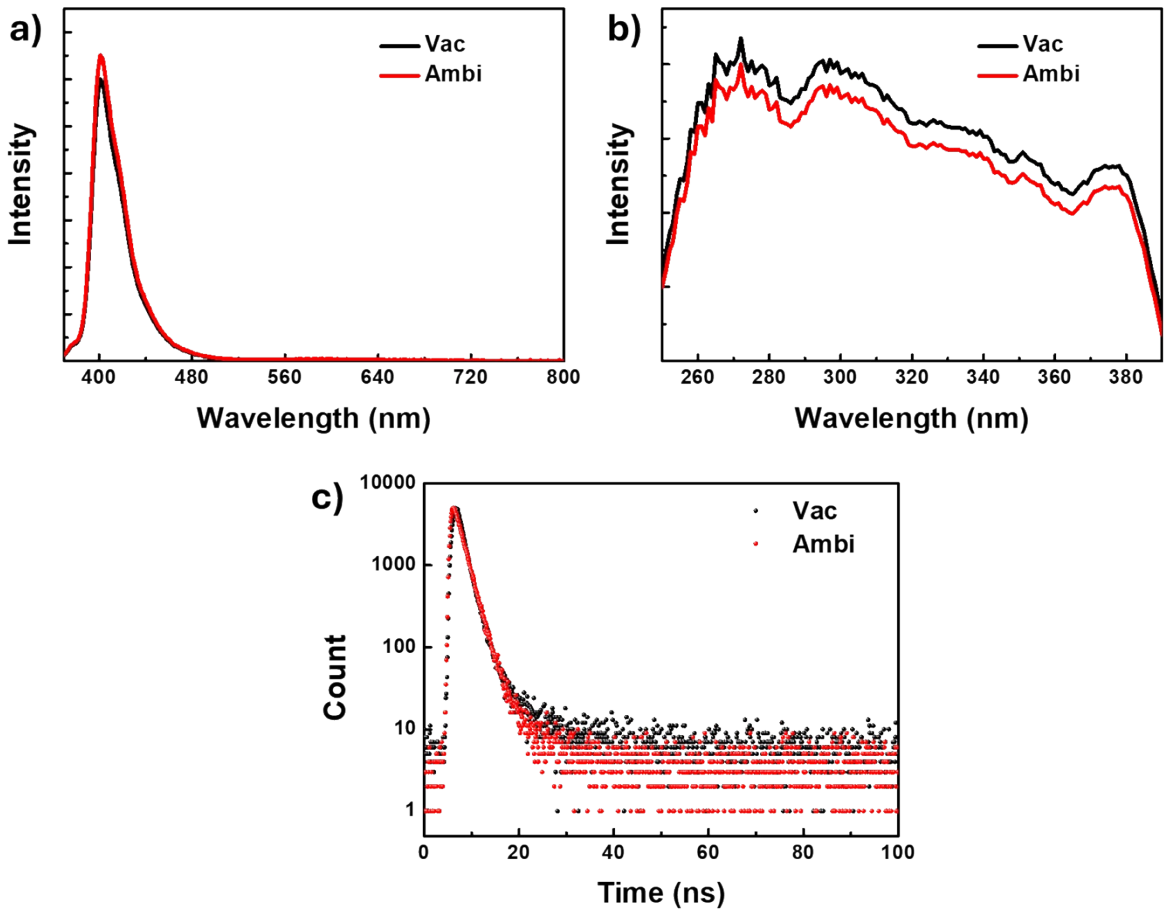

Figure S37. (a) Steady state FL spectra at λ_{ex} = 350 nm (b) Excitation spectra at λ_{em} = 401 nm and (c) Fluorescence lifetime decay [λ_{ex} = 350 nm, λ_{em} = 401 nm] for **NB-OMe** under vacuum and ambient conditions at 298 K.

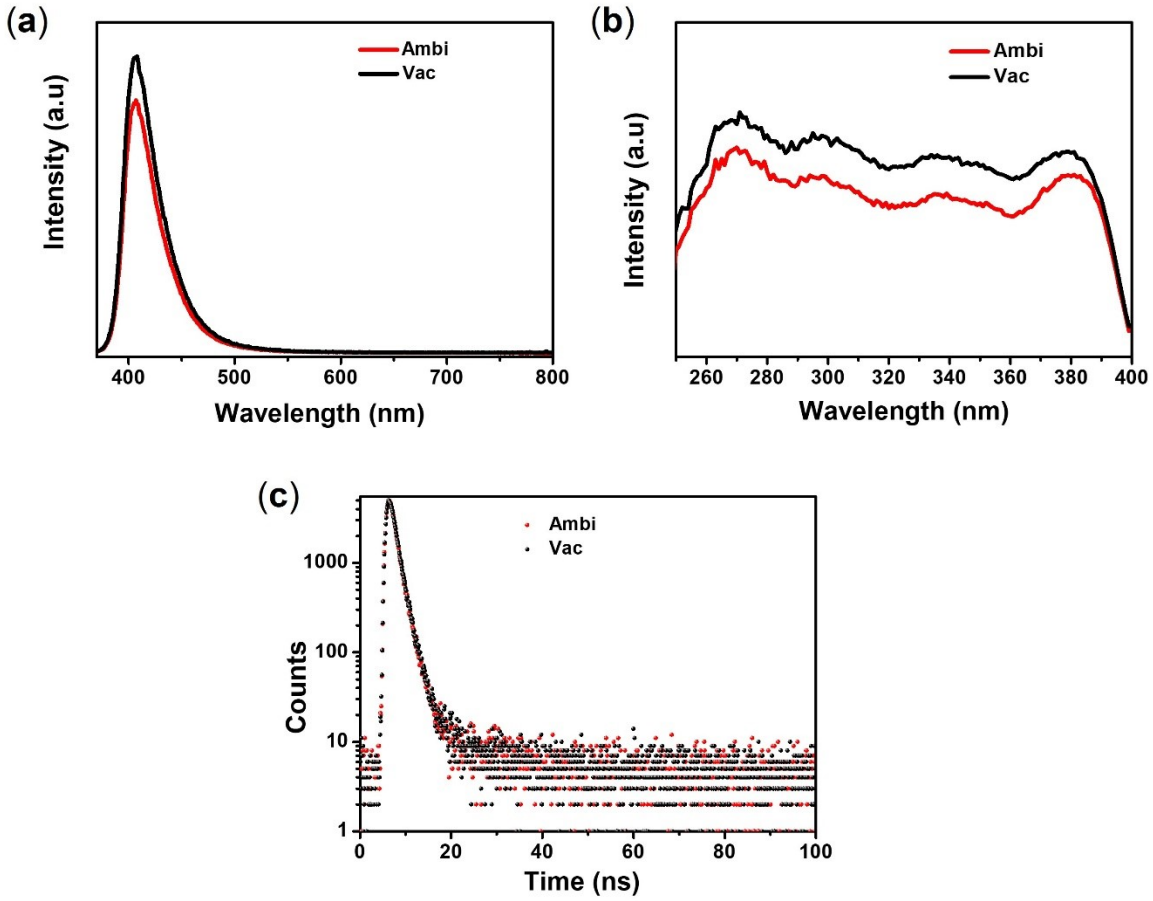

Figure S38. (a) Steady state FL spectra at λ_{ex} = 350 nm (b) Excitation spectra at λ_{em} = 405 nm and (c) Fluorescence lifetime decay [λ_{ex} = 350 nm, λ_{em} = 401 nm] for **NB-OH** under vacuum and ambient conditions at 298 K.

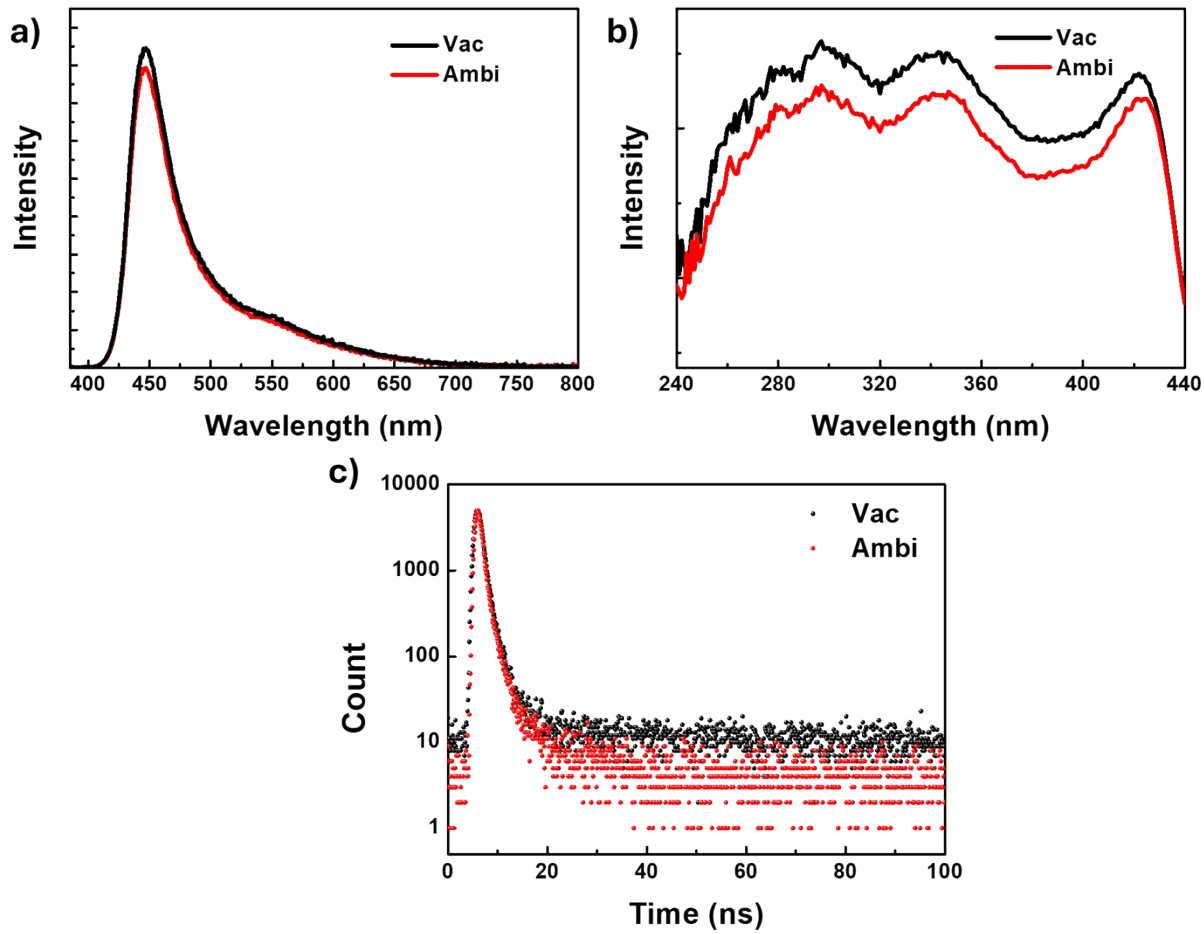

Figure S39. (a) Steady state FL spectra at λ_{ex} = 375 nm (b) Excitation spectra at λ_{em} = 447 nm and (c) Fluorescence lifetime decay [λ_{ex} = 375 nm, λ_{em} = 447 nm] for **NB-NH$_2$** under vacuum and ambient condition at 298 K.

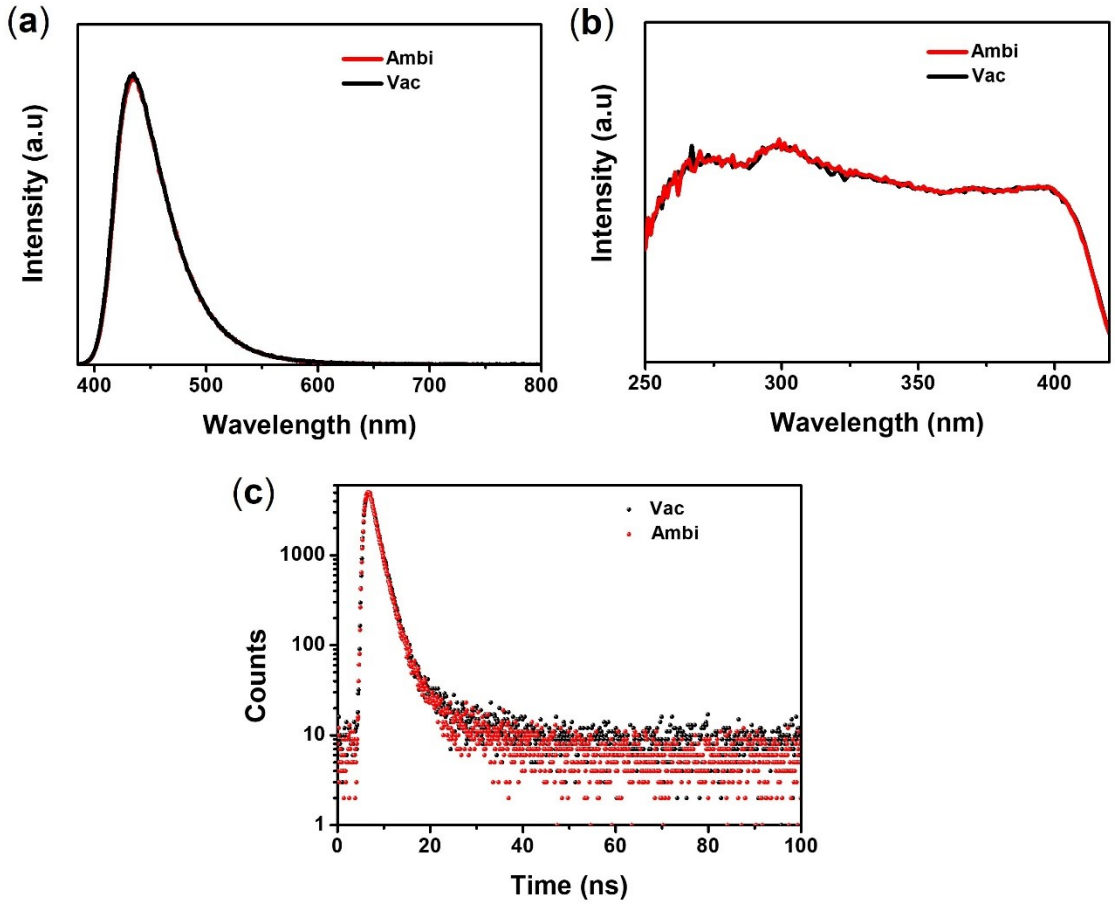

Figure S40. (a) Steady state FL spectra at λ_{ex} = 375 nm (b) Excitation spectra at λ_{em} = 434 nm and (c) Fluorescence lifetime decay [λ_{ex} = 375 nm, λ_{em} = 434 nm] for **NB-COOH** under vacuum and ambient condition at 298 K.

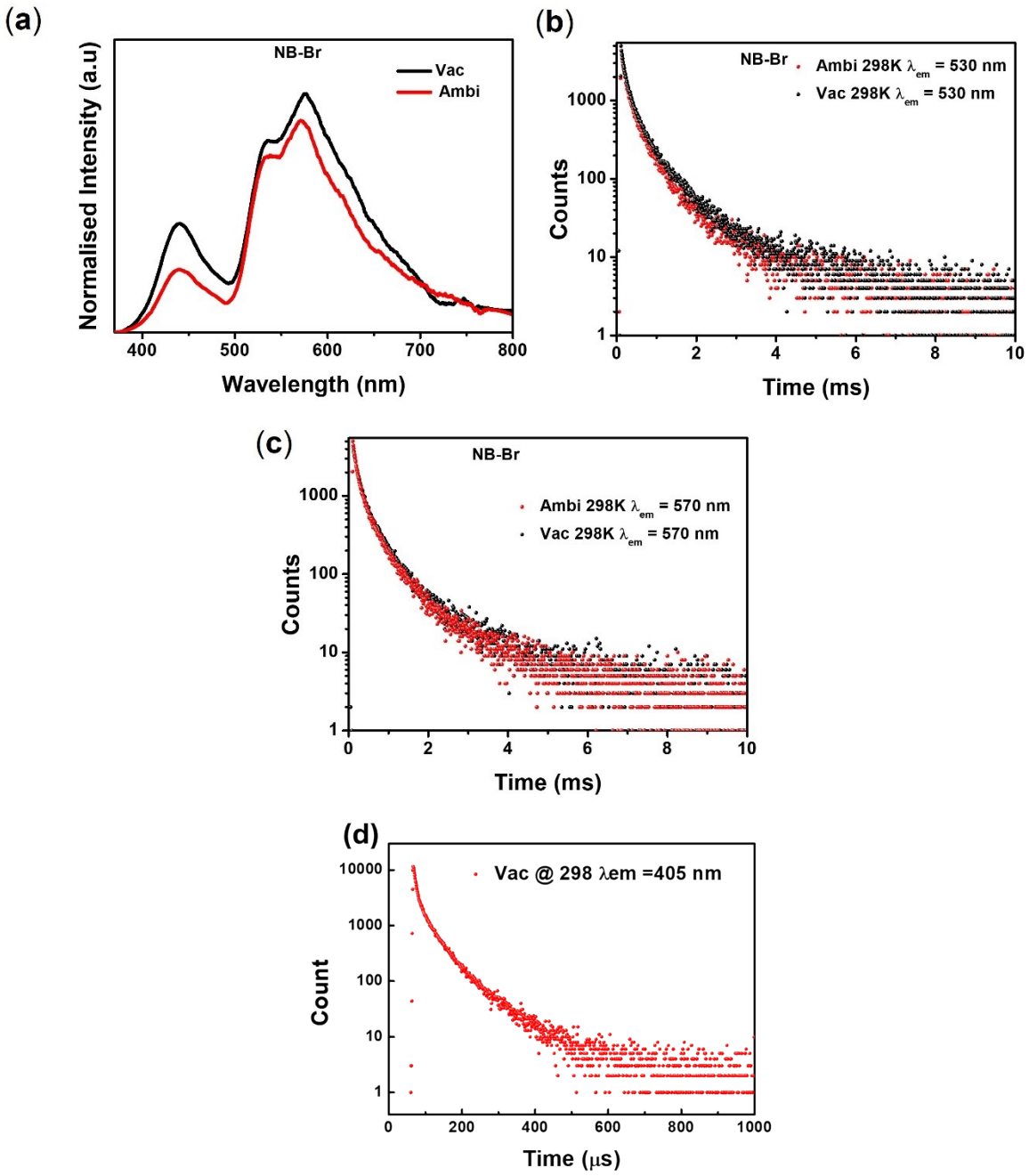

Figure S41. Time-gated PL spectra for (a) **NB-Br** and (b) and (c) Phosphorescence lifetime decay [λ_{ex} = 375 nm and λ_{em} = 530 nm, and 570 nm] and (d) delayed fluorescence decay [λ_{ex} = 375 nm and λ_{ex} = 430 nm] for **NB-Br** under vacuum [absence of oxygen] and ambient atmosphere [presence of oxygen] at 298 K in the solid state

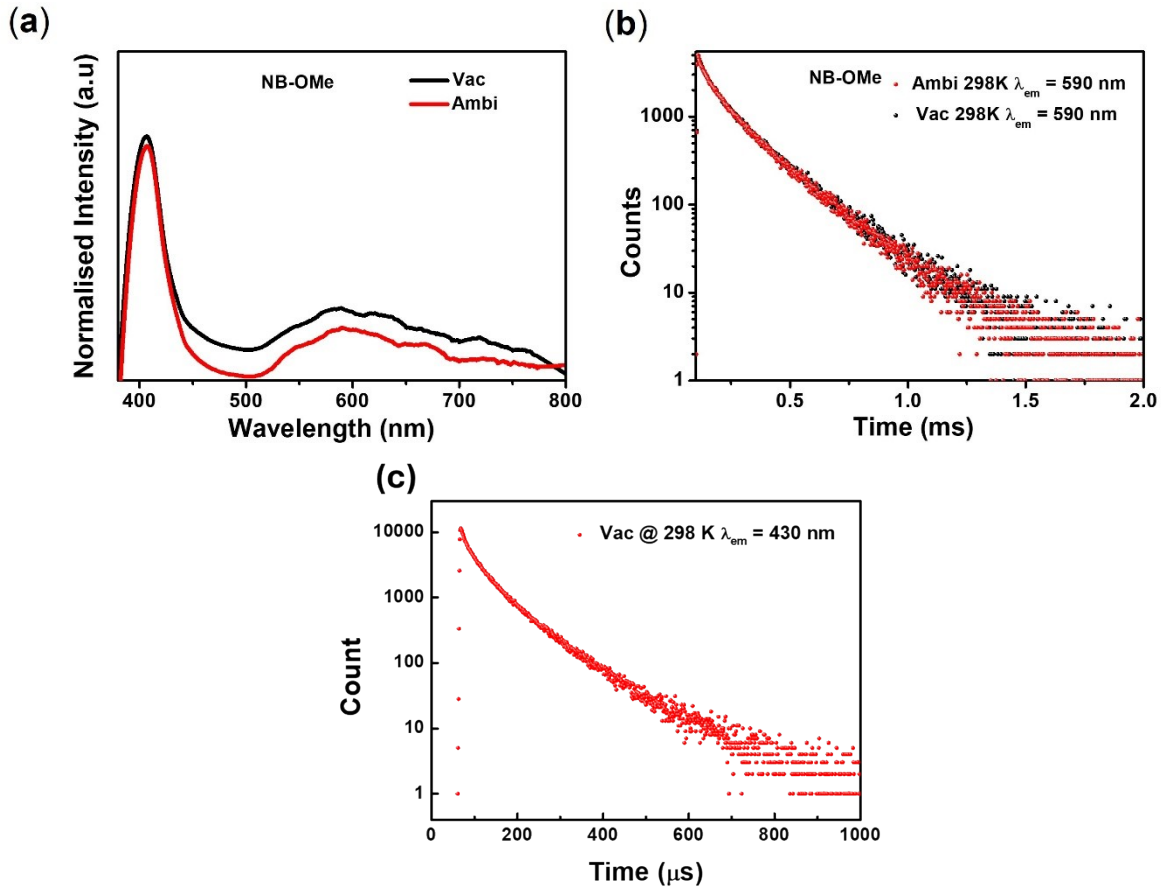

Figure S42. Time-gated PL spectra for (a) **NB-OMe,** (b) Phosphorescence lifetime decay [λ_{ex} = 375 nm and λ_{ex} = 590 nm] and (c) delayed fluorescence decay [λ_{ex} = 375 nm and λ_{ex} = 430 nm] for **NB-OMe** under vacuum [absence of oxygen] and ambient atmosphere [presence of oxygen] at 298 K in the solid state.

Table S8: Fluorescence lifetime for **NB-OH**, **NB-NH$_2$**, and **NB-COOH** under different atmospheric conditions and different temperatures, along with total PLQY under ambient conditions at 298 K.

Compound	**λ_{ex} (nm)**	**λ_{em} (nm)**	**τ_{av} [FL]**	**Φ_{PL}**	**k_r (x10^{7}S^{-1})**	**k_{nr} (x10^{8}S^{-1})**
NB-OH	350	405	1.72	3.60	2.09	5.60
NB-NH$_2$	375	447	2.51	6.50	2.59	3.72
NB-COOH	375	434	2.40	7.88	3.28	3.84

λ_{ex}, λ_{em} = excitation and emission wavelength, τ = fluorescence lifetime, A= amplitude of intensity, τ_{av} =average fluorescence lifetime, Φ_{PL} = total absolute photoluminescence quantum yield, k_r = radiative rate constant of fluorescence = Φ_{PL} / τ_{FL}, k_{nr} = non-radiative rate constant from singlet state (1 - Φ_{PL}) / τ_{av}.

Table S9: Delayed fluorescence (DF) and phosphorescence (PH) lifetime for **NB-Br** and **NB-OMe**, in solid state at 298 K.

	vaccum				Ambinet			
	λ_{ex}	λ_{em}	τ_1 (A_1 %)	τ_2 (A_2 %)	λ_{ex}	λ_{em}	τ_1 (A_1 %)	τ_2 (A_2 %)
NB-Br								
DF	350	430	103.59 µs (51.87)	368.40 µs (48.13)	350	430	-	-
Ph	350	530	212.83µs (52.96)	935.77µs (47.04)	375	530	199.54µs (55.11)	891.28µs (44.89)
		572	243.05µs (57.09)	1008.95µs (42.91)		572	227.41µs (56.22)	938.43µs (43.78)
NB-OMe								
DF	350	403	32.61 µs (42.22)	96.55 µs (57.78)	350	403	-	-
Ph	350	590	63.97µs (28.63)	199.91µs (71.37)	375	590	57.31µs (26.11)	199.97µs (73.89)

Table S10: Fluorescence decay kinetics for **NB-Br, NB-OMe** in the solid state

	Fluorescence lifetime (ns)								PLQY [%]
	298 K (Vacuum)				298 K (Ambient)				
	λ_{ex}	λ_{em}	τ_1 (A_1 %)	τ_2 (A_2 %)	λ_{ex}	λ_{em}	τ_1 (A_1 %)	τ_2 (A_2 %)	
NB-Br									
Solid	350	430	1.82 (80.37)	6.19 (19.63)	350	430	1.61 (68.26)	4.38 (31.74)	2.09
NB-OMe									
Solid	350	403	1.91 (96.37)	7.54 (3.63)	350	403	1.57 (89.61)	6.48 (10.39)	17.04
NB-OH									
Solid	350	405	1.43 (94.24)	6.32 (5.76)	350	405	1.40 (94.98)	7.35 (5.02)	3.60
NB-NH_2									
Solid	375	450	1.24 (77.95)	7.07 (22.05)	375	450	0.86 (76.75)	2.79 (23.25)	6.50
NB-COOH									
Solid	375	430	1.79 (91.79)	9.48 (8.21)	375	430	1.70 (90.78)	7.40 (9.22)	7.88

Table S11: Fluorescence and phosphorescence decay kinetics for **NB-Br, NB-OMe** in the solid state.

Compound	λ_{ex} (nm)	λ_{em}^{FL} (nm)	λ_{em}^{PH} (nm)	τ_{av}^{FL} (ns)	τ_{av}^{PH} (μs)	Φ_{Total} %	Φ_{PH} %	k_r^{FL} (x$10^7 S^{-1}$)	k_{nr}^{FL} (S^{-1})	k_r^{PH} (S^{-1})	k_{nr}^{T} (x10^2 S^{-1})
NB-Br	350	430	530	2.69	552.6	2.10	0.54	0.59	3.64	9.2	1.8
NB-OMe	375	401	550	2.11	160.5	17.04	0.72	7.73	3.93	44.86	6.1

λ_{ex} = excitation wavelength, λ_{em}^{FL} λ_{em}^{PH}= fluorescence and phosphorescence emission wavelength, τ_{av}^{FL}, τ_{av}^{PH} = average fluorescence and phosphorescence lifetime, Φ_{PL} = total absolute photoluminescence quantum yield. Φ_{FL}, Φ_{PH} = fluorescence and phosphorescence quantum yield, k_r^{FL} = radiative rate constant from singlet, k_{nr}^{FL} = non-radiative rate constant from singlet state. k_r^{PH} = radiative rate constant of phosphorescence, k_{nr}^{PH} = non-radiative rate constant from triplet state. $k_r^{FL} = \Phi_{FL} / \tau_{FL}$, $k_{nr}^{FL} = (1 - \Phi_{FL}-\Phi_{PH}) / \tau_{av}^{FL}$,$k_r^{PH} = \Phi_{PH} / \tau_{PH}$, $k_{nr}^{PH} = (1 - \Phi_{PH}) / \tau_{av}^{PH}$.

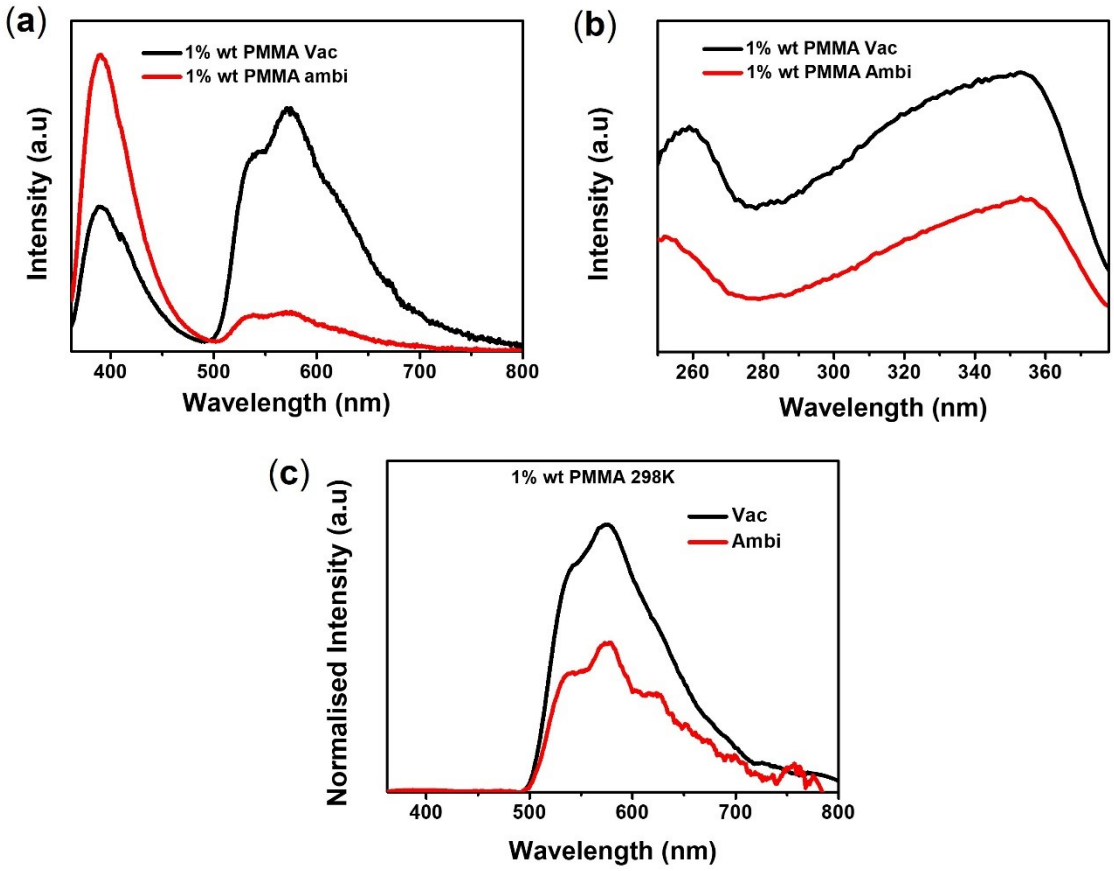

Figure S43. (a) PL spectra at λ_{ex} = 350 nm (b) Excitation spectra at λ_{em} = 390nm (c) Time gated [50μs delay] PL spectra at λ_{ex} = 350 nm for **NB-Br** under vacuum (absence of oxygen) and ambient conditions (presence of oxygen).

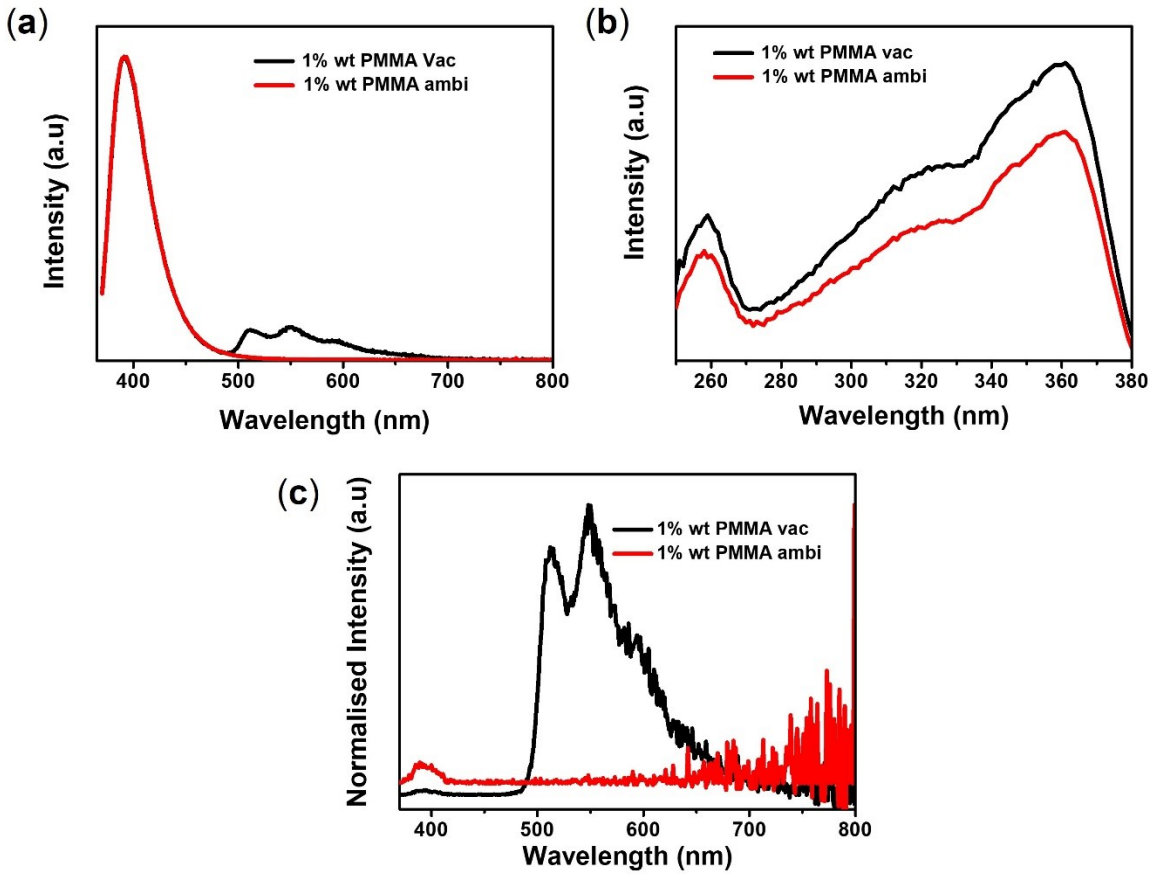

Figure S44. (a) PL spectra at λ_{ex} = 350 nm, (b) Excitation spectra at λ_{em} = 390nm, (c) Time-gated [50μs delay] PL spectra at λ_{ex} = 350 nm for **NB-OMe** under vacuum (absence of oxygen) and ambient conditions (presence of oxygen).

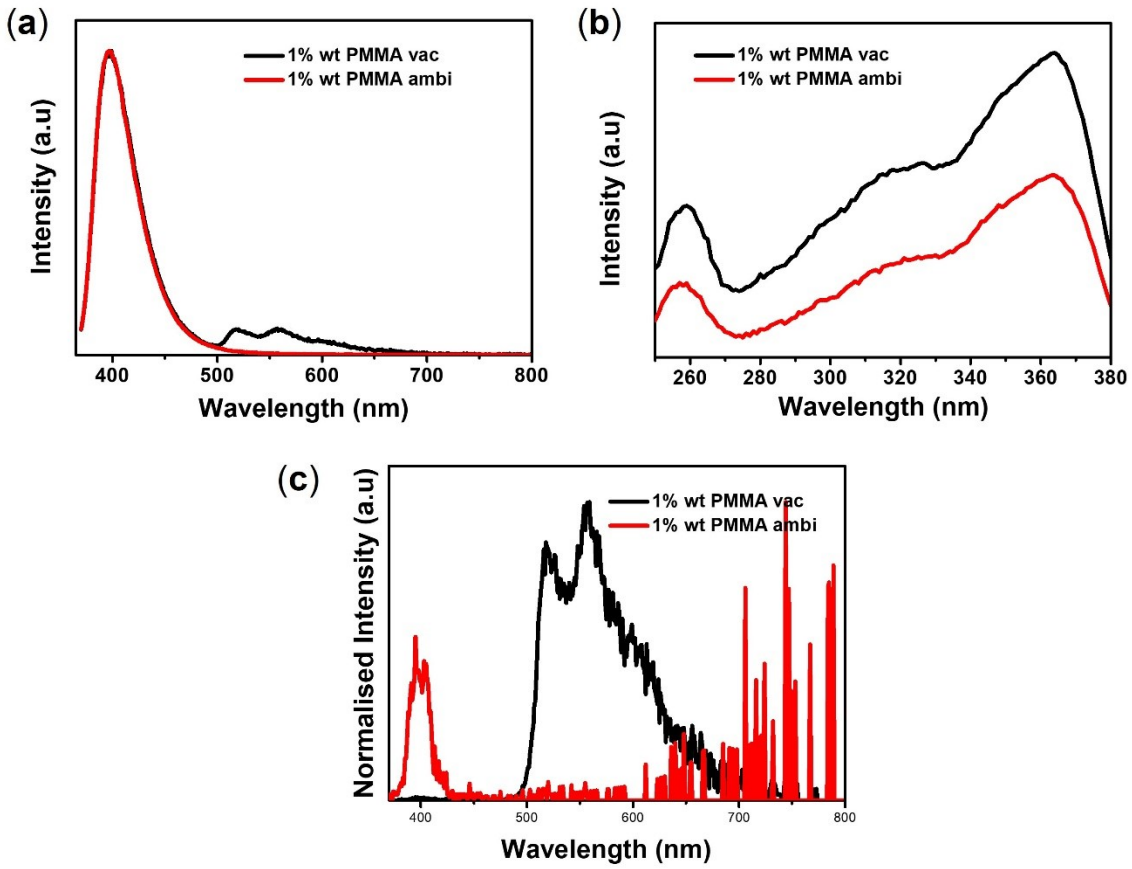

Figure S45. (a) PL spectra at λ_{ex} = 350 nm (b) Excitation spectra at λ_{em} = 390nm (c) Time-gated [50μs delay] PL spectra at λ_{ex} = 350 nm for **NB-OH** under vacuum (absence of oxygen) and ambient conditions (presence of oxygen).

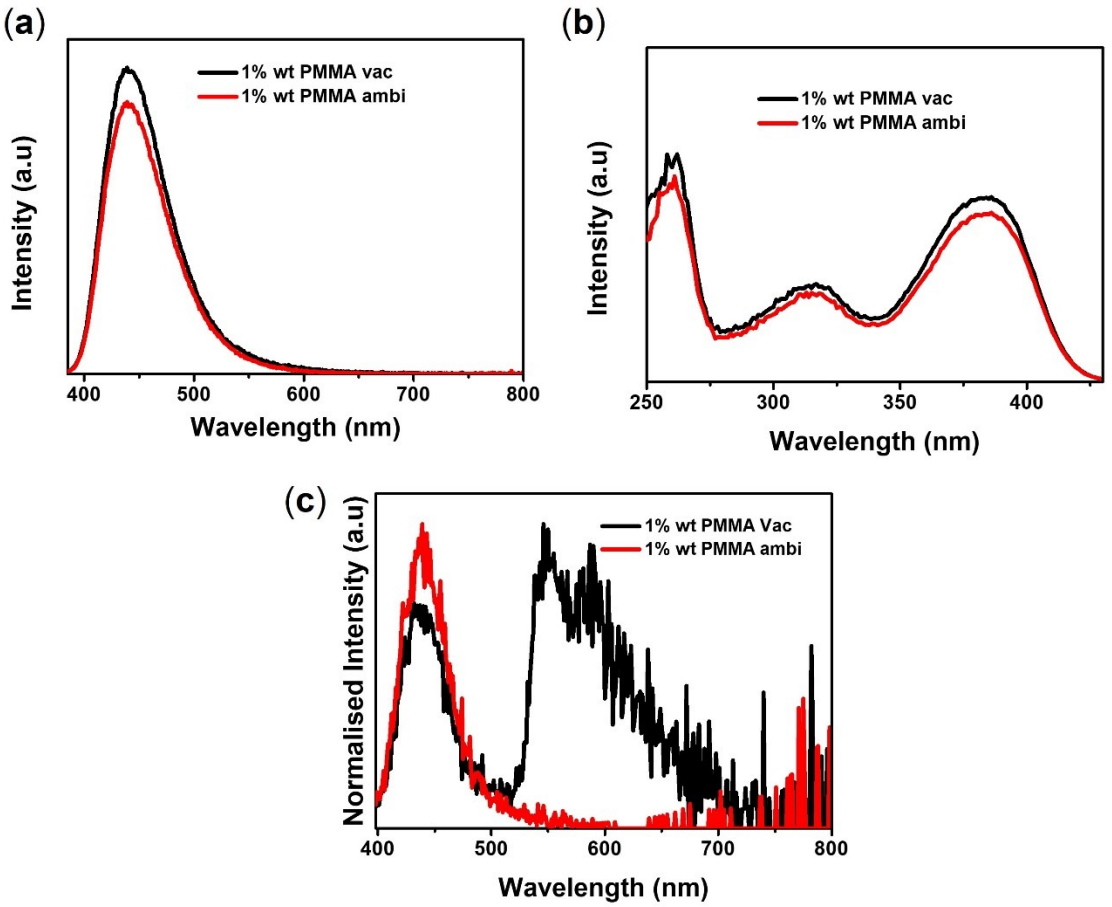

Figure S46. (a) PL spectra at λ_{ex} = 350 nm (b) Excitation spectra at λ_{em} = 450 nm, (c) Time-gated [50μs delay] PL spectra at λ_{ex} = 350 nm for **NB-NH_2** under vacuum (absence of oxygen) and ambient conditions (presence of oxygen).

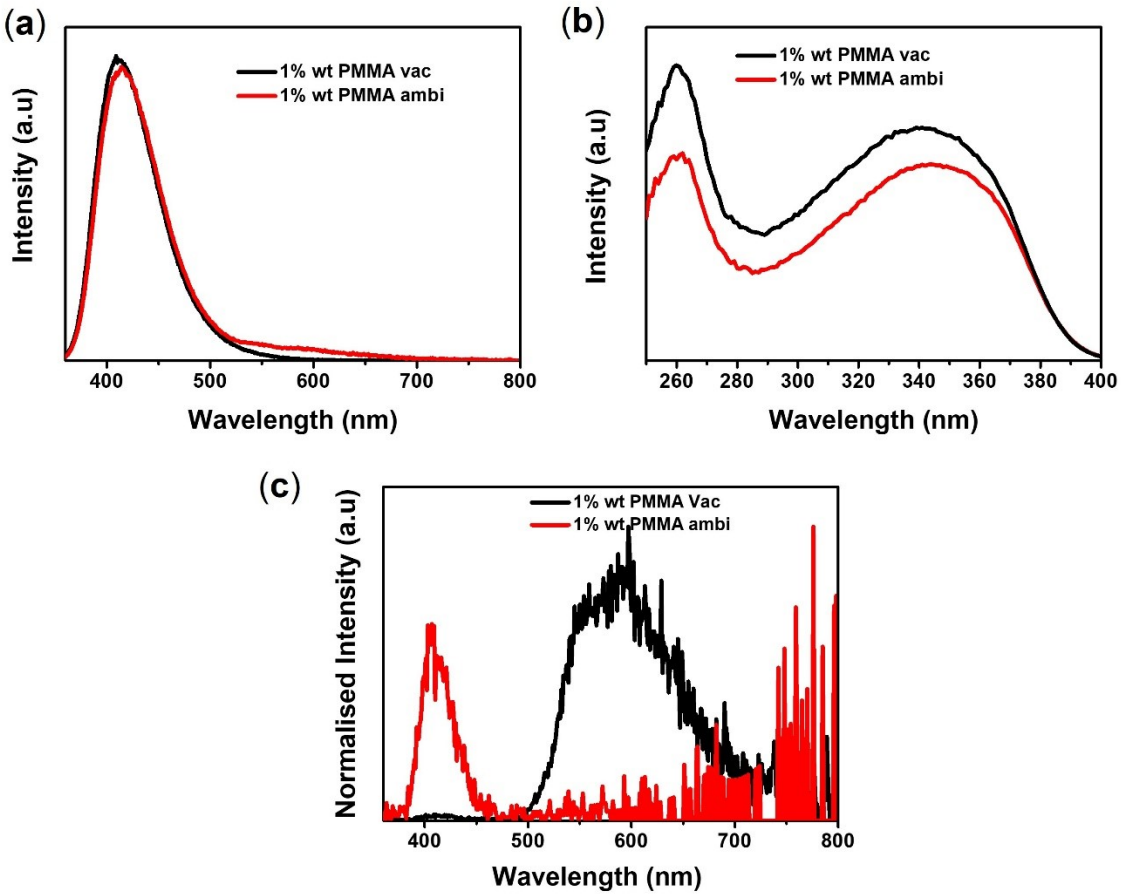

Figure S47. (a) PL spectra at λ_{ex} = 350 nm (b) Excitation spectra at λ_{em} = 450 nm, (c) Time-gated [50μs delay] PL spectra at λ_{ex} = 350 nm for **NB-COOH** under vacuum (absence of oxygen) and ambient conditions (presence of oxygen).

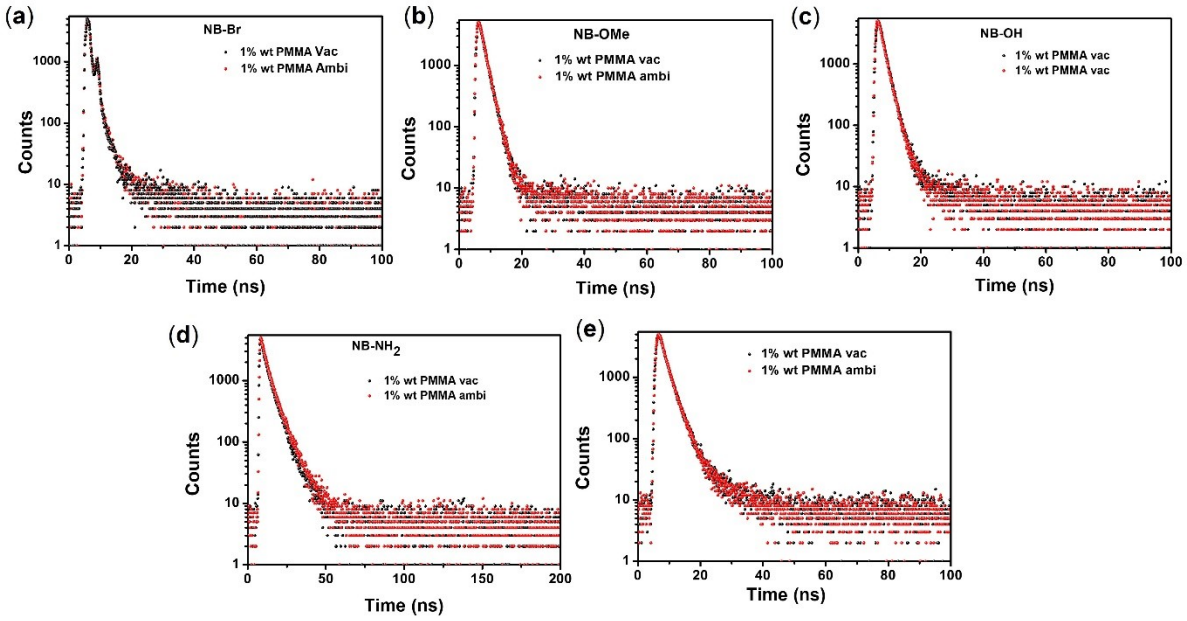

Figure S48: Fluorescence lifetime decay for **NB-Br** (λ_{em}=398 nm), **NB-Ome** (λ_{em}=390 nm), **NB-OH** (λ_{em}=397 nm), **NB-NH$_2$** (λ_{em}=440nm), and **NB-COOH** (λ_{em}=415nm) under different atmospheric conditions as a doped film on 1%wt PMMA matrix.

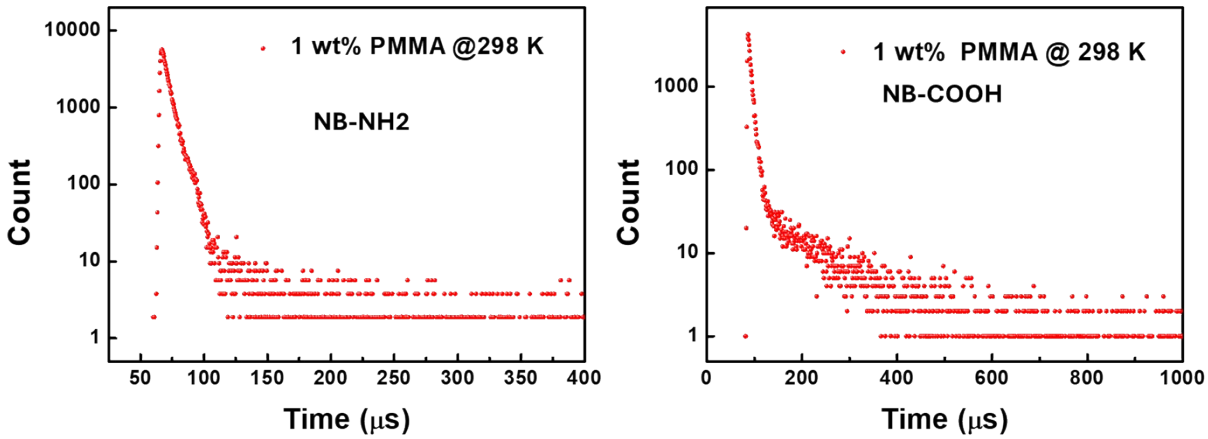

Figure S49: Delayed fluorescence lifetime decay for **NB-OH** (λ_{em}=397 nm), **NB-NH$_2$**(λ_{em}= 440 nm), and **NB-COOH** (λ_{em}= 415 nm) as a doped film on 1%wt PMMA matrix.

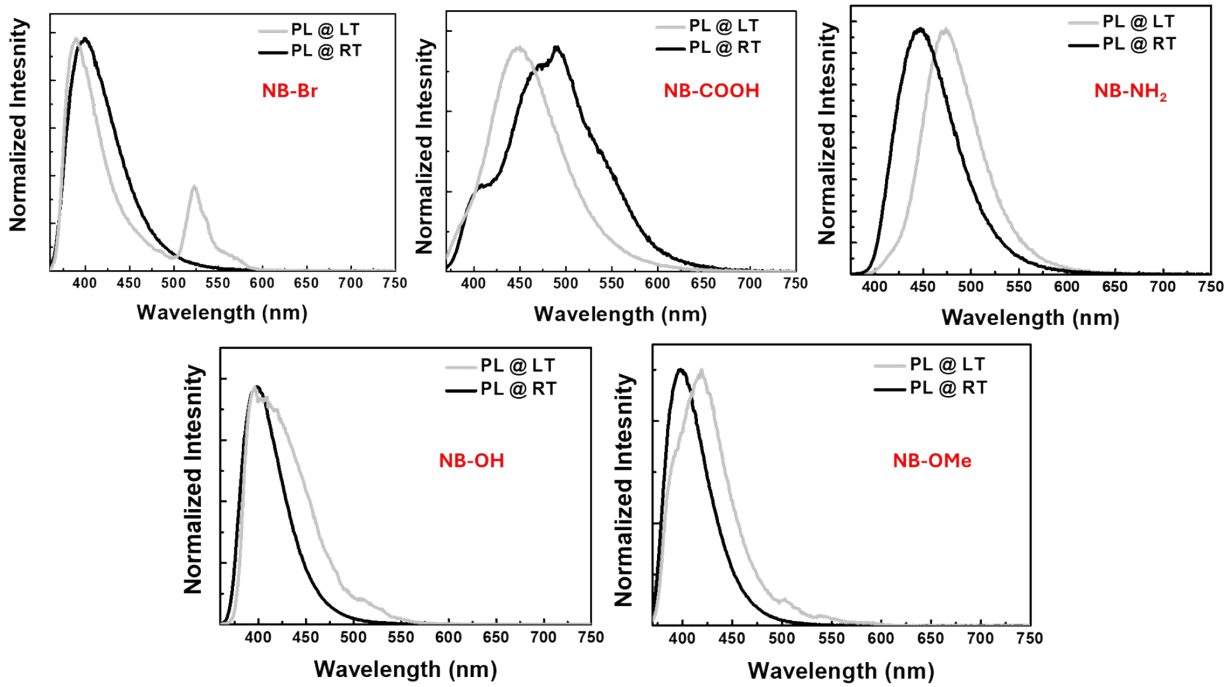

Figure 50. Photoluminescence (PL) spectra for **NB-Br**, **NB-OMe**, **NB-OH**, **NB-NH$_2$**, and **NB-COOH** in toluene (conc 10^{-5} M) at room temperature (RT, temperature = ~298 K) and low temperature (LT, temperature = ~77 K)

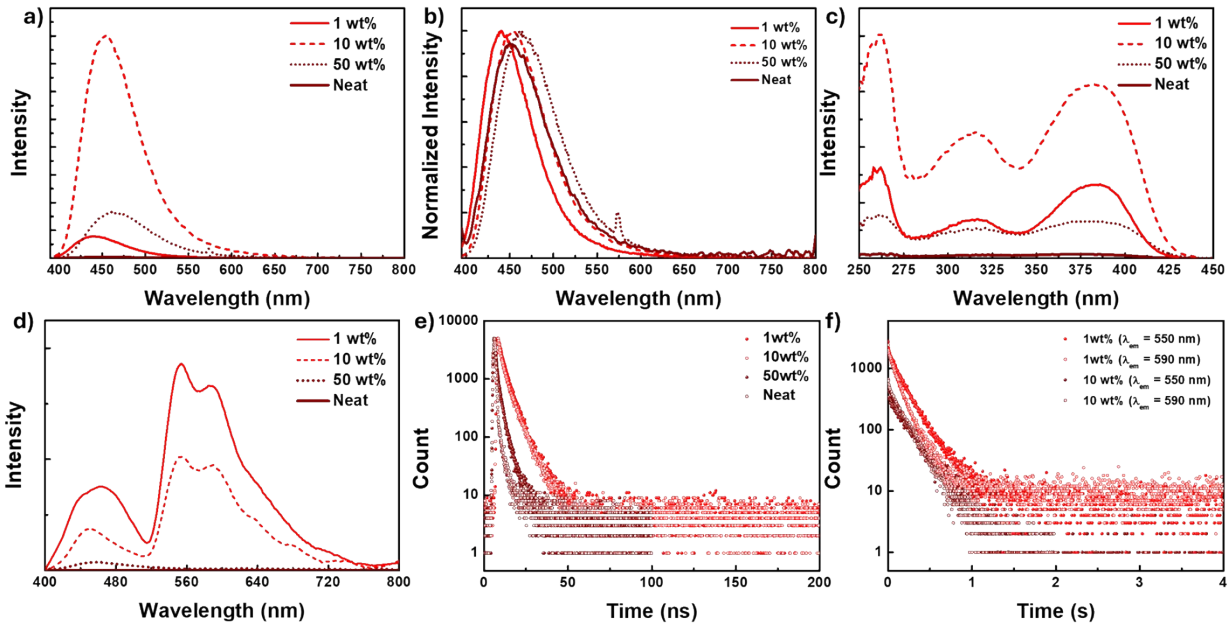

Figure S51. (a-d) Steady-state PL, excitation, and time-gated PL spectra of **NB-NH$_2$** in PMMA at different doping concentrations, and (e, f) fluorescence and phosphorescence lifetime decays at 298 K under vacuum (in the absence of oxygen), all measured upon λ_{ex}=375 nm.

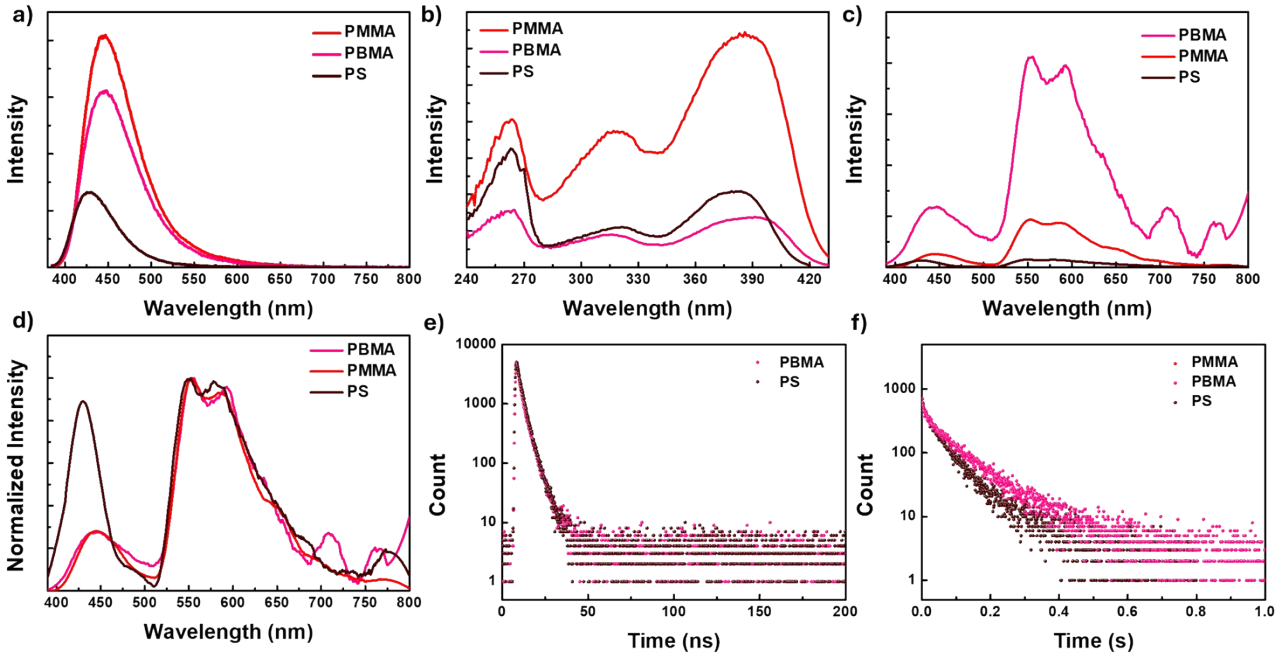

Figure S52. (a-c) Steady-state PL, excitation, and time-gated PL spectra of **NB-NH$_2$** at 1wt% doping concentrations in different polymer matrices and (d, e) fluorescence and phosphorescence lifetime decays at 298 K under vacuum (in the absence of oxygen), all measured upon λ_{ex}=375 nm. [PMMA-poly(methyl methacrylate, PBMA poly(butyl methacrylate) and PS- polystyrene],

Table S12: Fluorescence and phosphorescence decay kinetics for **NB-Br, NB-OMe** in the 1wt% doped PMMA film state.

Compound	**λ_{ex} (nm)**	**λ_{em}^{FL} (nm)**	**λ_{em}^{PH} (nm)**	**τ_{av}^{FL} (ns)**	**τ_{av}^{PH}** (ms)	**Φ_{Total} %**	**Φ_{PH} %**	**k_r^{FL} (x10^{7}S^{-1})**	**k_{nr}^{FL} (x10^{8}S^{-1})**	**k_r^{PH} (S^{-1})**	**k_{nr}^{T} (x10^2 S^{-1})**
NB-Br	350	398	570	2.03	4.52	7.50	5.73	0.87	4.55	12.67	2.08
NB-OMe	350	390	550	2.19	716.5	31.36	6.22	11.47	3.13	0.08	0.013
NB-OH	360	397	560	2.10	396.3	26.56	4.04	10.72	3.50	0.10	0.024
NB-NH$_2$	380	440	550	5.26	186.0	79.18	9.62	13.22	0.40	0.52	0.048
NB-COOH	350	415	550	2.89	195.80	70.80	13.49	19.83	1.10	0.69	0.041

λ_{ex} = excitation wavelength, λ_{em}^{FL} λ_{em}^{PH}= fluorescence and phosphorescence emission wavelength, τ_{av}^{FL}, τ_{av}^{PH} = average fluorescence and phosphorescence lifetime, Φ_{PL} = total absolute photoluminescence quantum yield. Φ_{FL}, Φ_{PH} = fluorescence and phosphorescence quantum yield, k_r^{FL} = radiative rate constant from singlet, k_{nr}^{FL} = non-radiative rate constant from singlet state. k_r^{PH} = radiative rate constant of phosphorescence, k_{nr}^{PH} = non-radiative rate constant from triplet state. $k_r^{FL} = \Phi_{FL} / \tau_{FL}$, $k_{nr}^{FL} = (1 - \Phi_{FL}-\Phi_{PH}) / \tau_{av}^{FL}$,$k_r^{PH} = \Phi_{PH} / \tau_{PH}$, $k_{nr}^{PH} = (1 - \Phi_{PH}) / \tau_{av}^{PH}$

Table S13: Fluorescence and phosphorescence lifetime for **NB-NH_2**, in PMMA at different doping concentrations, 298 K under vacuum (in the absence of oxygen).

	Lifetime							
	Fluorescence (ns)				**Phosphorescence (µs)**			
	λ_{ex}	**λ_{em}**	**τ_1 (A_1 %)**	**τ_2 (A_2 %)**	**λ_{ex}**	**λ_{em}**	**τ_1 (A_1 %)**	**τ_2 (A_2 %)**
1 wt%	375	440	3.04 (48.39)	7.32 (51.61)	375	550	122.59 (50.33)	249.41 (49.67)
						585	85.65 (53.27)	189.90 (46.73)
10 wt%	375	450	1.91 (39.60)	6.23 (60.40)	375	550	28.71 (6.02)	205.15 (93.98)
						585	38.24 (12.01)	168.08 (87.89)
50 wt%	375	465	1.04 (62.31)	3.75 (37.69)	No RTP			
Neat	375	450	0.47 (74.76)	3.97 (25.24)	No RTP			

Table S14: Fluorescence and phosphorescence lifetime for **NB-NH_2**, in 1wt% doping concentrations in different polymer matrices, 298 K under vacuum (in the absence of oxygen).

	Lifetime								**Φ_{PL} [%]**
	Fluorescence (ns)				**Phosphorescence (µs)**				
	λ_{ex}	**λ_{em}**	**τ_1 (A_1 %)**	**τ_2 (A_2 %)**	**λ_{ex}**	**λ_{em}**	**τ_1 (A_1 %)**	**τ_2 (A_2 %)**	
PMMA	375	440	3.04 (48.39)	7.32 (51.61)	375	550	122.59 (50.33)	249.41 (49.67)	
PBMA		445	1.78 (41.93)	5.02 (58.07)		550	16.7 (12.04)	107.59 (87.96)	16.2 %
PS	375	430	2.52 (61.63)	5.10 (38.37)	375	550	31.63 (41.39)	94.66 (58.61)	58.9 %

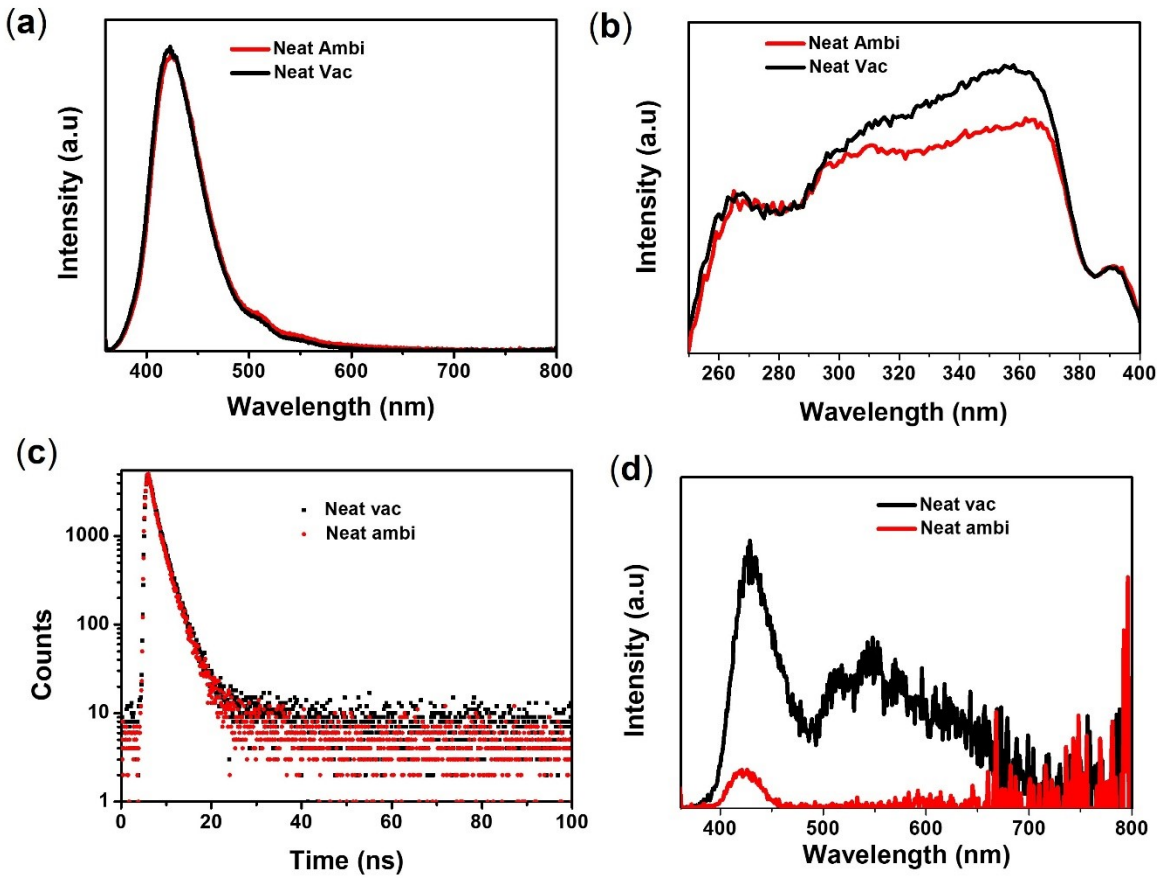

Figure S53. (a) PL spectra at λ_{ex} = 350 nm (b) Excitation spectra at λ_{em} = 425 nm, (c) Fluorescence lifetime decay for **NB-Br** (λ_{em}=425 nm), (d) Time gated [50μs delay] PL spectra at λ_{ex} = 350 nm for **NB-Br** under vacuum (absence of oxygen) and ambient conditions (presence of oxygen).

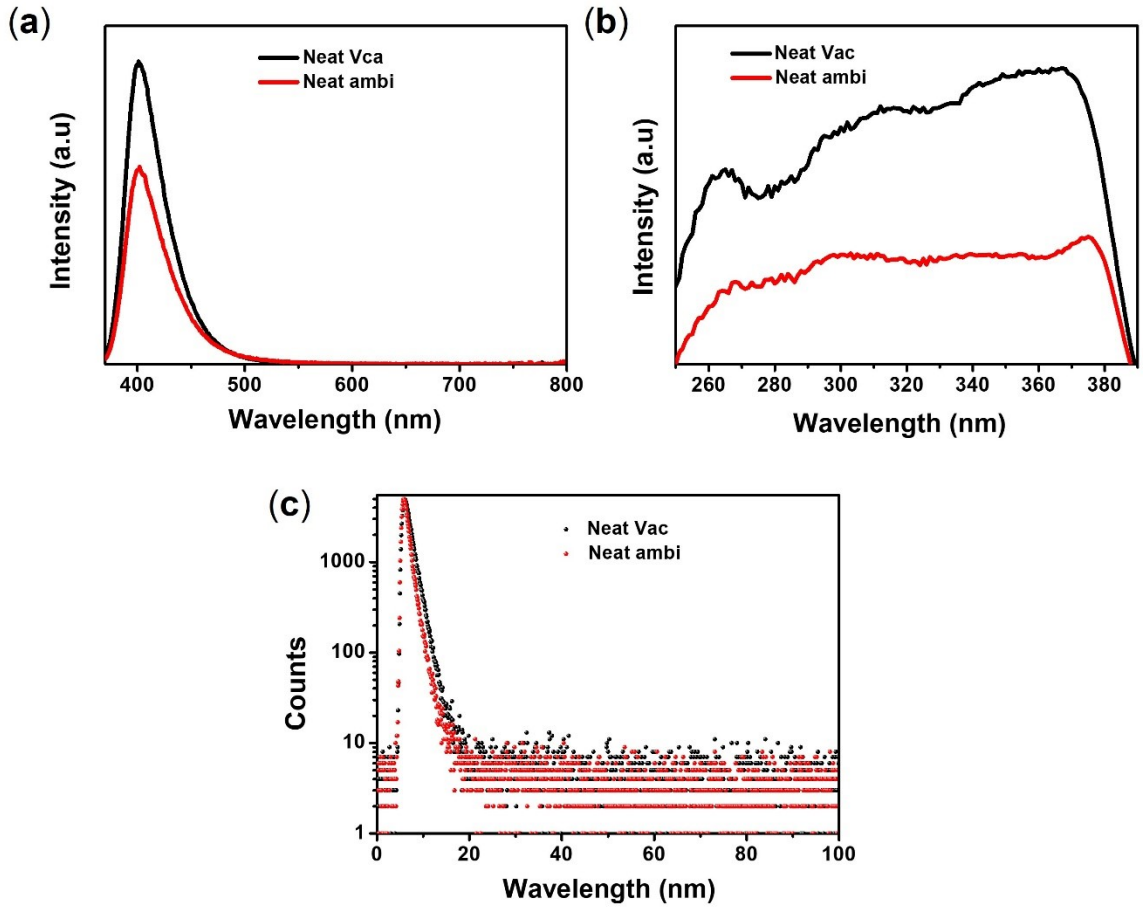

Figure S54. (a) PL spectra at λ_{ex} = 350 nm (b) Excitation spectra at λ_{em} = 400 nm (c) Fluorescence lifetime decay (λ_{em}=400 nm) for **NB-OMe** under vacuum (absence of oxygen) and ambient conditions (presence of oxygen).

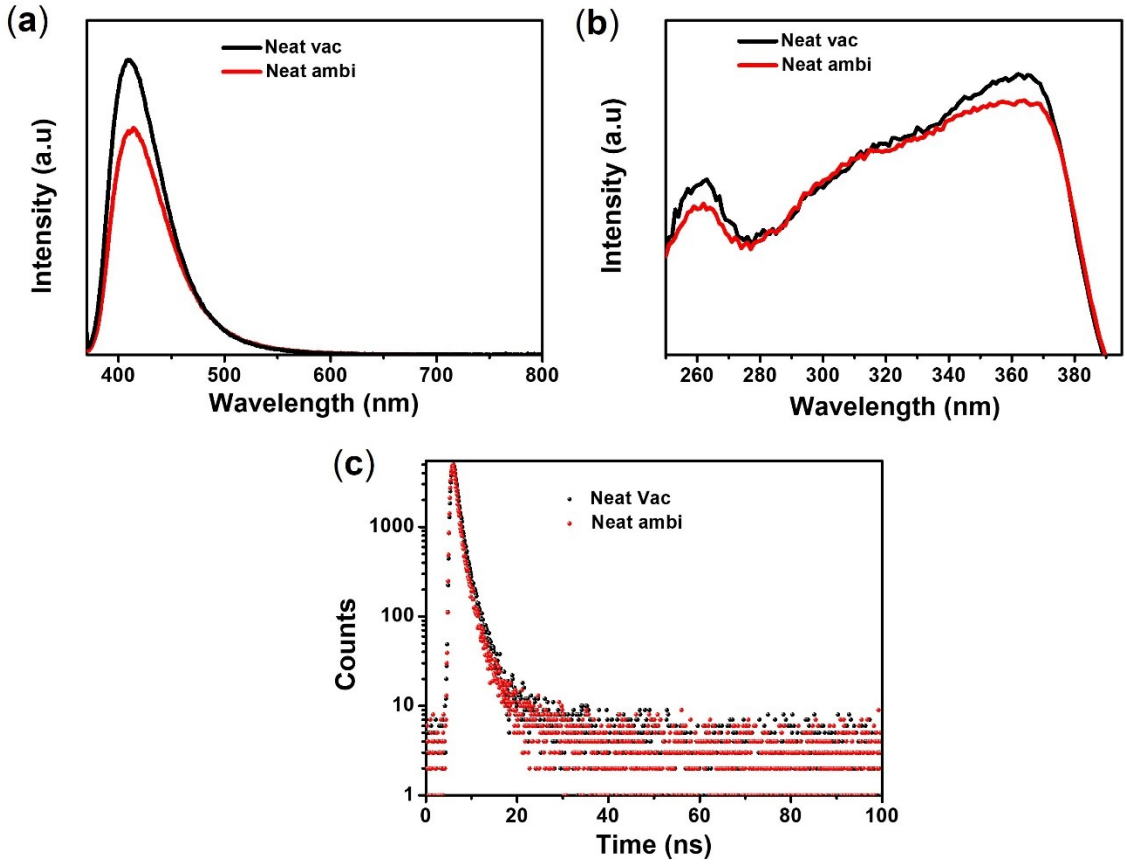

Figure S55. (a) PL spectra at λ_{ex} = 350 nm (b) Excitation spectra at λ_{em} = 409 nm (c) Fluorescence lifetime decay (λ_{em}=400 nm) for **NB-OH** under vacuum (absence of oxygen) and ambient conditions (presence of oxygen).

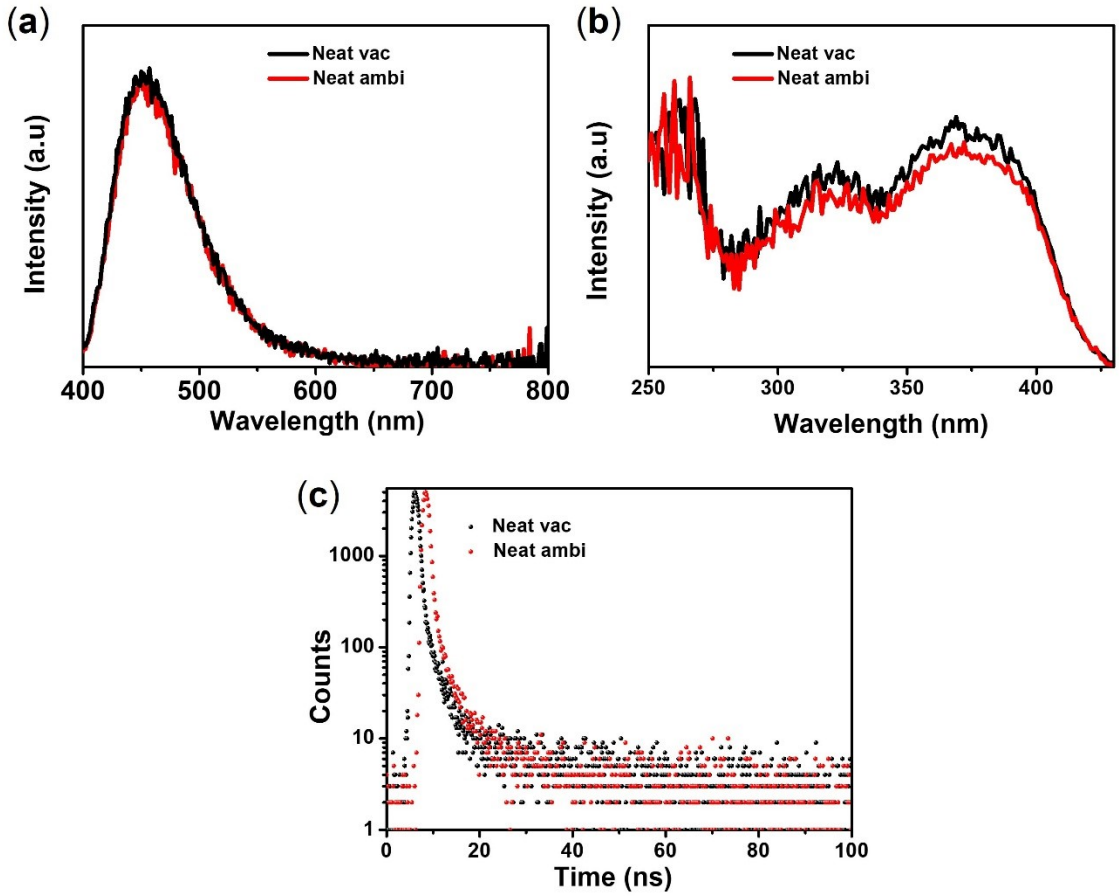

Figure S56. (a) PL spectra at λ_{ex} = 375 nm (b) Excitation spectra at λ_{em} = 450 nm (c) Fluorescence lifetime decay (λ_{em}=450nm) for **NB-NH2** under vacuum (absence of oxygen) and ambient conditions (presence of oxygen).

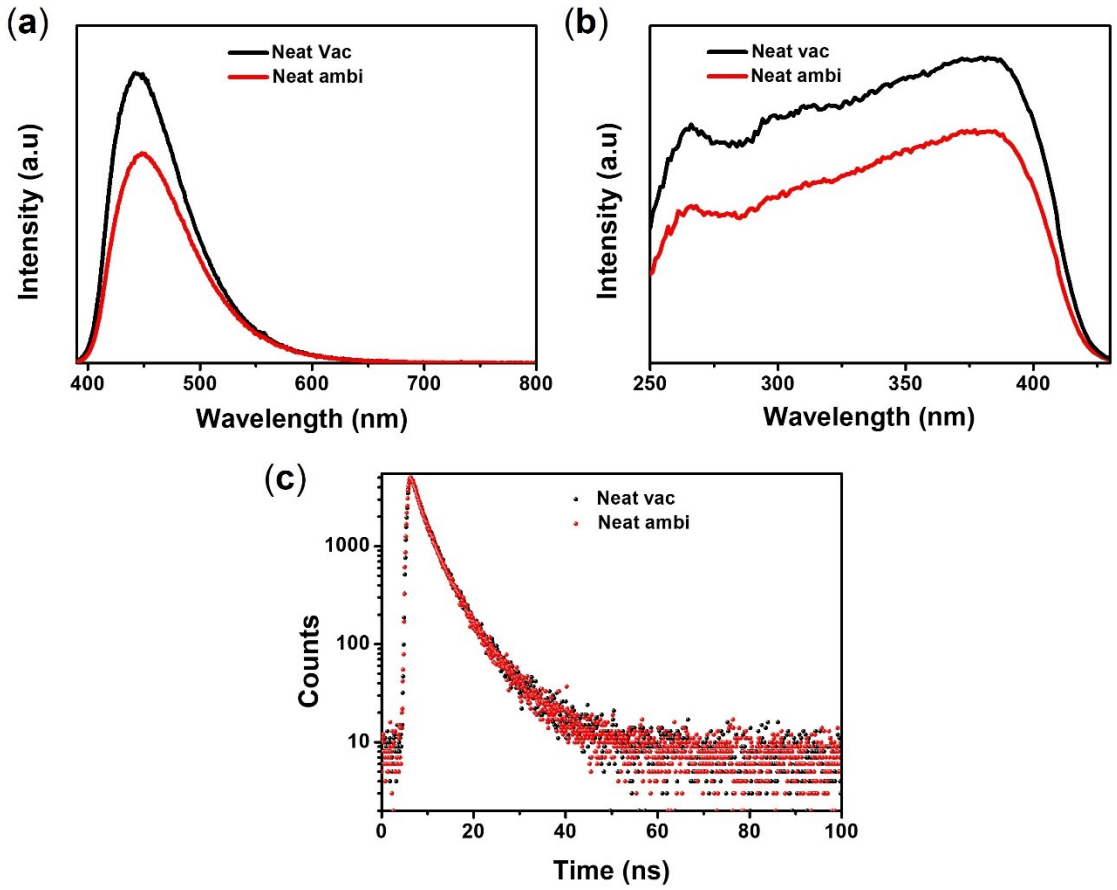

Figure S57. (a) PL spectra at λ_{ex} = 375 nm (b) Excitation spectra at λ_{em} = 450 nm,(c) Fluorescence lifetime decay (λ_{em}=450 nm) for **NB-COOH** under vacuum (absence of oxygen) and ambient conditions (presence of oxygen).

Table S15: Fluorescence lifetime for **NB-Br**, **NB-OMe**, **NB-OH**, **NB-NH_2**, and **NB-COOH** under different atmospheric conditions along with total PLQY under ambient conditions at 298 K, as a doped film on PMMA matrix.

	Fluorescence lifetime (ns)								**PLQY [%]**
	298 K (Vaccum)				**298 K (Ambient)**				
	λ_{ex}	**λ_{em}**	**τ_1 (A_1 %)**	**τ_2 (A_2 %)**	**λ_{ex}**	**λ_{em}**	**τ_1 (A_1 %)**	**τ_2 (A_2 %)**	
NB-Br									
Neat	375	425	1.57 (64.28)	3.67 (35.72)	375	425	1.52 (62.62)	3.44 (37.38)	5.01
1 wt% PMMA		390	0.62 (56.20)	3.84 (43.80)		390	0.58 (49.58)	3.82 (50.42)	7.50
NB-OMe									
Neat	375	401	1.48 (98.32)	10.25 (1.68)	375	400	0.86 (72.25)	2.16 (27.75)	17.99
1 wt% PMMA		390	1.75 (97.40)	16.59 (2.60)		390	1.72 (97.51)	12.32 (2.49)	31.36
NB-OH									
Neat	375	409	0.99 (63.03)	3.17 (36.97)	375	413	0.89 (63.66)	3.15 (36.34)	11.05
1 wt% PMMA		397	1.81 (96.88)	11.12 (3.12)		397	1.78 (96.24)	8.38 (3.76)	26.56
NB-NH_2									
Neat	375	450	0.47 (74.76)	3.97 (25.24)	375	450	0.44 (66.47)	2.47 (24.88)	21.17
1 wt% PMMA		440	3.04 (48.39)	7.32 (51.61)	375	440	2.74 (44.68)	6.61 (55.32)	79.18
NB-COOH									
Neat	375	450	2.69 (60.19)	7.17 (39.81)	375	450	2.68 (64.03)	7.25 (35.97)	27.69
1 wt% PMMA		415	2.28 (88.28)	7.35 (11.72)		415	2.27 (89.31)	7.29 (10.69)	70.80

Nb: No phosphorescence bands were observed at 298 K for any of the compounds except **NB-Br.**

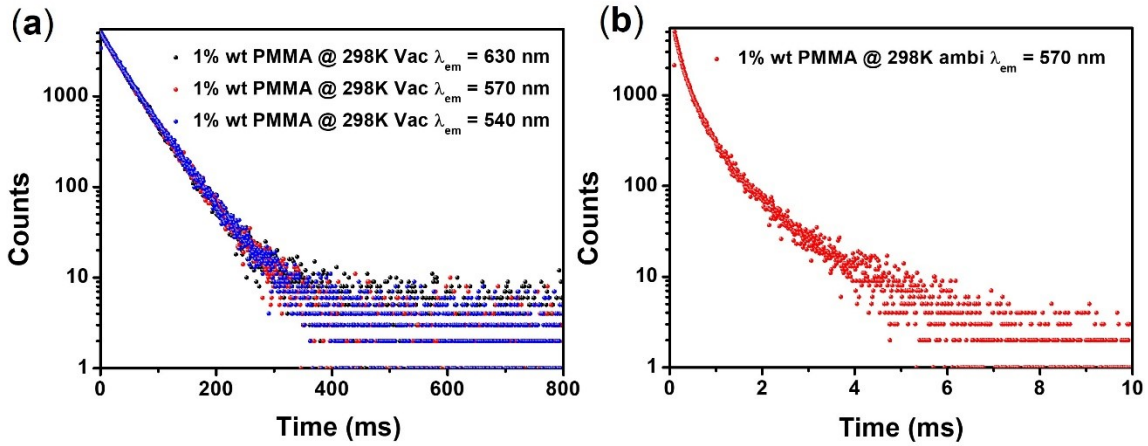

Figure S58. (a) Phosphorescence lifetime decay [λ_{ex} = 375 nm and λ_{ex} = 630 nm, 570 nm and 540 nm] under vacuum [absence of oxygen] at 298 K for **NB-Br** doped in PMMA matrix (1 wt%) (b) Phosphorescence lifetime decay [λ_{ex} = 375 nm and λ_{ex} = 570 nm] under ambient atmosphere at 298 K for **NB-Br** doped in PMMA matrix (1 wt%)

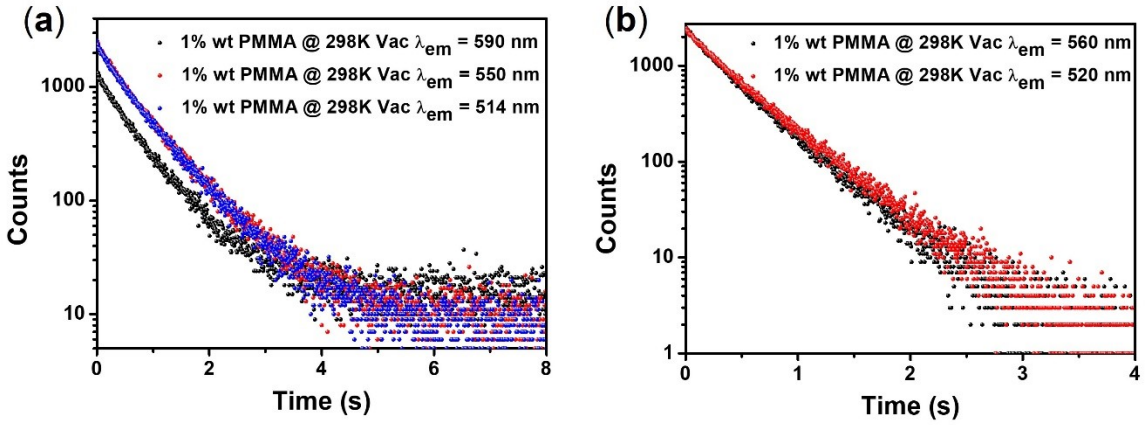

Figure S59. (a) Phosphorescence lifetime decay [λ_{ex} = 375 nm and λ_{ex} = 590 nm, 550nm and 514 nm] for **NB-OMe** under vacuum [absence of oxygen] and ambient atmosphere [presence of oxygen] at 298 K as a doped in PMMA matrix (1 wt%) (b) Phosphorescence lifetime decay [λ_{ex} = 375 nm and λ_{ex} = 560 nm, and 520 nm] for **NB-OH** under vacuum [absence of oxygen] and ambient atmosphere [presence of oxygen] at 298 K as a doped in PMMA matrix (1 wt%) [λ_{ex} = 380 nm].

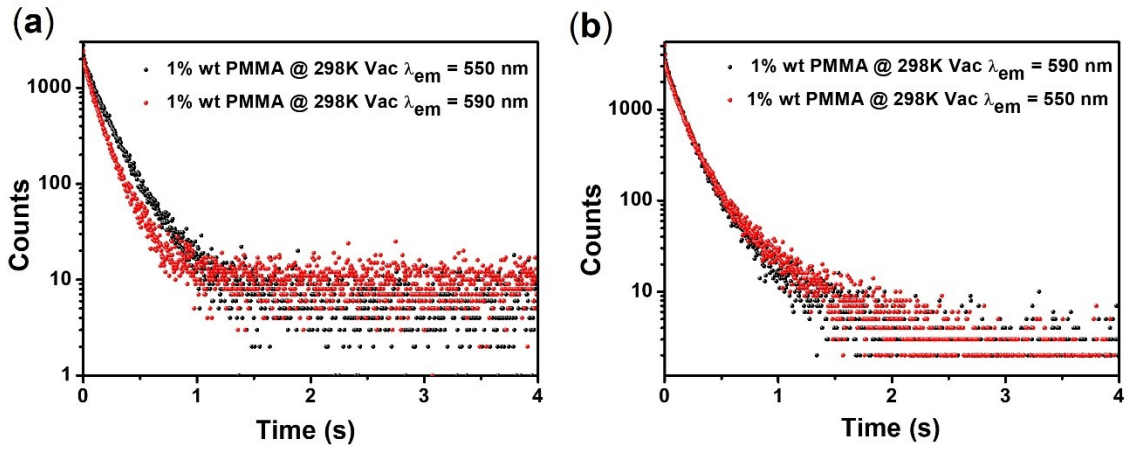

Figure S60. (a) Phosphorescence lifetime decay [λ_{ex} = 375 nm and λ_{ex} = 590 nm, and 550 nm] for **NB-NH$_2$** under vacuum [absence of oxygen] and ambient atmosphere [presence of oxygen] at 298 K as a doped in PMMA matrix (1 wt%). (b) Phosphorescence lifetime decay [λ_{ex} = 375 nm and λ_{ex} = 590 nm, and 520 nm] for **NB-COOH** under vacuum [absence of oxygen] and ambient atmosphere [presence of oxygen] at 298 K as a doped in PMMA matrix (1 wt%).

Table S16: Phosphorescence lifetime for **NB-Br**, **NB-OMe**, **NB-OH**, **NB-NH_2**, and **NB-COOH** under different atmospheric conditions, along with total PLQY under ambient conditions at 298 K as a doped film on PMMA matrix

	Delayed lifetime							
	Delayed Fluorescence (μs)				**Phosphorescence (ms)**			
	λ_{ex}	**λ_{em}**	**τ_1 (A_1 %)**	**τ_2 (A_2 %)**	**λ_{ex}**	**λ_{em}**	**τ_1 (A_1 %)**	**τ_2 (A_2 %)**
NB-Br								
1 wt% @ PMMA (vacuum)	No delayed Fluorescence				375	540	3.33 (41.08)	5.35 (58.92)
						570	3.44 (45.04)	5.43 (54.96)
1 wt% @ PMMA (ambinet)	No delayed Fluorescence					540	0.20 (55.51)	0.89 (44.89)
						570	0.24 (57.09)	1.01 (42.91)
Neat	350	425	ND*		350	550	97.36μs (72.55)	926.38μs (27.45)
NB-OMe								
1 wt%@ PMMA	No delayed Fluorescence				375	517	419.71 (30.71)	862.16 (69.29)
						550	373.83 (23.69)	824.81 (76.31)
						603	390.14 (31.70)	800.43 (68.30)
Neat	No delayed component							
NB-OH								
1 wt%@ PMMA	No delayed Fluorescence				375	524	242.11 (20.71)	484.95 (79.29)
						560	206.20 (18.51)	440.96 (81.49)
Neat	No delayed component							
NB-NH_2								
1 wt%@ PMMA	375	440	3.66 (41.70)	7.86 (58.30)	375	550	122.59 (50.33)	249.41 (49.67)
						585	85.65 (53.27)	189.90 (46.73)
Neat	No delayed component							
NB-COOH								
1 wt%@ PMMA	375	415	5.99 (86.47)	94.65 (13.53)	375	550	117.56 (74.01)	418.74 (25.99)
						590	113.86 (76.97)	361.97 (23.03)
Neat	No delayed component							

ND: Not detectable**.**

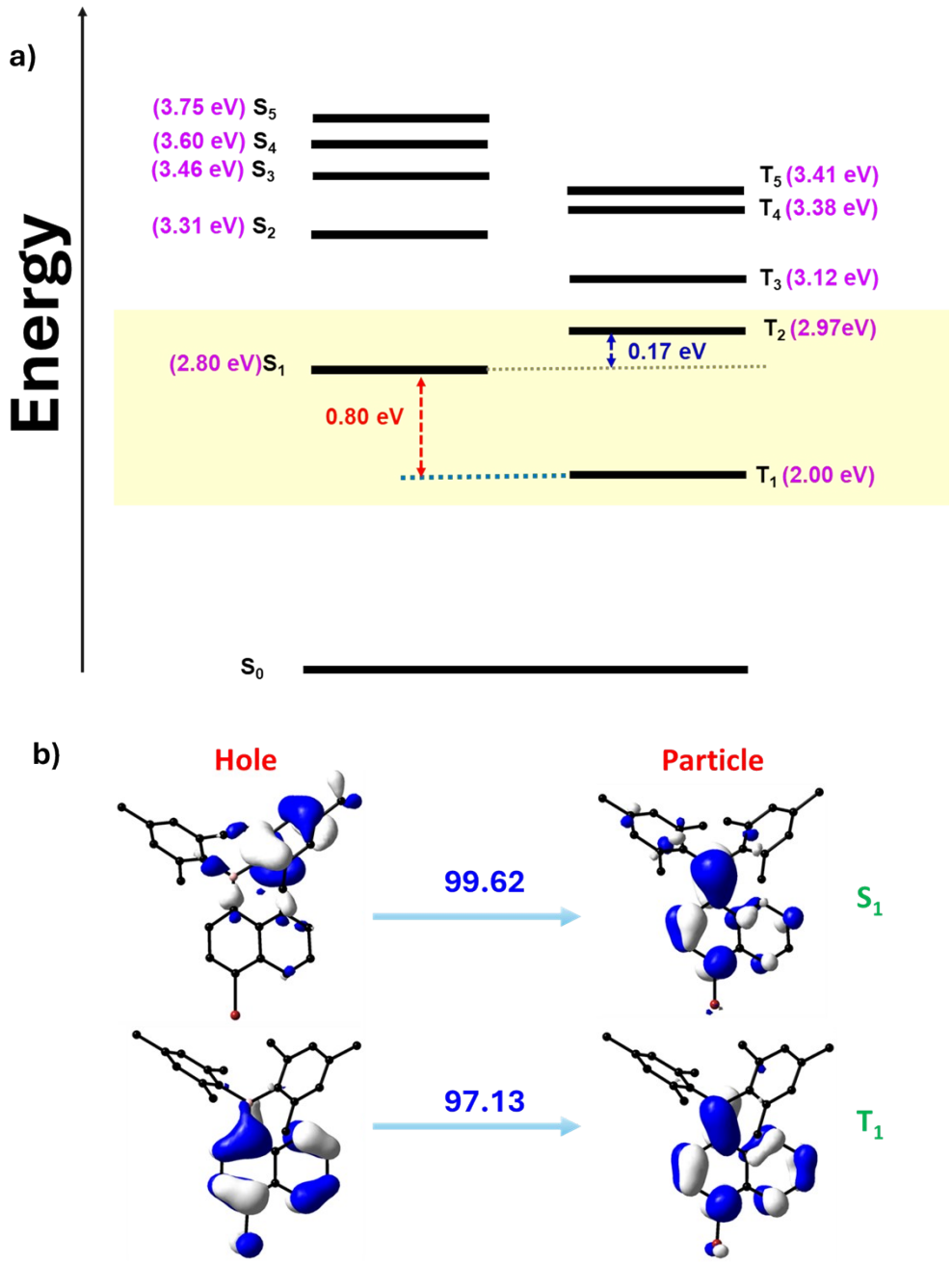

Figure S61. (a) Energy level diagram showing singlet-triplet energy gap, and possible ISC channel (b) Natural transition orbital (NTO's) for **NB-Br** [energy levels in the diagram are not up-to-scale, the most possible T_n state involved in spin-crossover according to the energy difference is highlighted in a yellow box]. (b) Natural transition orbital (NTO's) for **NB-Br**. The energy levels and NTO's are calculated from singlet and triplet vertical transitions through TD-DFT using 6-31G (d, p)/B3LYP level of theory.

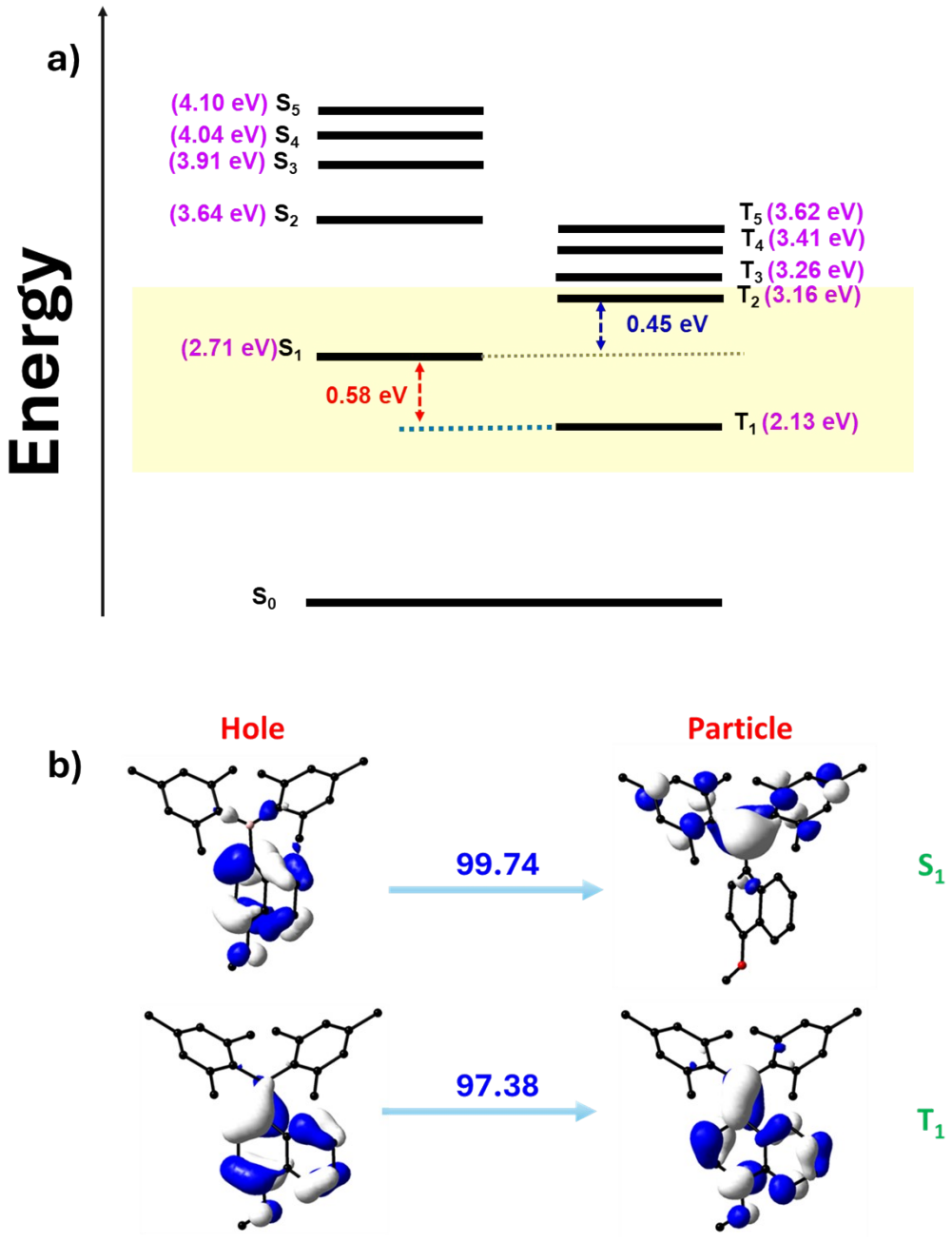

Figure S62. (a) Energy level diagram showing singlet-triplet energy gap, and possible ISC channel (b) Natural transition orbital (NTO's) for **NB-OMe** [energy levels in the diagram are not up-to-scale, the most possible T_n state involved in spin-crossover according to the energy difference is highlighted in a yellow box]. (b) Natural transition orbital (NTO's) for **NB-OMe**. The energy levels and NTO's are calculated from singlet and triplet vertical transitions through TD-DFT using 6-31G (d, p)/B3LYP level of theory.

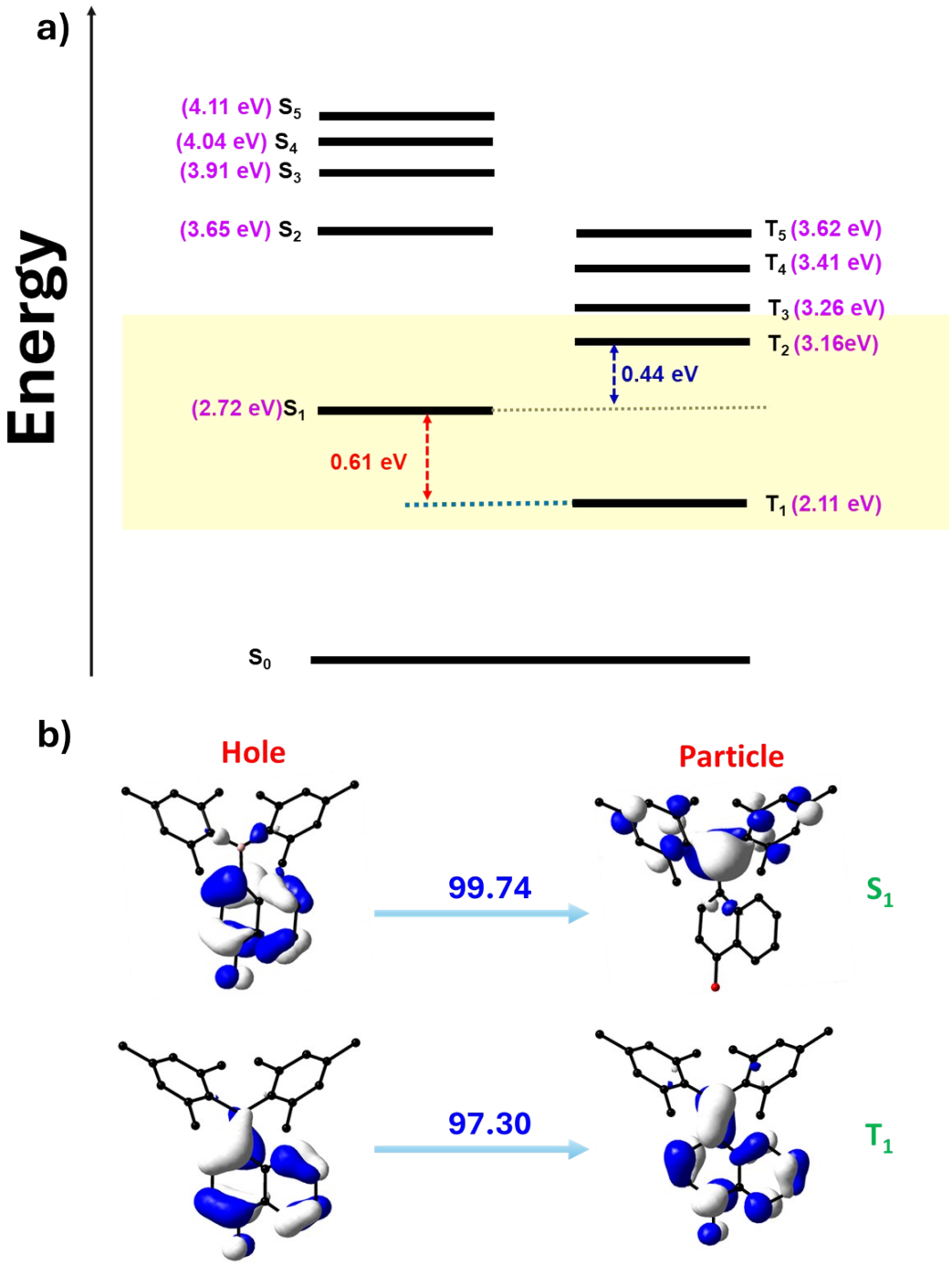

Figure S63. (a) Energy level diagram showing singlet-triplet energy gap, and possible ISC channel (b) Natural transition orbital (NTO's) for **NB-OH** [energy levels in the diagram are not up-to-scale, the most possible T_n state involved in spin-crossover according to the energy difference is highlighted in a yellow box]. (b) Natural transition orbital (NTO's) for **NB-OH**. The energy levels and NTO's are calculated from singlet and triplet vertical transitions through TD-DFT using 6-31G (d, p)/B3LYP level of theory.

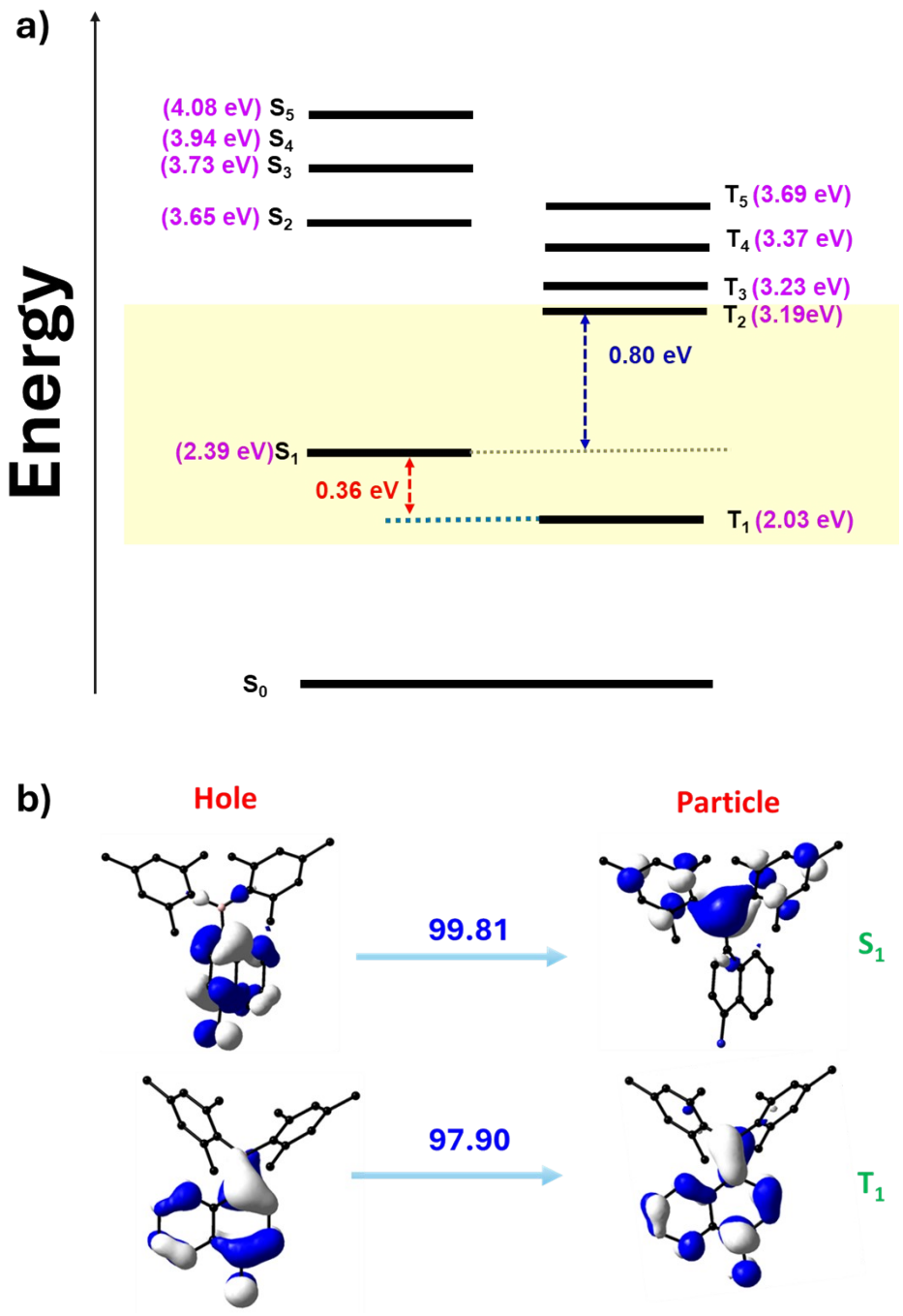

Figure S64. (a) Energy level diagram showing singlet-triplet energy gap, and possible ISC channel (b) Natural transition orbital (NTO's) for **NB-NH$_2$** [energy levels in the diagram are not up-to-scale, the most possible T_n state involved in spin-crossover according to the energy difference is highlighted in a yellow box]. (b) Natural transition orbital (NTO's) for **NB-NH$_2$**. The energy levels and NTO's are calculated from singlet and triplet vertical transitions through TD-DFT using 6-31G (d, p)/B3LYP level of theory

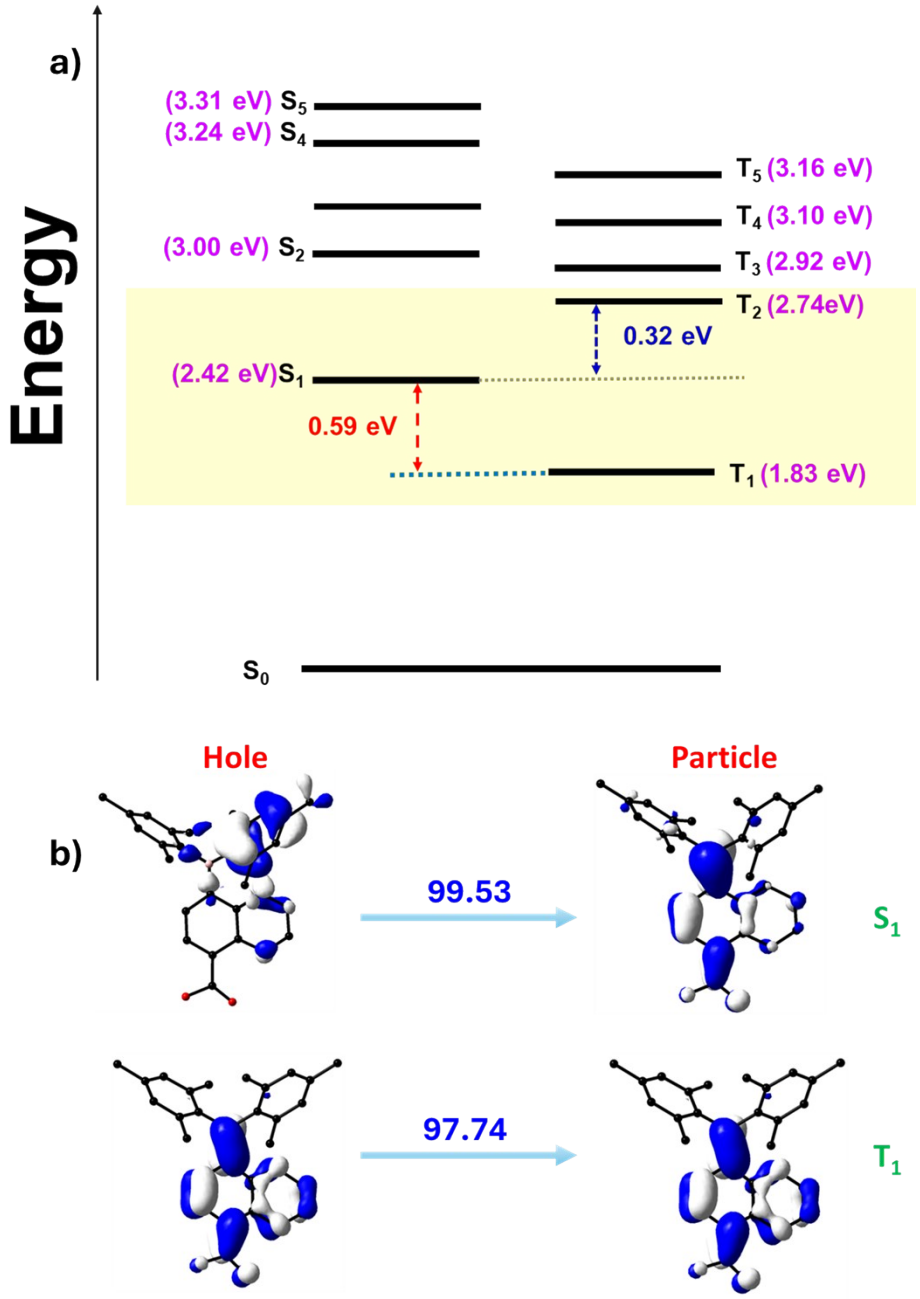

Figure S65. (a) Energy level diagram showing singlet-triplet energy gap, and possible ISC channel (b) Natural transition orbital (NTO's) for **NB-COOH** [energy levels in the diagram are not up-to-scale, the most possible T_n state involved in spin-crossover according to the energy difference is highlighted in a yellow box]. (b) Natural transition orbital (NTO's) for **NB-COOH**. The energy levels and NTO's are calculated from singlet and triplet vertical transitions through TD-DFT using 6-31G (d, p)/B3LYP level of theory

Table S17: List of spin-orbital coupling values for **NB-Br, NB-OMe, NB-OH, NB-NH_2, NB-COOH** between different singlet and triplet energy levels obtained theoretically using B3LYP/6-31G(d,p) level of theory

Transition	SOC (cm^{-1})				
	NB-Br	**NB-OMe**	**NB-OH**	**NB-NH_2**	**NB-COOH**
S0→T1	6.0144	0.2529	0.2894	0.1954	0.2539
S0→T2	2.1673	0.5481	0.5488	0.5270	1.723
S0→T3	1.0616	0.3361	0.3672	0.4379	0.3885
S1→T1	5.3296	0.3832	0.4442	0.2519	0.7153
S1→T2	3.2884	1.1356	1.1531	1.0337	0.9039
S1→T3	1.6196	0.5741	0.6110	0.5233	0.9854
S1→T4	0.2930	0.0519	0.0412	0.1876	0.1236
S1→T5	0.3343	0.1268	0.1529	0.1630	0.2111

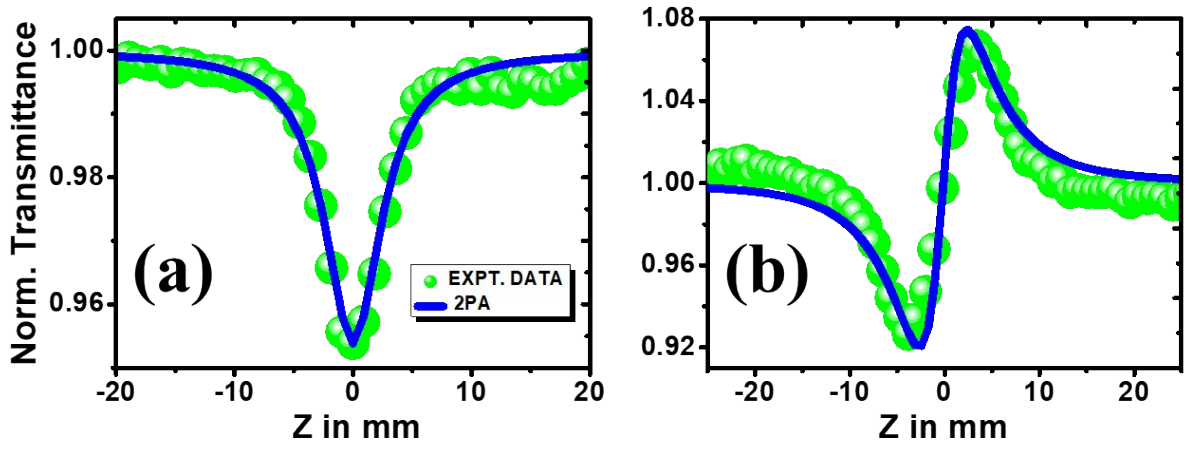

Figure S66: Femtosecond Z-Scan (a) open aperture and (b) close aperture plots of the solvent chloroform. Green circles demonstrate experimentally obtained data, and the blue line represents the theoretical fit to 2PA.

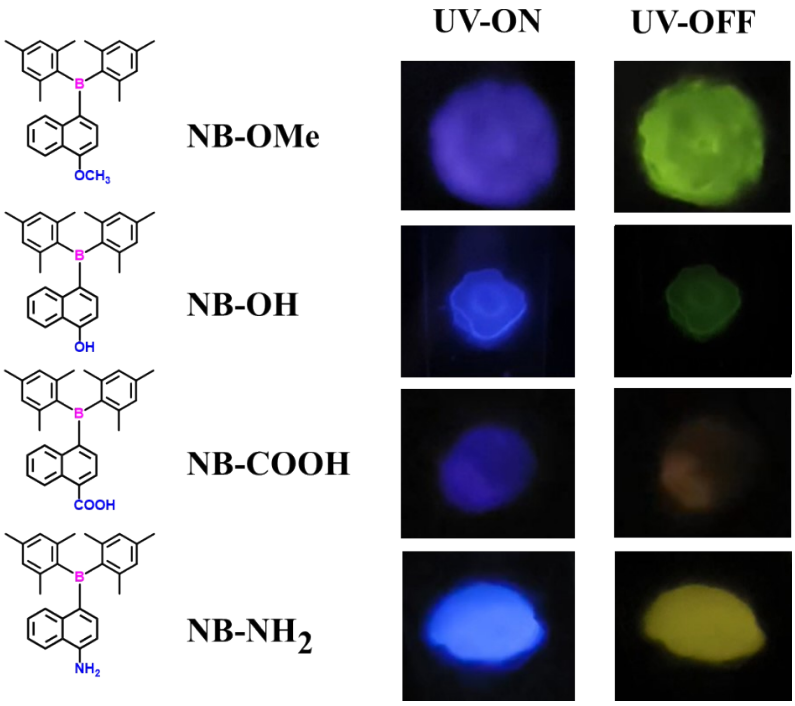

Figure S67: Photographs of PMMA (1 wt%) films containing NB–OMe, NB–OH, NB–COOH, and NB–NH_2 under UV light (λ_{ex} = 365 nm) and after turning off the UV source. NB–Br shows negligible phosphorescence and could not be captured.

References

1. R. J. Errington, Advanced practical inorganic and metal organic chemistry, Blackie academic & professional, London, 1997.

2. W. F. Armarego and C. L. L. Chai, Purification of laboratory chemicals, Elsevier, UK, 2013.

3. (a) G. M. Sheldrick, Crystal structure refinement with SHELXL, Acta Crystallogr., Sect. C: Struct. Chem., **2015**, 71, 3-8; (b) G. M. Sheldrick, A short history of SHELX, Acta Crystallogr., Sect. A: Found. Crystallogr., **2008**, 64, 112; (c) A. L. Spek, Single-crystal structure validation with the program PLATON, J. Appl. Crystallogr., **2003**, 36, 7; (d) G. M. Sheldrick, Program for Crystal Structure Solution. SHELXS-97, University of Göttingen, Göttingen, Germany, 1997.

4. a) Frisch, M. J.; Trucks, G. W.; Schlegel, H. B.; Scuseria, G. E.; Robb, M. A.; Cheeseman, J. R.; Scalmani, G.; Barone, V.; Mennucci, B.; Petersson, G. A., et al. Gaussian 09, Revision D.01, Gaussian, Inc., Wallingford CT, **2013**. b) Lee, C.; Yang, W.; Parr, R. G. Development of the Colic-Salvetti Correlation-Energy Formula into a Functional of the Electron Density. *Phys. Rev. B*., **1988**, *37*, 785-789.

5. Chen, J.-F.; Yin, X.; Zhang, K.; Zhao, Z.; Zhang, S.; Zhang, N.; Wang, N.; Chen, P. Pillar[5]arene-Based Dual Chiral Organoboranes with Allowed Host Guest Chemistry and Circularly Polarized Luminescence. *J. Org. Chem*. **2021**, *86*, 12654.

6. Li, B., Gong, Y., Wang, L., Lin, H., Li, Q., Guo, F., Li, Z., Peng, Q., Shuai, Z., Zhao, L. and Zhang, Y., 2019. Highly efficient organic room-temperature phosphorescent luminophores through tuning triplet states and spin–orbit coupling with incorporation of a secondary group. *J. Phys. Chem. Lett.,***2019**,10(22), pp.7141.

7. Wei, J., Liu, C., Duan, J., Shao, A., Li, J., Li, J., Gu, W., Li, Z., Liu, S., Ma, Y. and Huang, W., 2023. Conformation-dependent dynamic organic phosphorescence through thermal energy driven molecular rotations. Nat. Commun., **2023**, 14(1), p.627.

8. Wu, Z., Nitsch, J., Schuster, J., Friedrich, A., Edkins, K., Loebnitz, M., Dinkelbach, F., Stepanenko, V., Wgrthner, F., Marian, M. C., Ji, L., Marder, B. T., Persistent Room Temperature Phosphorescence from Triarylboranes: A Combined Experimental and Theoretical Study. Angew. Chem. Int. Ed. **2020**, *59*, 17137.